

**Synthesis of positron emitter-labelled amino acids:
Application to the investigation of metabolic
preferences and vulnerabilities in a mouse prostate
cancer model**

Pilar Castellnou Arenas

Donostia 2022





Synthesis of positron emitter-labelled amino acids: Application to the investigation of metabolic preferences and vulnerabilities in a mouse prostate cancer model

PhD Thesis

to obtain the Doctor of Philosophy degree in

Synthetic and Industrial Chemistry

at the University of the Basque Country (UPV/EHU)

by

Pilar Castellnou Arenas

Donostia 2022

Thesis supervisors: Dr. Jordi Llop Roig (Radiochemistry and Nuclear Imaging Group, CIC biomaGUNE) and Prof. Arkaitz Carracedo Pérez (Cancer Cell Signaling and Metabolism Groupm CIC bioGUNE)

University Tutor: Dr. María Esther Lete Expósito (Department of Organic Chemistry II, Faculty of Science and Technology, University of the Basque Country (UPV/EHU))

List of Abbreviations and Acronyms

ACN	Acetonitrile
AMF	Ammonium formate
ATP	Adenosine triphosphate
BSA	Bovine Serum Albumin
CH₃I	Iodomethane
CH₃OH	Methanol
CT	Computed Tomography
EC	Electron Capture
FDG	2-deoxy-2-[¹⁸ F]fluoro-D-glucose
GEM	Genetically Engineered Models
HPLC	High Performance Liquid Chromatography
HRP	Horseradish peroxidase
LOR	Line of Response
MIP	Maximum Intensity Projections
MRI	Magnetic Resonance Imaging
NADPH	Nicotinamide adenine dinucleotide phosphate
NADH	Nicotinamide adenine dinucleotide
NaOH	Sodium Hydroxide
PC	Prostate Cancer
PIN	Prostatic Intraepithelial Neoplasm
PET	Positron Emission Tomography
PTC	Phase transfer catalyst
PTEN	Phosphate and tensin homolog deletion
RCY	Radiochemical Yield
SPECT	Single Photon Emission Tomography

SUV	Standardized Uptake Value
TAC	Time Activity Curve
TCA	Tricarboxylic acid cycle
t_{1/2}	Half-life time
VOI	Volume of Interest

Table of Contents

SUMMARY	i
RESUMEN	iv
Chapter 1. General Introduction.....	1
1.1 Prostate carcinoma	1
1.1.1 Animal models of prostate cancer	1
1.1.2 Cancer cell metabolism	3
1.2 Molecular Imaging	4
1.2.1 General aspects	4
1.2.2 Nuclear imaging techniques	5
1.2.3 PET (Positron emission tomography) General aspects.....	6
1.2.4 PET radionuclides – General aspects.....	8
1.2.5 PET radionuclides – Production.....	11
1.2.6 PET radionuclides - Radiochemistry	13
1.2.7 PET Imaging study	18
1.3 Radiolabelled amino acids	20
1.3.1 Radiolabelling by synthetic pathways	21
1.3.2 Radiolabelling by biocatalytic pathways	25
1.4 D-amino acids	32
1.5 Imaging prostate cancer	33
1.5.1 PSMA Imaging	34
1.6 References	35
Chapter 2. Motivation and objectives of the thesis	47
2.1 Justification of the study, hypothesis and objectives	47
2.2 Objectives	49
Chapter 3. Radiolabelled alanine.....	53
3.1 Introduction.....	53
3.2 Objectives	55

3.3 Materials and methods	56
3.3.1 Reagents.....	56
3.3.2 Synthesis of phase transfer catalyst 2 (PTC-2)	56
3.3.4 Animal experimentation	59
3.3.5 Image quantification	60
3.3.6 Alanine dehydrogenase enzyme production	61
3.3.7 Determination of the protein concentration	61
3.3.8 Determination of enzyme activity.....	62
3.3.9 Enzymatic synthesis of L-[¹³ N]alanine	62
3.4 Results and discussion	63
3.4.1 Synthesis of L-[<i>methyl</i> - ¹¹ C]alanine and D-[<i>methyl</i> - ¹¹ C]alanine	63
3.4.2 Automatization	67
3.4.3 Radio-Enzymatic synthesis of L-[¹³ N]alanine.....	70
3.4.4 Whole body dynamic <i>in vivo</i> PET studies.....	73
3.4.5 Prostate-specific Pten deletion cancer model: <i>ex vivo</i> studies.....	80
3.4.6 Histological analysis	81
3.5 Summary and conclusions.....	85
3.6 References	85
Chapter 4. Radiolabelled Glutamine	89
4.1 Introduction.....	89
4.2 Objectives	92
4.3 Materials and methods	92
4.3.1 Reagents.....	92
4.3.2 Enzyme production	93
4.3.3 Determination of the protein concentration	94
4.3.4 Determination of enzyme activity.....	94
4.3.5 Synthesis of L-glutamine	96
4.3.6 Synthesis of L-[¹³ N]glutamine	97
4.3.6 HPLC and radio-HPLC analysis.....	97

4.4	Results and discussion	98
4.4.1	Multi-enzymatic system under non-radioactive conditions.....	98
4.4.2	Multi-enzymatic system under radioactive conditions	104
4.4.3	Separated synthesis of 2-oxoglutaramate.....	108
4.4.4	Enzymatic synthesis starting from cyclic LiOGA	110
4.4.5	Future perspectives	116
4.5	Summary and conclusions	118
4.6	References	119
	Chapter 5. General conclusions	123
	ACKNOWLEDGEMENTS	127

SUMMARY

Prostate carcinoma is one of the most common cancer-related causes of death worldwide. Human prostate cancer begins with a primary tumour formation, that sometimes develops in metastasis, leading to a poor patient's prognosis. Because of that, the study of this disease in an animal model which mimics the disease in humans is paramount to elucidate pathophysiological aspects of the disease and develop diagnostic and therapeutic tools. Within that context, "La Caixa" Foundation funded a project to study prostate cancer progression. The aim of the project was to investigate molecular markers which provide cancer cells with metastatic capacity, and to exploit them to develop imaging biomarkers. This thesis, which is part of that project, was developed in a collaborative effort between the Cancer Cell Signaling and Metabolism Laboratory led by Prof. Arkaitz Carracedo (CIC bioGUNE, Bilbao, Spain), and the Radiochemistry and Nuclear Imaging Group (led by Dr. Llop) and the Heterogeneous Biocatalysis Laboratory (led by Prof. López-Gallego) both in CIC biomaGUNE (San Sebastian, Spain).

The main objective of this thesis was the development of radiolabelled amino acids, to use them as imaging probes in Positron Emission Tomography (PET) in a mice prostate cancer model. Together with other imaging modalities, PET has gained notable attention during the last years. It constitutes the most sensitive nuclear imaging technique and relies on the administration of short-lived positron emitter-labelled molecules. The location of the labelled molecule can be quantitatively monitored as a function of time, providing valuable information at the molecular level of different biological and physiological processes within living organisms.

To achieve the general objective mentioned above, two major milestones were defined: (i) to develop new strategies to produce radiolabelled amino acids in high yields and

Summary

purity to use them as PET probes; and (ii) to investigate labelled amino acids using *in vivo* imaging in a mouse prostate cancer model.

The experimental work included in this PhD thesis has been divided in two chapters. **Chapter 3** covers all the work related to the amino acid alanine. First, strategies for the preparation of L-[*methyl*-¹¹C]alanine and D-[*methyl*-¹¹C]alanine using a chemical route, and for the preparation of L-[¹³N]alanine following an improved biocatalytic strategy, were developed. Both synthetic strategies resulted in radiochemically pure, ready to inject compounds. The *in vivo* biodistribution of the three labelled amino acids was investigated in a mouse model of prostate cancer using PET imaging. Complementary techniques, such as *ex vivo* imaging and histological analysis, were applied to corroborate *in vivo* results. The *in vivo* studies showed that the three labelled species have different biodistribution profiles, with highest uptake in the prostate observed for D-[*methyl*-¹¹C]alanine, as demonstrated by *in vivo* imaging and corroborated by *ex vivo* imaging. Histological analysis proved the presence of malignant tissue.

Chapter 4 covers all the work related to the amino acid glutamine. First, a multi-enzymatic system for the preparation of L-[¹³N]glutamine was assayed. The reaction conditions were initially assayed under non-radioactive conditions. First attempts focused on the stereoisomeric inversion from D-glutamine to L-glutamine. Although the formation of the L-amino acid could be detected, translation into radioactive conditions did not yield the labelled amino acid, probably due to the low concentration of the labelling agent ([¹³N]NH₄OH), and the equilibrium between the linear and cyclic forms of the reaction intermediate, oxoglutaramate (OGA), which results in a very low concentration of the linear form (this being the substrate for the second enzymatic reaction). In view of these results, OGA was prepared using a chemical route, in order to enable the preparation of L-[¹³N]glutamine using a mono-enzymatic reaction. Increasing the concentration of OGA and the enzyme (glutamate dehydrogenase) enabled the preparation of the labelled amino acid, although radiochemical yields were low (20% chromatographic yield) and long reaction times were applied (60 min). These long

Summary

reaction times are incompatible with the short half-life of the radionuclide. Hence, although our works seeds the basis for the preparation of L-[¹³N]glutamine using biocatalytic reactions, further development and refinement of the experimental conditions is required in future works.

RESUMEN

El carcinoma de próstata es una de las principales causas de muerte por cáncer en todo el mundo. El cáncer de próstata humano frecuentemente comienza con la formación de un tumor primario, el cual en algunos casos puede acabar generando metástasis, lo que se traduce en un mal pronóstico para el paciente. Por ello, el estudio de esta enfermedad en un modelo animal que mimetice a la perfección el desarrollo de la enfermedad en humanos se convierte en un tema de interés en la comunidad científica. En este contexto, la fundación “La Caixa” financió un proyecto para estudiar la progresión de este tipo de cáncer. El objetivo de este proyecto era investigar los marcadores moleculares directamente relacionados con la capacidad metastática celular, para aprovecharlos como sondas de imagen e identificar así las células metastáticas. Esta tesis forma parte de este proyecto, y requiere de un enfoque multidisciplinar. Por ello, ha sido llevada a cabo en colaboración con el grupo de Señalización y Metabolismo de Células Cancerosas dirigido por el Prof. Arkaitz Carracedo (CIC bioGUNE, Bilbao, España), el grupo de Radioquímica e Imagen Molecular dirigido por el Dr. Llop y el grupo de Biocatálisis Heterogénea dirigido por el Prof. López-Gallego (ambos en CIC biomaGUNE, San Sebastián, España).

El principal objetivo de esta tesis fue el desarrollo de aminoácidos radiomarcados, para utilizarlos como sondas en Tomografía por Emisión de Positrones (PET, de sus siglas en inglés) en un modelo animal de cáncer de próstata.

Entre otras técnicas de imagen, la Tomografía por Emisión de Positrones ha adquirido gran relevancia durante los últimos años, ya que es capaz de proporcionar datos de gran valor para la identificación de moléculas en organismos vivos. Se trata de la técnica de imagen nuclear más sensible, y se basa en la administración de radiotrazadores marcados con isótopos emisores de positrones, obteniendo así imágenes

tridimensionales de los procesos biológicos y fisiológicos que suceden en el interior de los organismos vivos.

En este contexto, esta tesis tiene dos objetivos principales: (i) el desarrollo de nuevas estrategias para producir aminoácidos radiomarcados, con rendimiento suficiente para poder ser utilizados como sondas PET; y (ii) llevar a cabo el estudio de imagen *in vivo* y *ex vivo* de estos radiotrazadores en un modelo animal de cáncer de próstata, así como complementar estos resultados con análisis histológico.

Por ello, el trabajo llevado a cabo en esta tesis se ha dividido en dos partes principales, que se corresponden así con los dos capítulos experimentales. El **capítulo 3** recoge todo el trabajo experimental llevado a cabo en relación al aminoácido alanina. En primer lugar, se han desarrollado estrategias sintéticas para la preparación de L-[*metil*-¹¹C]alanina, D-[*metil*-¹¹C]alanina y L-[¹³N]alanina.

En el caso de la síntesis con carbono-11 se ha seguido una ruta sintética basada en la catálisis por transferencia de fase. Como agente para el radiomarcaje, se ha utilizado yoduro de metilo marcado con carbono-11 ([¹¹C]CH₃I). Esta ruta está basada en la alquilación asimétrica de una base de Schiff derivada de glicina, y su posterior desprotección. De esta forma, según el catalizador utilizado, la metilación se produce de forma que el aminoácido mayoritario obtenido es L- o D- (Figura 1, A). Siguiendo este proceso, ha sido posible obtener ambos radiotrazadores marcados con carbono-11 con un rendimiento radioquímico (no corregido por decaimiento) de 10.2±1.2% y 10.3±1.1% para las formas L-y D- respectivamente, una pureza radioquímica >99% y una pureza enantiomérica del 90%, en ambos casos.

En el caso de la síntesis de alanina marcada con nitrógeno-13, se ha elegido una estrategia sintética diferente, esta vez, basada en la biocatálisis. Para ello, se ha seguido una ruta previamente descrita por nuestro laboratorio, pero con modificaciones que la han mejorado. Esta ruta se basa en la utilización de la enzima Alanina deshidrogenasa, como biocatalizador, para producir la aminación reductiva de piruvato y, gracias al uso de amonio radiomarcado como agente de radiomarcaje ([¹³N]NH₄OH), producir alanina

radiomarcada con nitrógeno-13 (Figura 1, B). Ha sido obtenida con un rendimiento radioquímico (corregido por decaimiento) del $40.3 \pm 2.1\%$.

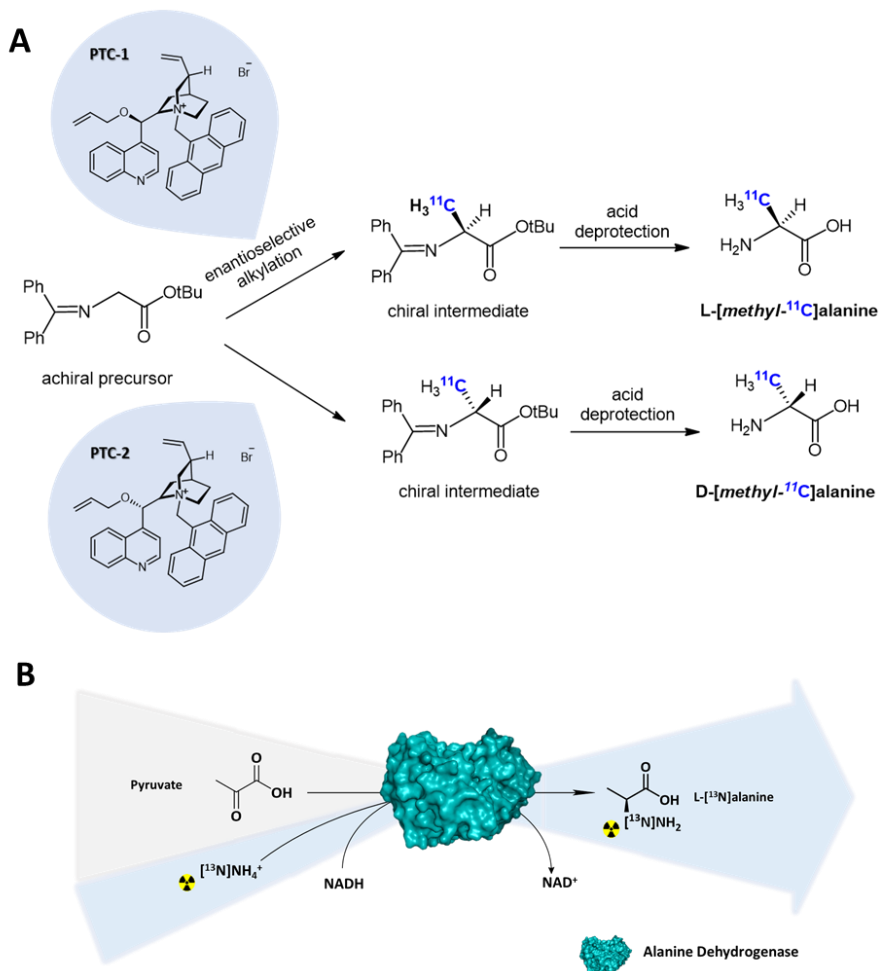


Figura 1. A) Ruta sintética para la radiosíntesis enantioselectiva de L- y D-[*metil*-¹¹C]alanina basada en una alquilación asimétrica de una base de Schiff derivada de glicina con yoduro de metilo radiomarcado [¹¹C]CH₃I como agente alquilante. B) Síntesis radio-enzimática de L-[¹³N]alanina partiendo de piruvato y utilizando [¹³N]NH₄OH como fuente de amonio y NADH como cofactor enzimático.

Una vez finalizada la producción de los tres radiotrazadores, se llevó a cabo el estudio de imagen por PET en el modelo de cáncer de próstata en ratones. El estudio de su biodistribución *in vivo*, mostró diferentes resultados para ambos trazadores (Figura 2, A). Además, fue posible la visualización de alanina radiomarcada con carbono-11 en la próstata de los animales (Figura 2, B), así como de su cuantificación de forma diferencial de la vejiga, como se observa en las curvas de actividad-tiempo correspondientes a los volúmenes de interés (VOIs) definidos en próstata y vejiga (Figura 2, C).

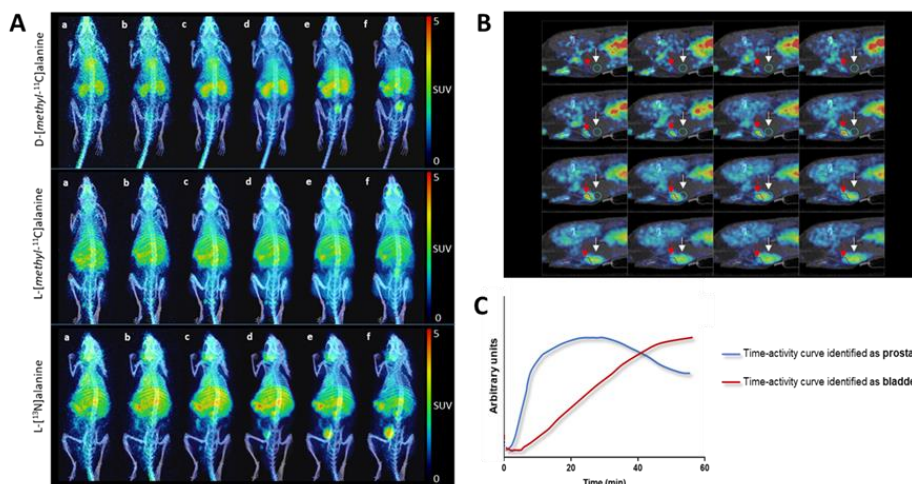


Figura 2. A) Imágenes PET (proyecciones coronales) corregistradas con sus correspondientes CT para localizar la señal radiactiva obtenida a diferentes tiempos, tras la administración intravenosa de los tres aminoácidos radiomarcados. Las imágenes son proyecciones de máxima intensidad (MIP por sus siglas en inglés) expresadas como valores estándar de absorción (SUV, por sus siglas en inglés). B) Proyecciones sagitales del estudio PET *in vivo* en el que se puede observar la captación de la próstata (flecha roja) y la captación de la vejiga (flecha blanca). C) Curvas de actividad-tiempo en los volúmenes de interés dibujados en la próstata (línea azul) y la vejiga (línea roja).

De hecho, se pudo observar una acumulación superior en las próstatas de los animales inyectados con D-[*metil*-¹¹C]alanina, en comparación de las próstatas de los animales inyectados con L-[*metil*-¹¹C]alanina, demostrando así que las células cancerosas pueden

presentar una captación superior de D-aminoácidos. Estos resultados se confirmaron realizando un estudio *ex vivo* por imagen PET de las próstatas todavía radioactivas. Además, la naturaleza del tejido de las próstatas se analizó utilizando técnicas histológicas, que confirmaron así la malignidad del tejido.

Por otra parte, el **capítulo 4** recoge todo el trabajo relacionado con el aminoácido glutamina, incluyendo el proceso biocatalítico y de radiomarcaje que ha sido necesario para su producción como L-[¹³N]glutamina. En primer lugar, se diseñó un sistema multi-enzimático capaz de producir la estereoinversión de D-glutamina en L-glutamina en condiciones no radioactivas (Figura 3).

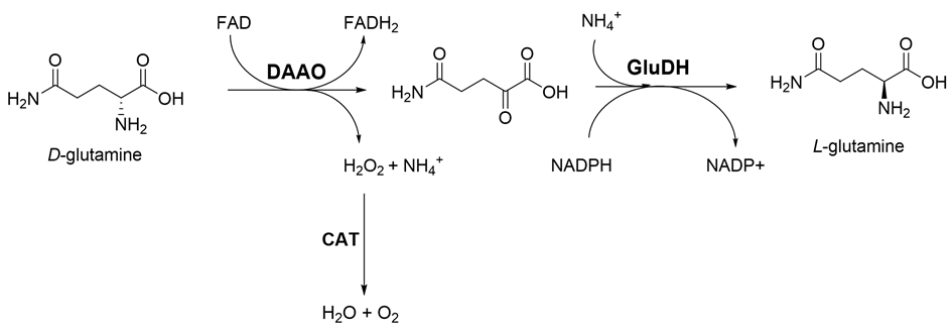


Figura 3. Sistema multi-enzimático capaz de producir la estereoinversión de D-glutamina en L-glutamina, compuesto por D-amino ácido oxidasa (DAAO), Catalasa (CAT) y Glutamato deshidrogenasa (GluDH).

El sistema consiste en dos pasos: El primero es la producción del ceto-ácido de glutamina, también conocido como ácido oxoglutarámico (OGA) utilizando la combinación enzimática DAAO/CAT (D-aminoácido oxidasa/Catalasa); el segundo consiste en la aminación reductiva de este cetoácido por la enzima GluDH (Glutamato Deshidrogenasa).

Después de encontrar unas condiciones óptimas en las que se obtuvo un rendimiento del 30% de conversión, se probó el sistema utilizando condiciones radioactivas. Para ello, se eligió amonio radioactivo como agente de radiomarcaje ($[^{13}\text{N}]\text{NH}_4\text{OH}$). Sin embargo, la traslación de las condiciones al entorno radioquímico no es siempre directa, ya que las condiciones de reacción se ven alteradas. De hecho, no pudo observarse la formación de L- $[^{13}\text{N}]$ glutamina utilizando el sistema multienzimático, muy probablemente debido a la baja concentración del $[^{13}\text{N}]\text{NH}_4\text{OH}$, así como al equilibrio entre las formas lineal y cíclica del compuesto OGA, que conlleva a una concentración baja de la forma lineal (sustrato de la segunda reacción enzimática). En vista de los resultados, se llevaron a cabo diferentes modificaciones del sistema. Una de las principales modificaciones fue la producción sintética del cetoácido (OGA), eliminando así el primer paso enzimático y simplificando el método al uso de una única enzima (GluDH). Mediante utilización de OGA sintetizada mediante métodos químicos (lo cual permitió aumentar su concentración de manera significativa) y el aumento de concentración de la enzima glutamato deshidrogenasa, pudo llevarse a cabo la producción del aminoácido marcado deseado (Figura 4).

Para analizar los productos de reacción, se eligió la derivatización de Marfey como método analítico, para así poder seguir la reacción mediante cromatografía líquida de alta resolución (HPLC, de sus siglas en inglés). Este método de derivatización de aminoácidos encaja perfectamente con las necesidades del estudio, ya que permite la diferenciación entre aminoácidos y enantiómeros. Los resultados de HPLC mostraron la presencia de L- $[^{13}\text{N}]$ glutamina con un rendimiento cromatográfico radioactivo del 20% (Figura 4, B). El bajo rendimiento y el tiempo de reacción largo que fue necesario emplear (60 minutos) impiden la utilización del aminoácido en estudios in vivo. Así pues, si bien el trabajo descrito supone la apertura de una nueva ruta biosintética para la síntesis de L-glutamina radiomarcada con nitrógeno-13, es necesario llevar a cabo una optimización de las condiciones experimentales en trabajos futuros.

Resumen

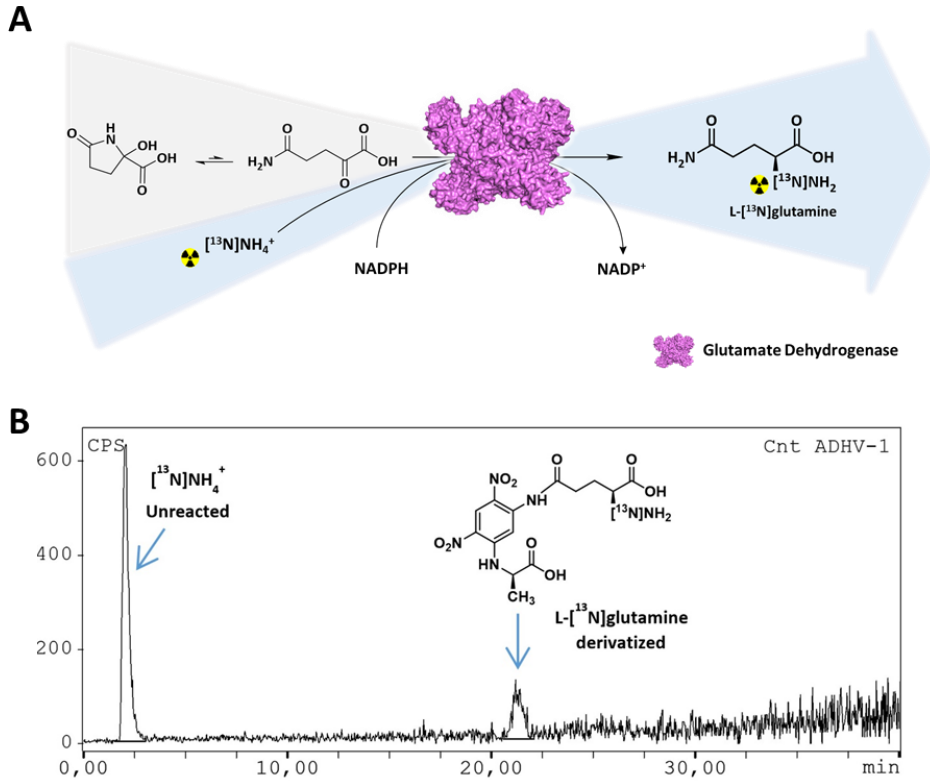


Figura 4. A) Radiomarcaje enzimático de L-[¹³N]glutamina, partiendo del cetoácido (ácido oxoglutarámico, LiOGA) en su forma de hidroxilactama y [¹³N]NH₄OH como agente de radiomarcaje. B) radio-HPLC correspondiente a la derivatización de Marfey tras la reacción enzimática para la producción de L-[¹³N]glutamina, con un rendimiento cromatográfico del 20%.

CHAPTER 1

General Introduction

Chapter 1. General Introduction

1.1 Prostate carcinoma

Prostate carcinoma is the most common visceral tumour in males and one of the most common cancer-related causes of death. There were an estimated 1.4 million new prostate cancer cases and 375.000 prostate cancer deaths worldwide in 2020¹. Human prostate cancer begins with a primary tumour formation. It sometimes results in metastasis and cell growth in secondary tissue sites, associated with poor prognosis.

1.1.1 Animal models of prostate cancer

Although prostate cancer typically shows slow progression, only few animal models are able to mimic its progression in detail to study tumorigenesis and to develop an effective treatments². This lack of relevant preclinical models to study the tumour progression is a key point in the establishment of good prevention and therapeutic strategies. The incomplete understanding of the human prostate cancer biology has hampered the development of relevant model systems that can faithfully mimic the human disease.

Preclinical models of prostate cancer currently available are obtained from mouse, rat, canine and human sources. They can be classified in two broad groups, those created from prostate cancer cell lines and those that are genetically engineered models (GEM) (Table 1.1).

Genetically engineered models reproduce the tumour conditions associated to the human disease^{3,4,5}. These GEM models are divided into two main groups, those created by overexpression of an oncogene with a prostate specific promoter and those with targeted deletion of specific genes. One of the best characterized models based on the disruption or overexpression of a gen, is the model that produces the loss of the tumour suppressor gene PTEN (Phosphate and tensin homolog deleted on chromosome 10)^{6,7,8}.

Chapter 1. General introduction

Table 1.1 Examples of most used prostate cancer preclinical models.

PROSTATE CANCER PRECLINICAL MODELS	FROM CELL LINES	SPECIES	MODEL	SOURCE
		Canine	Ace-1	Cell line from primary adenocarcinoma.
		Rat	Dunning	Spontaneous from primary adenocarcinoma.
		Human (top 3)	PC-3	Cell line from bone metastasis.
	DU145		Cell line from dural metastasis.	
	LNCaP		Cell line from lymph node metastasis.	
	GEM (Genetically Engineered Models)	<u>By overexpression of an oncogen</u>	TRAMP (Transgenic mouse model of Prostate)	Results in the development of prostate cancer which mimics the human prostate cancer histopathology.
<u>By deletion of specific genes</u>		PTEN (Phosphate and tensin homolog deletion)	Results in invasive prostate cancer that metastasizes.	

Functional loss of tumour suppressor PTEN is thought to be present in more than 40 % of metastatic prostate cancers. In consequence, PTEN loss is associated with advanced stages of the disease and poor outcome^{9,10}. Having an orthotopic prostate cancer model based on the conditional deletion of the tumour suppressor PTEN offers a great opportunity to mimic the disease in humans. Contrary to the common heterotopic cancer models, this PTEN deletion model results in hyperproliferative lesions which culminate in prostate cancer within 6 months of age. In spite of the advantages of orthotopic models, it is important to consider the morphological differences between prostates in mice in comparison with human prostates (Figure 1.1).

Mouse prostate presents a lobular structure composed of four lobes (anterior, ventral, dorsal and lateral) whereas human prostate has one lobe divided into three zones (central, transitional and peripheral). Despite the obvious inter-species differences, mice are, similarly to humans, vulnerable to cancer. Additionally, they are the most widely used and experimentally accessible mammalian model, thus representing a powerful experimental tool for understanding the complexity of human cancer pathogenesis¹¹

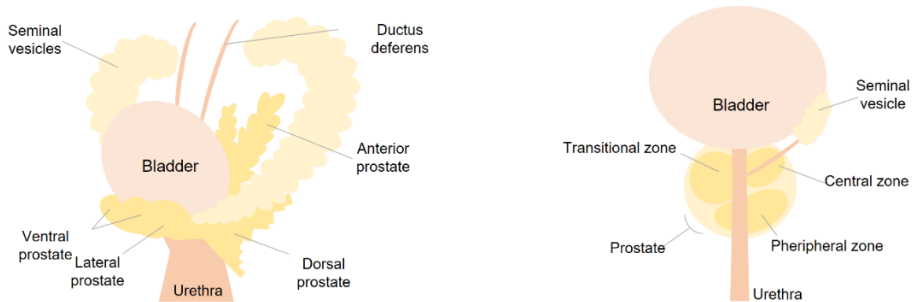


Figure 1.1 Schematic illustration of the anatomy of the mouse (left) and human (right) prostate, showing its position regarding bladder and urethra.

1.1.2 Cancer cell metabolism

A remarkably different metabolism is found in tumour cells in comparison with a normal differentiated cell. Tumour cells take up high levels of nutrients such as glucose and amino acids to support their anabolic growth¹². This aberrant cellular metabolism present in cancer cells was first described by Otto Warburg, who demonstrated the anaerobic use of glucose in the presence of oxygen¹³. This so-called Warburg effect occurs in many cancer cells, but it is not predominant in prostate cancer (PC) cells, which are often not glycolytic. Prostate cancer cells show altered fatty acid and amino acid metabolism. Fatty acid metabolism comprehend *de novo* lipid biosynthesis, β -oxidation and oxidative phosphorylation¹⁴, membrane synthesis and post-translational modification of signalling molecules¹⁵.

Also, amino acid transport is usually increased in malignant transformation. Concerning amino acids metabolism, a high rate of glutamine consumption is exhibited by transformed cells. Glutaminolysis (conversion of glutamine to lactate) produces NADPH to support fatty acid synthesis and also, α -ketoglutarate derived from glutamine metabolism enters tricarboxylic acid (TCA) cycle to produce energy in the form of cellular adenosine triphosphate (ATP)^{16,17}.

Chapter 1. General introduction

The Warburg effect established the basis of the broad clinical use of fluorodeoxyglucose ($[^{18}\text{F}]\text{FDG}$) in positron emission tomography (PET) to identify primary and metastatic tumours¹⁸. The importance of $[^{18}\text{F}]\text{FDG}$ in the clinic is undeniable. It is used in many types of cancer, for tumour diagnosis, staging, restaging, radiation therapy planning and treatment monitoring. Because of that, PET oncologic imaging has gained notable attention during the last decades, to identify new and effective therapies and to understand the role of some molecular biomarkers¹⁹.

In spite of its wide applicability, $[^{18}\text{F}]\text{FDG}$ cannot be applied to all cancer types, *e.g.* when the tumour is located in a tissue with high glucose consumption (such as the brain), or when there is inflammation, or in the vicinity of regions with high accumulation of the tracer due to elimination. One clear example of the latter is prostate cancer, as the prostate is located close to the bladder and $[^{18}\text{F}]\text{FDG}$ is mainly eliminated via urine. In these cases, other radiotracers may offer significant advantages over $[^{18}\text{F}]\text{FDG}$. Among these, amino acids are less influenced by inflammation and may show higher selectivity in regions with high basal $[^{18}\text{F}]\text{FDG}$ uptake. Based on this narrative, radiolabelled amino acids have become an attractive family of compounds to be used as PET radiotracers²⁰. To label natural and unnatural amino acids ^{11}C ($t_{1/2}=20.4$ min), ^{13}N ($t_{1/2}= 9.96$ min), ^{18}F ($t_{1/2}=109.65$ min) and ^{124}I ($t_{1/2}=4.2$ d) are frequently used as PET radionuclides²¹.

1.2 Molecular Imaging

1.2.1 General aspects

The term molecular imaging comprises a group of non-invasive techniques that allow the monitoring of molecular processes in living organisms. Several biological, physiological, and medical processes can be investigated in clinical and preclinical studies by using these techniques. Positron emission tomography (PET), single photon emission computerized tomography (SPECT), optical/fluorescence imaging, magnetic

Chapter 1. General introduction

resonance imaging (MRI) and computed tomography (CT) are considered molecular imaging techniques (Table 1.2).

Table 1.2 Properties of most common clinical and preclinical imaging modalities.

Modality	Energy used	Common contrast agents	Penetration depth	Temporal resolution	Spatial resolution	Sensitivity of detection
CT	X rays	I or Ba agents	>300 mm	Minutes	0.03-1 mm	0.1mol.l ⁻¹
MRI	Radiofrequency waves	Gd ⁺³ agents	>300 mm	Minutes-hours	0.03-1 mm	10 ⁻⁵ mol.l ⁻¹
PET	Annihilation photons	β ⁺ emitters	>300 mm	Seconds-Minutes	1-10 mm	10 ⁻¹² mol.l ⁻¹
SPECT	γ rays	γ emitters	>300 mm	Minutes	0.5-15 mm	10 ⁻¹¹ mol.l ⁻¹
Optical	Light (visible to infrared)	Fluorophores or lanthanides	1-20 mm	Seconds-Minutes	2-10 mm	10 ⁻¹¹ mol.l ⁻¹

The combination of these techniques (multimodality) can provide anatomical, functional, and molecular information.

1.2.2 Nuclear imaging techniques

Nuclear imaging techniques include positron emission tomography (PET) and single photon emission computerized tomography (SPECT). Both techniques are highly sensitive and minimally invasive and rely on the administration of a molecule or material previously labelled with a radionuclide. This radionuclide will spontaneously decay into a more stable atom, resulting in the emission of positrons or gamma rays. When positrons are emitted, the annihilation process ultimately results in the formation of gamma rays (see below for more detailed explanation). Gamma rays, which are highly energetic photons, escape from the organism and can be detected in a way that the concentration of the radiolabelled compound can be determined. As far as the radioisotope remains bound to the molecule, its biodistribution inside a living organism can be measured.

Nuclear imaging techniques only provide molecular information, this is, the concentration of the labelled specie over time. They are usually combined with CT or MRI to obtain anatomical information.

This PhD thesis is focused on PET imaging. Because of this, a brief introduction to the basic principles of the technique and the main positron emitters currently used both in the clinical and preclinical settings is provided below.

1.2.3 PET (Positron emission tomography) - General aspects

Positron emission tomography is based on the emission of a positron (β^+), the electron antiparticle with same mass but opposite charge, from a radionuclide. PET imaging starts with the administration of a positron emitter-labelled radiotracer to a living organism. The spontaneous decay of the positron emitter results in the emission of positrons, which after being emitted, travel a few millimetres while losing their kinetic energy. When the positron is almost at rest, it interacts with its antiparticle (one electron) from the surroundings and annihilates. The annihilation results in the emission of a pair of highly energetic gamma rays (511 keV each) with opposite directions²². The PET scanner has a series of detectors arranged in a circular ring, that detect the two gamma rays (Figure 1.2).

When two detectors detect a gamma ray simultaneously, this is considered by the imaging system as a coincidence event, which means that the annihilation occurred somewhere in the line between the two detectors (so called “line of response” or LOR). The detection of hundreds of thousands of coincident events allows the reconstruction of an image which provides information about the concentration of the labelled specie within the organism.

As mentioned above, PET cannot provide anatomical information. Because of this, PET imaging is usually combined with CT, which provides detailed anatomical images to unambiguously located the radioactive signal^{23,24}. Additionally, CT images are used to

generate the attenuation map of the subject investigated, in order to correct the PET images during the reconstruction process.

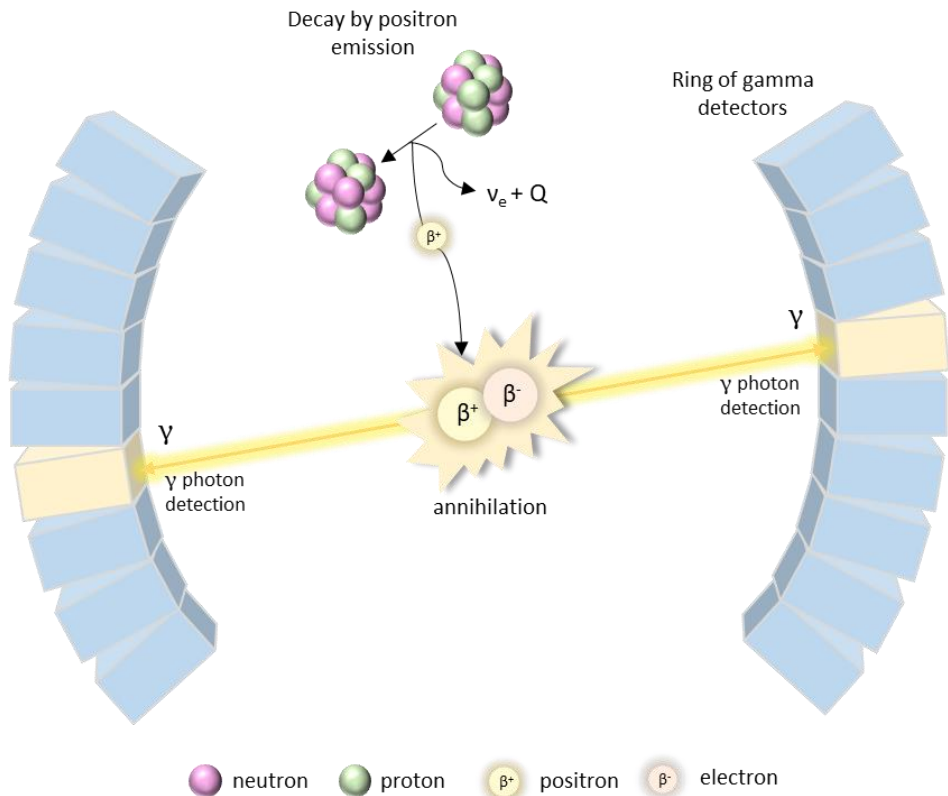


Figure 1.2 Schematic representation of the principle behind PET, radioactive decay by positron emission and its annihilation and detection of the two gamma rays. A positron is emitted and after travelling a certain distance (positron range) it annihilates with an electron, forming 2 photons (511 keV each), that are emitted in opposite directions and detected as coincidence events by special detectors. β^+ = positron, β^- = electron, ν_e = neutrino, γ = gamma ray, Q describes the energy of the decay and the difference of the mass of the transformation ($E = mc^2$).

Chapter 1. General introduction

1.2.4 PET radionuclides - General aspects

There are many positron emitters. However, because of their physicochemical properties, only a few of them are routinely used in preclinical and clinical studies (Table 1.3).

Table 1.3 The most employed PET isotopes with their half-life, maximum energy, and production method.

Isotope	Half-life	β^+ Energy _{max} [MeV]*	Production method
¹⁵ O	2.03 min	1.73	¹⁴ N(d,n) ¹⁵ O ¹⁵ N(p,n) ¹⁵ O
¹³ N	9.96 min	1.19	¹² C(d,n) ¹³ N ¹⁶ O(p, α) ¹³ N
¹¹ C	20.40 min	0.96	¹⁰ B(d,n) ¹¹ C ¹⁴ N(p, α) ¹¹ C
¹⁸ F	109.65 min	0.63	¹⁸ O(p,n) ¹⁸ F
⁶⁸ Ga	67.71 min	1.90	⁶⁸ Ge/ ⁶⁸ Ga-Generator
⁶⁴ Cu	12.70 h	0.65	⁶⁴ Ni(p,n) ⁶⁴ Cu ⁶⁴ Ni(d,2n) ⁶⁴ Cu
⁸⁹ Zr	78.41 h	0.90	⁸⁹ Y(p,n) ⁸⁹ Zr

*Positrons are not emitted with a unique energy. Radionuclides emit positrons with different energies, which follow a Poisson distribution. The maximum value of this distribution is presented in this table.

One important characteristic of the radionuclides is the half-life. The radioisotope half-life is defined as the time required for a quantity of radioactivity to decrease to one half of the starting value. Half-life values for PET radionuclides typically used in biomedical applications range from few minutes to few days. The selection of a radionuclide with an appropriate half-life is paramount to guarantee successful *in vivo* studies. Mainly, the

physical half-life of the selected radionuclide should match the biological half-life of the molecule to be investigated. If the half-life is too short, only partial information about the pharmacokinetics will be obtained, because the radionuclide will completely decay before the compound is eliminated from the organism. Contrarily, if the half-life is too long, the subject under investigation will receive a high (and unnecessary) radiation dose. The latter is especially relevant for clinical studies and when repeated administration is required. The radionuclide half-life is closely related with its availability, that is another critical aspect. The use of radionuclides with relatively long half-life (e.g. ^{18}F) enables the centralized production of the radiotracer and distribution to end users. But when positron emitters with shorter half-lives are used, they require *in situ* production, which is carried out using particle accelerators. The infrastructure required to produce positron emitters and the subsequent preparation of the radiotracers has a huge cost and requires trained personnel. This has historically limited the consolidation of PET imaging, particularly at the preclinical level and in the process of drug development.

Another relevant aspect of positron emitters is the positron range. The line of response (LOR) identifies the positron where the annihilation occurred, and not the position in which the positron is emitted. The positron range, defined as the linear distance between the points where the disintegration and the annihilation occur, is proportional to the energy of the emitted positron (which is an intrinsic property of the radionuclide) and the media. Positrons which are emitted with high-energy, result in a high positron range, and vice-versa. The image resolution is negatively affected by the positron range: the larger the positron range, the lower the spatial resolution that can be achieved. Nevertheless, latest devices are able to statistically correct for this effect to a certain extent, and the resolution of modern PET scanners is close to (or even below) the positron range²⁵. Positron emitters that are typically used in nuclear medicine present positron ranges ranging from a few mm to a few cm in water.

Chapter 1. General introduction

Besides the decay via positron emission, another relevant way for proton-rich nuclei to stabilize is to decay via electron capture (EC; Figure 1.3). Electron capture consists of the electron absorption from a proton in the nucleus. This proton is converted into a neutron with the emission of a neutrino. The generated daughter nuclide is in an excited state and will release excitement via x-ray or Auger electrons. Differently to the β^+ decay, where the released energy is split between the positron and the neutrino, which leads to a continuous energy spectrum, here the entire energy is carried by the neutrino and gives a single sharp energy profile. However, this decay mode does not result in the emission of a positron, and hence is not useful for PET imaging. Radionuclides need to be selected carefully: a higher percentage of β^+ decay will be preferable, as other radiation types do not contribute to image quality but increase the radiation dose to the investigated subject.

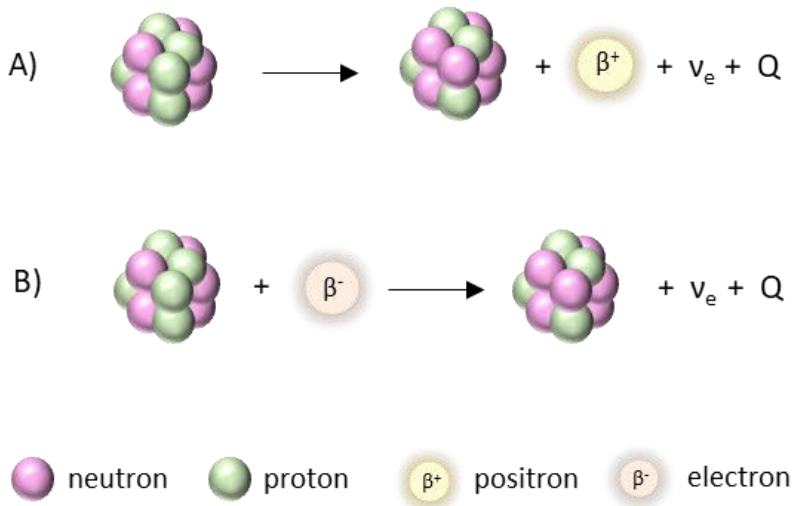


Figure 1.3. Schematic representation of the radioactive decay of a proton-rich nuclei by positron emission (A) and electron capture (B). β^+ = positron, β^- = electron, v_e = neutrino, γ = gamma ray, Q describes the energy of the decay and the difference of the mass of the transformation ($E = mc^2$)

1.2.5 PET radionuclides - Production

During the selection process of a radionuclide, availability is a key aspect. Some positron emitters can be produced in generators (*e.g.* ^{68}Ga , which is produced in commercially available $^{68}\text{Ge}/^{68}\text{Ga}$ generators) that are usually easy to handle for routine hospital work. But many others need to be produced in particle accelerators, usually cyclotrons (*e.g.* ^{15}O , ^{13}N , ^{11}C , ^{18}F , ^{64}Cu and ^{89}Zr). This production requires equipment much more complex and expensive in maintenance, consequently not widely available.

A cyclotron (Figure 1.4) is a particle accelerator in which an electric field is used to accelerate ions, such as H^+ and D^+ , guided with a magnetic field. The electric field is generated by the application of an electric potential between two electrodes (called “dees” and “counter-dees”), connected to an alternating current source. Negative ions are generated in the ion source (which is placed in the center of the cyclotron) by applying a high voltage to hydrogen or deuterium gas. When the so-called “dee” is positively charged, the “counter-dee” is negatively charged and vice versa. Then, when the “dee” is positively charged, the negative ions extracted from the ion source, are accelerated towards the “dee” by the electric field. Thanks to the presence of the magnetic field, the charged particles describe a curved trajectory. When the ion leaves the “dee”, it is accelerated again towards the “counter-dee”, because the polarity on the “dees”/“counter-dees” is reversed. This process is repeated several times, and the orbit radius becomes larger while the speed of the ion increases. The ion describes a spiral outward towards the border of the magnetic field. Then, when a certain value of radius is reached, the negative ions hit a carbon foil (named stripper) which removes the electrons. The charged ion is now positively charged, and the direction of the rotation is inverted. In consequence, the accelerated ion leaves the magnetic field and impacts in one of the targets, that are situated along the periphery of the cyclotron. The target, which is composed of a stable material, is irradiated with the high energy protons or deuterons to produce the nuclear reaction, and generate the radioisotopes (Figure 1.5).

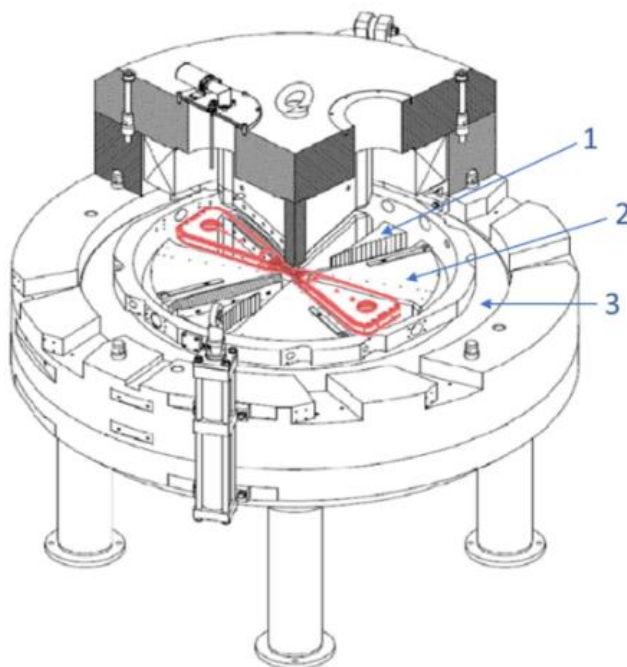


Figure 1.4 General view of the main body of an IBA Cyclone 18/9 cyclotron. Some parts (such as ion sources, strippers and targets) have been removed from the drawing for clarity. The magnetic field is created by the electrical current in the coils (3) that surround the four wedge-shaped steel sectors (2). “Dees” (drawn in red) are placed between the steel sectors, and “counter-dees” (not drawn) are placed on the edges of the four steel sectors close to the “dees”. For dual particle cyclotrons (acceleration of H- and D-), small steel sectors called flaps (1) can be introduced or removed to modulate the magnetic field when particle is changed from H- to D-. Adapted from the PhD Thesis: Gómez-Vallejo, V., Synthesis of Radiotracers Labeled with Short-Lived Isotopes: application to ^{11}C and ^{13}N . Universitat Ramon Llull, 09.07.2010)

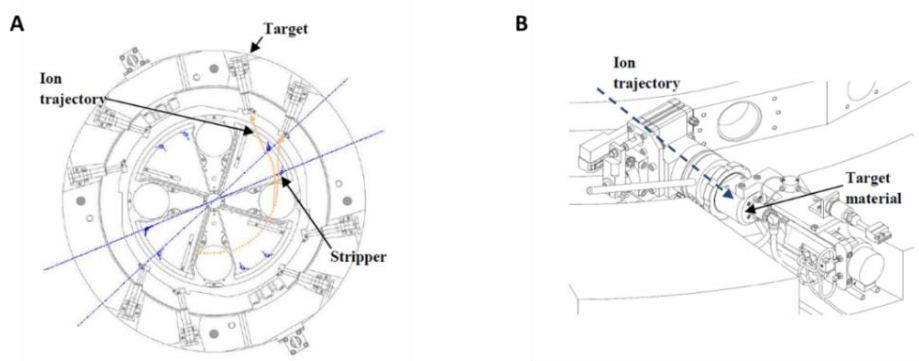


Figure 1.5 A) Negative ions accelerated until they reach a stripping foil (Stripper), then the stripper removes the electrons and the ion charge, now positive, escapes from the cyclotron and hits the selected target; B) Disposition of a target in an IBA Cyclone 18/9 cyclotron. Positive ions collision with the target material to produce the radioisotope. Adapted from the PhD Thesis: Gómez-Vallejo, V., Synthesis of Radiotracers Labeled with Short-Lived Isotopes: application to ^{11}C and ^{13}N . Universitat Ramon Llull, 09.07.2010).

1.2.6 PET radionuclides - Radiochemistry

The radioactive labelling is the chemical reaction in which a radionuclide is incorporated into the desired molecule, to produce a radiotracer. Two main strategies are used to incorporate the radionuclide into a molecule: (i) when the desired radiotracer is a small organic molecule, radiolabelling can be achieved by preparing a precursor which enables the direct incorporation of the radionuclide by a chemical reaction; and (ii) in the radiolabelling of large molecules, such as peptides, proteins, antibodies, polymers or nanoparticles, radiolabelling is usually achieved by attaching a functional group in which the radionuclide is present.

Radiochemistry work have three major considerations that need to be considered: (i) radionuclides emit ionizing radiation. This means that a protection equipment is required (*e.g.* hot cells as described below), and all processes need to be automated and conducted using remote-controlled system, avoiding personnel exposure; (ii) PET

Chapter 1. General introduction

radionuclides have a short half-life, and hence the chemical reactions must be fast and efficient, and the radiolabelling step must be at the end of the procedure; and (iii) only a few labelling agents can be produced in the cyclotron as primary species.

Radiochemistry laboratories are equipped with “hot cells”, which are basically lead-shielded versions of a classical chemical hood. The radionuclide, generated in the cyclotron, is transferred from there to the hot cell, where it is transformed into the desired radioactive chemical species after a series of reactions. Hot cells usually house computer-controlled robotic modules, which are used to track the reaction and minimise exposure to radioactivity by the user (Figure 1.6).

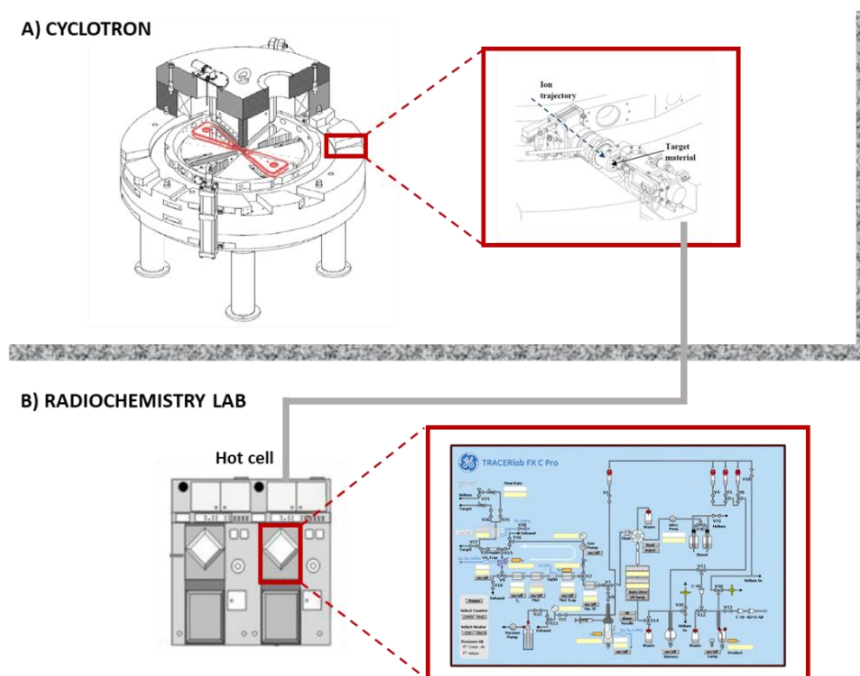


Figure 1.6 Schematic representation of the radiolabelling process. A) The positron-emitter is produced in the cyclotron by proton irradiation of the target (which will vary according to the desired radioisotope). B) The radionuclide is transferred from the cyclotron to the “Hot-cell” in the radiochemistry laboratory, where it is transformed in the derided chemical specie by computer-controlled reaction.

Radiolabelling is the first step to investigate the biodistribution of a molecule inside a living organism using nuclear imaging techniques. Radiochemists are doing a continuous effort to develop novel PET tracers. Large number of strategies to incorporate these positron and gamma emitters to provide interesting radiotracers have been developed. Regarding the half-life of the radioisotope selected for the radiosynthesis, the whole process (including synthesis, purification, and analysis) must consume no more than three half-lives, which in some cases, becomes a real challenge.

In this PhD thesis, ^{11}C and ^{13}N have been employed, as they enable the radiolabelling and *in vivo* investigation of amino acids without altering its native structure. A brief description of the production and radiochemical application of these radionuclides is included below.

Carbon - 11

Carbon-11 is considered as an optimal radionuclide. Due to the presence of carbon atoms in all organic molecules, C-11 constitutes an opportunity to produce labelled molecules without altering the chemical structure of the compound under evaluation. Moreover, carbon-11 presents a 99 % β^+ -decay, becoming a favorable PET nuclide. Thus, as explained in the Section 2.3.2, the almost absence of another competitive ways of decay (as Electron Capture) is a positive aspect, as all the radiation results in the emission of gamma rays that are detected, which means that no “useless” radiation dose is posed on the investigated subject.

However, its short half-life (20.4 min), makes its transport from manufacturing centers to surrounding hospitals not viable, thus limiting its application to facilities equipped with a cyclotron on site. Still, the half-life is long enough to enable multi-step radiosynthesis and imaging studies.

Carbon-11 is produced by proton irradiation of nitrogen gas which contains small amounts of oxygen or hydrogen via the $^{14}\text{N}(\text{p},\alpha)^{11}\text{C}$ reaction. Depending on the

Nitrogen - 13

Nitrogen-13 is also considered is a convenient radionuclide, as its presence in some organic molecules, such as amino acids, constitute an opportunity to label these molecules without altering its chemical structure. However, its short half-life (9.97min) requires its production on demand and limits its application to centers equipped with a cyclotron *on site*. Nitrogen-13 can be generated by proton irradiation of pure water via the $^{16}\text{O}(p,\alpha)^{13}\text{N}$ nuclear reaction and it will decay into carbon-13 by emission of a positron. There are several ways to produce nitrogen-13, but it is usually produced by proton irradiation of water. When water is irradiated, the major radioactive species produced are nitrate ($[^{13}\text{N}]\text{NO}_3^-$), nitrite ($[^{13}\text{N}]\text{NO}_2^-$) and ammonia ($[^{13}\text{N}]\text{NH}_3$)²⁷. The $[^{13}\text{N}]\text{NO}_3^-$ can be reduced to $[^{13}\text{N}]\text{NO}_2^-$, that can be used for the radiolabeling of a large variety of species, such as nitrosothiols, nitrosamines, azo derivatives and triazoles^{28,29,30,31,32,33}. The cyclotron-produced $[^{13}\text{N}]\text{NO}_3^-$ can also be reduced to $[^{13}\text{N}]\text{NH}_3$. Classical reduction methods consist of the treatment with Raney-nickel catalyst³⁴, titanium hydroxide or Devarda's alloy³⁵.

More commonly, $[^{13}\text{N}]\text{NH}_3$ is produced directly in the target, by just adding free radical scavengers to the irradiated solution, which prevent radiolytic oxidation of ammonia^{36,37}. By using 5 mM ethanol in water as the irradiated material, $[^{13}\text{N}]\text{NH}_3$ is produced as the major specie. It can be easily purified with a cation exchange resin and it can be directly used as perfusion marker^{38,39} or further incorporated into organic molecules, such as amino acids⁴⁰, which are the purpose of these thesis.

Based on the narrative above, in this PhD thesis, Carbon-11 and Nitrogen-13 have been selected as favorable radionuclides to produce radiolabelled amino acids.

1.2.7 PET Imaging study

Every radiotracer production and its corresponding imaging study in an animal model comprehends some basic steps, that are schematically represented in Figure 1.7.

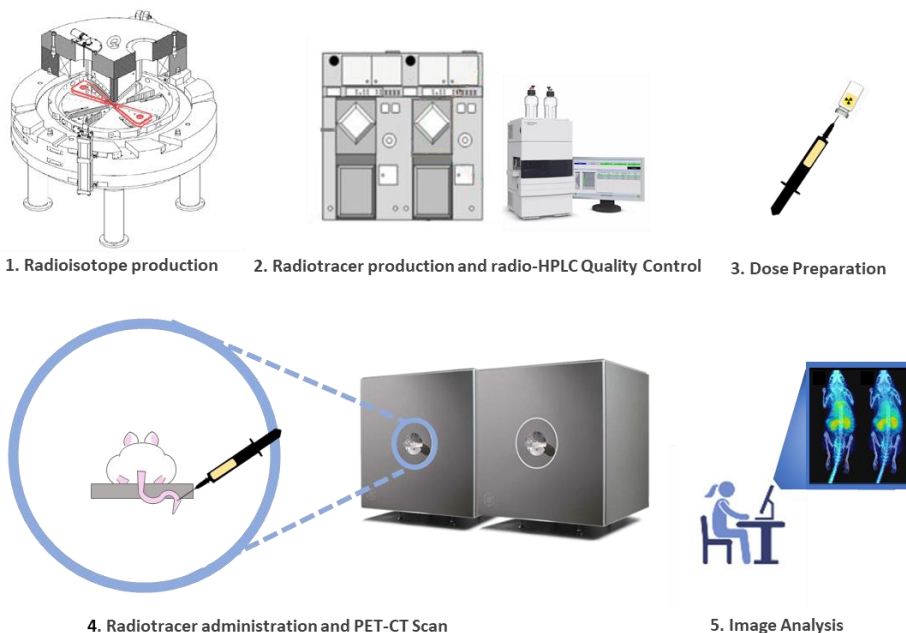


Figure 1.7 Key steps involved in a PET imaging study in chronological order from the radioisotope production in the cyclotron until the software image analysis.

As explained in section 1.2.5 the first step consists of the radioisotope production in the cyclotron; the radioisotope is then transferred to the radiochemistry laboratory (section 1.2.6) in which the synthesis of the radiotracer is carried out. After production, the radiotracer is submitted to an exhaustive quality control by analytical techniques such as high-performance liquid chromatography coupled to a radioactive detector (radio-HPLC) and gas chromatography (GC) among others. After quality control, a dose (which is prepared taking into consideration the radioisotope half-life and the specie under study) is prepared for the *in vivo* administration.

1.2.7.1 *In vivo* administration

There are a wide variety of routes of substances administration to laboratory animals⁴¹. The substance can be delivered onto, into, under or across the skin or into muscle (epicutaneous, intradermal, subcutaneous, transdermal and intramuscular administration, respectively); delivered into the mouth or directly into the stomach (orally and gastric gavage, respectively); delivered into the brain (intracerebral) or in the surrounding space from the dura mater or the distal spinal cord (epidural and intrathecal); delivered into the peritoneal cavity (intraperitoneal); delivered into the eye (transcorneal or intraocular); sprayed into the nose (intranasal) or delivered into the lungs (intratracheal); delivered into the marrow cavity (intraosseous) and delivered into a blood vessel (intravenous). In particular, the most common routes for the administration of substances to mice are subcutaneous, intraperitoneal and intravenous injection⁴². A key factor to select a route is based on whether the agent is being administered for a local or systemic effect. In this PhD thesis, intravenous administration though the tail vein has been selected as a route of delivery of radiolabelled amino acids. Intravenous administration bypasses the need for solute absorption, which is crucial when radioisotopes with short half-life are used, and it is also the best way to deliver a precise dose quickly and in a well-controlled manner throughout the body. After the administration, the corresponding animal under study is placed into the PET-CT scan to acquire the images.

1.2.7.2 Parameters in small PET scanners

In this PhD thesis, PET have been used for the *in vivo* evaluation of radiolabelled amino acids in a mouse prostate cancer model. The wide use of this technique in pre-clinical research boosts the need for the development of sophisticated small animal scanners. When a small animal PET is used, the resolution and sensitivity are critical. Due to the low body weight of small animals, the amount of radioactivity that can be injected is low. Thus, the number of events detected is considerably lower than those detected in human scans, and consequently the sensitivity is compromised. Moreover, the size of

animals is much smaller than a human subject, in particular when small rodents are studied. Therefore, improved spatial resolution is required.

Usually, PET detectors consist of an array of scintillation crystals optically coupled to several photomultipliers. The high-energy photons from the positron and electron annihilation, interact with the crystal, removing electrons from the valence band. These electrons return to the stationary phase dissipating energy as light, which is finally amplified by a photosensitive photomultiplier. The size of the scintillation crystal and the diameter of the ring of detectors, as well as physical parameters such as the positron range, the non-linearity of the annihilation photons and parallax error will determine the spatial resolution⁴³. Nowadays, small animal PET scanners can achieve resolution close to 0.8 mm in the center of the field of view, while resolution of clinical scanners is *ca.* 3 mm⁴⁴.

The second important factor to be considered is the sensitivity. It is defined as the fraction of events effectively detected as a coincidence. Increasing the length of the scintillation crystal can improve the sensitivity, while minimizing the size in the axial and transaxial directions can improve the spatial resolution. Therefore, designing a PET scanner involves a compromise between spatial resolution and sensitivity.

The data obtained during the PET scan is obtained as sinograms that are reconstructed into tomographic images, and then the images are analyzed and quantified by using specific software tools.

1.3 Radiolabelled amino acids

During decades, radiolabelled amino acids have been used for human studies, and they continue under an active investigation due to recent insights into the role of amino acid transporters and amino acids in tumor metabolism. The natural presence of carbon and nitrogen in organic molecules such as amino acids, makes the PET isotopes carbon-11

and nitrogen-13 attractive and valuable radionuclides for PET imaging. Radiolabelling of amino acids with ^{11}C and ^{13}N offers several advantages over other commonly used radionuclides, such as fluorine-18: (i) they structurally preserve the native molecule, which translates into equivalent biological properties; (ii) due to their favourable nuclide characteristics, multiple injections per day are feasible and the patient receives low radiation burden. On the other hand, the incorporation of radionuclides such as ^{18}F modify the native structure of the amino acid, altering its physico-chemical and biological properties. Because of that, different synthetic strategies to produce ^{11}C and ^{13}N -labelled amino acids have been developed, and they must contemplate the labelling position and the chirality of the amino acid native structure. These strategies can be divided into two large groups, those which have been synthesized by following a classical synthetic pathway and those whose synthetic pathway involves the use of enzymes as biocatalyst. In this PhD thesis, we have used both approaches to prepare labelled amino acids. Because of that, a brief explanation about these two groups is given below.

1.3.1 Radiolabelling by synthetic pathways

Traditional synthetic pathways have been widely used to the development of radiolabelled amino acids.

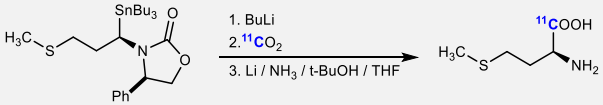
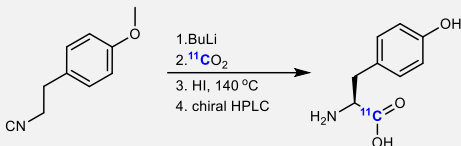
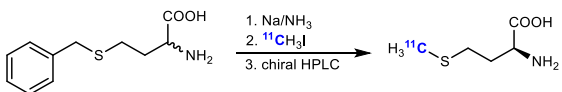
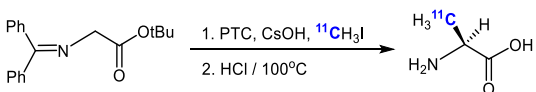
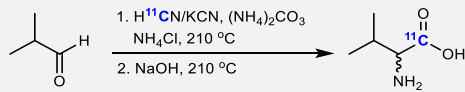
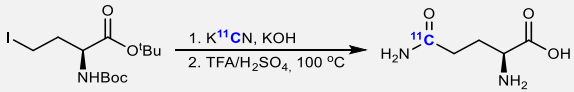
^{11}C -Amino acids

Classical catalysis based on organic synthetic pathways offers many possibilities for the radiosynthesis of ^{11}C -labelled amino acids. Over time, many strategies for the labelling have been transferred from organic synthesis, which offer two distinct positions for the radiolabelling: the α -atom and the carboxylic group. Although several methods have been developed, most of them resulted in racemic mixtures of amino acids, requiring time-consuming procedures for purification. Because of that, asymmetric catalysis is an attractive tool for radiosynthetic chemistry and the use of chiral catalyst for stereospecific radiosynthesis demonstrated to be successful^{45,46,47}.

Chapter 1. General introduction

As explained in the Section 2.3.4, carbon-11 can be produced as primary precursors directly from the cyclotron, such as $[^{11}\text{C}]\text{CH}_4$ and $[^{11}\text{C}]\text{CO}_2$, which can be directly used or transformed into radioactive secondary precursors such as $[^{11}\text{C}]$ hydrogen cyanide, $[^{11}\text{C}]$ acetate, $[^{11}\text{C}]$ methanol, $[^{11}\text{C}]$ methyl iodine, $[^{11}\text{C}]$ propionate and $[^{11}\text{C}]$ carbonate. Some examples for ^{11}C -labelled amino acids synthetic routes are shown in (Table 1.4).

Table 1.4 Examples of $[^{11}\text{C}]$ amino acids synthesized by following organic synthetic routes starting from different carbon-11 precursors.

Radioactive precursor	Reaction	Amino acid synthesized
$[^{11}\text{C}]$ Carbon dioxide	 <ol style="list-style-type: none"> 1. BuLi 2. $[^{11}\text{C}]\text{CO}_2$ 3. Li / NH_3 / t-BuOH / THF 	$[^{11}\text{C}]$ Methionine ⁴⁸
$[^{11}\text{C}]$ Methyl iodide	 <ol style="list-style-type: none"> 1. BuLi 2. $[^{11}\text{C}]\text{CO}_2$ 3. HI, 140 °C 4. chiral HPLC 	$[^{11}\text{C}]$ Tyrosine ⁴⁹
$[^{11}\text{C}]$ Methyl iodide	 <ol style="list-style-type: none"> 1. Na/NH_3 2. $[^{11}\text{C}]\text{H}_3\text{I}$ 3. chiral HPLC 	$[^{11}\text{C}]$ Methionine ⁵⁰
$[^{11}\text{C}]$ Hydrogen cyanide	 <ol style="list-style-type: none"> 1. PTC, CsOH, $[^{11}\text{C}]\text{H}_3\text{I}$ 2. HCl / 100 °C 	$[^{11}\text{C}]$ Alanine ⁴⁵
$[^{11}\text{C}]$ Hydrogen cyanide	 <ol style="list-style-type: none"> 1. $\text{H}^{11}\text{C}\text{N}/\text{KCN}$, $(\text{NH}_4)_2\text{CO}_3$, NH_4Cl, 210 °C 2. NaOH, 210 °C 	$[^{11}\text{C}]$ Valine ⁵¹
$[^{11}\text{C}]$ Hydrogen cyanide	 <ol style="list-style-type: none"> 1. $\text{K}^{11}\text{C}\text{N}$, KOH 2. TFA/$\text{H}_2\text{SO}_4$, 100 °C 	$[^{11}\text{C}]$ Glutamine ⁵²

When synthetic routes are used for the development of radioactive amino acids, it can be observed that the most used radioactive precursors are the primary precursor carbon dioxide [^{11}C] CO_2 or the secondary precursors [^{11}C]hydrogen cyanide and [^{11}C]methyl iodine.

L- and D-[*methyl*- ^{11}C]methionine can be radiolabelled in two different positions, depending on the synthetic route chosen. When it is radiolabelled in the terminal methyl position, the synthetic route consists of the alkylation of L- or D-S-benzyl-homocysteine by using sodium in liquid ammonia to produce the corresponding sodium salt of the sulphide anion, and then [^{11}C]methyl iodine as alkylating agent. By following this route, a racemic mixture is obtained, which can be purified by semi-preparative HPLC. On the other hand, when it is radiolabelled in the carboxylic position, the reaction consists of using butyl lithium with a methionine precursor, and the posterior carboxylation with [^{11}C] CO_2 . L-[^{11}C]methionine is extensively studied for tumour imaging (*e.g.* gliomas)⁵³. Not only the passive diffusion in the blood-brain barrier (BBB) promotes the uptake of L-[^{11}C]methionine, also the active amino acid transport into the cell contributes⁵⁰. It is also used in combination with [^{18}F]FDG for the determination of brain lesions and tumours⁵⁴, because several studies using both tracers conclude that they offer complementary information⁵⁵.

[^{11}C]Tyrosine can be synthesized using [^{11}C] CO_2 or [^{11}C]cyanide as carbon-11 sources. When [^{11}C] CO_2 is used, the reaction is based on the use of butyl lithium with a tyrosine precursor, and the posterior carboxylation. On the other hand, when the carbon-11 precursor is [^{11}C]cyanide, L- and D- [1- ^{11}C]tyrosine synthesis is carried out by the Bücherer-Strecker reaction, starting from the non-radioactive precursor p-hydroxyphenylacetaldehyde-bisulphite⁵⁶. The enantiomeric mixture can be purified by chiral HPLC. [^{11}C]Tyrosine was firstly used as a racemic mixture in 1984 during preliminary studies conducted in rat tumour models by Vaalburg *et al.*⁴⁹ and later by Daemen *et al.*⁵⁷ Both enantiomers present tumour uptake and interestingly, tumour uptake was slightly higher for the D-enantiomer⁴⁹. L-[^{11}C]Tyrosine metabolism shows that decarboxylation

is the first metabolic reaction and $[^{11}\text{C}]\text{CO}_2$ is the predominant product. This metabolite ($[^{11}\text{C}]\text{CO}_2$) can be released through the respiratory system not disturbing PET measurements⁵⁸. Regardless its use has not been so extensive, a small scale study in patients with prolactinoma (a type of benign brain tumour), L- $[^{11}\text{C}]\text{tyrosine}$ proved to be preferable to $[^{18}\text{F}]\text{FDG}$ for the visualization of this type of tumour after radiotherapy⁵⁷.

$[^{11}\text{C}]\text{Valine}$ can also be synthesized by following a modification of the Bücherer-Strecker reaction, using isobutyraldehyde as non-radioactive precursor and $[^{11}\text{C}]\text{cyanide}$ as carbon-11 source. In 1978 $[^{11}\text{C}]\text{Valine}$ demonstrated to be a potential pancreas-imaging agent by Washburn *et al.*⁵⁹ Valine was also rapidly decarboxylated as it happens with L- $[^{11}\text{C}]\text{tyrosine}$, but studies performed in patients with pancreatic disease showed high uptake of the racemic mixture in the diseased tissue⁵¹. There are no sufficient studies to make a strong conclusion about its use as promising imaging agent.

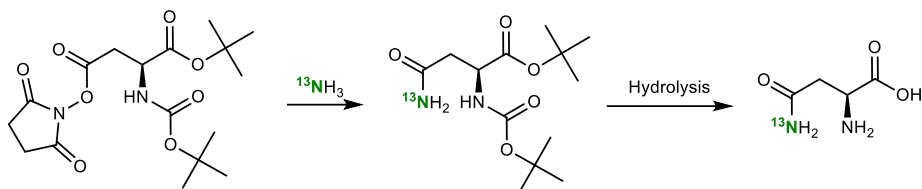
L- $[^{11}\text{C}]\text{glutamine}$ is synthesized using $[^{11}\text{C}]\text{cyanide}$ as carbon-11 source, by doing the $[^{11}\text{C}]\text{CN}$ -insertion in the non-radioactive precursor (S)-*tert*-butyl 2-((*tert*-butoxycarbonyl)amino)-4-iodobutanoate, and the subsequent deprotection. Despite not being an essential amino acid, glutamine has gained notable attention during the last years. Some preclinical studies have demonstrated that the tumour progression and development relies on the use of glutamine as nutrient, the so-called glutaminolysis pathway^{17,52}. Tumour cells can use different energetic sources to obtain their energy to grow and proliferate. Because of that, the use of L- $[^{11}\text{C}]\text{glutamine}$ in addition to $[^{18}\text{F}]\text{FDG}$ can result very interesting to discriminate tumour's reliance on different nutrients for growth.

$[^{11}\text{C}]\text{alanine}$ can be synthesized as L-*[methyl- $^{11}\text{C}]\text{alanine}$* by asymmetric alkylation of the non-radioactive precursor *N*-(diphenylmethylene)glycine *tert*-butyl ester using $[^{11}\text{C}]\text{methyl iodine}$ as carbon-11 source. $[^{11}\text{C}]\text{alanine}$ was firstly synthesized by Langstrom *et al.* in the late 1970's and they obtained a 48% of enantiomeric excess yield by following an asymmetric synthetic pathway. But it took some years to develop a synthesis whose yield was 80 % ee of L- $[^{11}\text{C}]\text{alanine}$. Finally in 1997 Corey *et al.*

developed a methodology based on phase transfer catalysis and using methyl iodine as alkylating agent, which reach an enantiomeric excess of 97 % of L-[^{11}C]alanine⁶⁰.

^{13}N -Amino acids

Amino acids have been also labelled with nitrogen-13 at the R group by using chemical methods. Only a few examples of chemical methods by using nitrogen-13 are found in the literature, due to their time-consuming methodology and the low efficiency. One of these examples is the synthesis of L-[^{13}N]asparagine shown in Scheme 2.



Scheme 2. Synthetic pathway for the synthesis of L-[^{13}N]asparagine.

The synthetic route is based on the reaction of the activated ester L- α -N-Boc-aspartate, using radioactive ammonia [^{13}N] NH_3 to form the corresponding amide and the subsequent hydrolysis of the protecting groups.

However, there are only few examples in the literature due to the nitrogen-13 half-life (9.96 min), which results short for its use in traditional synthetic procedures. These synthetic pathways also produce intermediates and usually yield racemic mixtures of the compound, which are not desirable in the synthesis of amino acids. Because of that, in those cases in which classical synthetic routes present some drawbacks, biocatalysis can offer a great opportunity to perform the radiolabelling.

1.3.2 Radiolabelling by biocatalytic pathways

Enzymes are the life's catalysts. They catalyse the chemical reactions that involve the metabolism of all living cells. Each biochemical reaction of the cell metabolism is catalysed by one specific enzyme.

Chapter 1. General introduction

The enzymes exhibit excellent properties as catalysts which make them very attractive to perform a plethora of chemical processes. Enzymes are biodegradable and environment-friendly catalysts with high regio-, chemo-, and stereoselectivity⁶¹. The discipline that exploits enzymes as process catalyst under non physiological conditions is named as Biocatalysis and offers some advantages over conventional synthetic routes. Synthetic chemistry frequently needs the time-consuming protection/deprotection/activation steps, and the use of enzymes avoid these steps. The possibility of using shorter synthetic routes with less generation of waste products makes them more environmentally and economically attractive. Therefore, biocatalysis is becoming a key tool of chemical manufacturing⁶².

Due to its natural origin, enzymes present also some disadvantages: i) its reactivity towards artificial substrates (non-natural reactions) could be limited; (ii) its low stability under extreme pH values, high temperatures or in the presence of non-polar solvents, and (iii) its high solubility in water limit their reusability in batch reactions or their use in continuous-flow processes⁶³. But the advances of genomics and computational biology have resulted in novel experimental and computational protein engineering tools, which have enhanced the toolbox of available enzymes⁶⁴.

Biocatalysis in radiochemistry

Due to the enzyme properties explained above, the exploitation of biocatalysis in radiochemistry represents an attractive alternative to conventional chemistry. Consequently, by harnessing the enzyme properties in PET radiochemistry, radiochemists can synthesize radiotracers through selective and fast biosynthetic routes, thus minimizing the formation of side products and preventing the racemic mixtures formation. During the 70's and 80's biocatalysis in radiochemistry lived its greatest period⁶⁵, but new biocatalytic approaches have been reported during the last decades for the synthesis of PET radiotracers using Nitrogen-13, Carbon-11 and Fluorine-18. Enzymes have been employed to radiosynthesize [¹³N/¹¹C]amino acids,

[^{18}F]nucleoside derivatives and [$^{11}\text{C}/^{18}\text{F}$]proteins. Moreover, enzymatic reactions have been also employed to regio- and stereospecifically introduce radioactive precursors into a plethora of biological molecules^{66,67}.

Several enzymes and multi-enzymatic systems have been used as heterogeneous biocatalyst to synthesize ^{13}N - and ^{11}C -labelled amino acids which are very relevant in the contexts of this PhD thesis.

^{11}C -amino acids

During the last decades of the 20th century, biocatalysis played an important role in the developments of carbon-11 radiochemistry. As explained in the Section 2.3.4, carbon-11 can be produced as primary precursors directly from the cyclotron, such as [^{11}C]CH₄ and [^{11}C]CO₂, which can be directly used or transformed into radioactive secondary precursors such as [^{11}C]hydrogen cyanide, [^{11}C]acetate, [^{11}C]methanol, [^{11}C]methyl iodine, [^{11}C]propionate and [^{11}C]carbonate. These carbon-11 precursors have been used to incorporate the radioisotope in several biological targets through biocatalytic reactions. Some examples of ^{11}C -labelled amino acids are represented in Table 5.

Table 5. Some examples of [^{11}C]amino acids synthesized by following a biocatalytic route by using carbon-11 primary and secondary precursors as ^{11}C source. Adapted from the PhD thesis: da Silva, E., Application of enzymes in Nitrogen-13 radiochemistry: biocatalytic synthesis of PET radionuclides with biomedical interest. University of the Basque Country, 2017.

Radioactive precursor	Biosynthetic route	Reaction	Amino acid synthesized
^{11}C Carbon dioxide	Phosphoenolpyruvate carboxylase	Decarboxylation	<i>L</i> -[4- ^{11}C]Aspartic acid ⁶⁸
	Aspartate transaminase	Transamination	
	Glutamate-pyruvate transaminase	Transamination	<i>L</i> -[^{11}C]Glutamate ⁶⁹
	D-amino acid oxidase/Catalase	Resolution/Redox reaction	<i>L</i> -[3- ^{11}C]Tyrosine ⁷⁰
	Aspartate transaminase	Transamination	[3- ^{11}C]Phenylalanine ⁷¹

Chapter 1. General introduction

[¹¹C]Methyl iodine	γ -cyano- α -aminobutyric acid synthetase	Elimination	<i>L</i> -[methyl- ¹¹ C]Methionine ⁷²
	Glutamic-pyruvic transaminase	Transamination	<i>L</i> -[¹¹ C]Alanine ⁷³
	D-amino acid oxidase/Catalase	Resolution/Redox reaction	<i>L</i> -[β - ¹¹ C]Tryptophan ⁷⁴
	Glutamate-pyruvate transaminase	Transamination	5-Hydroxy- <i>L</i> -[β - ¹¹ C]Tryptophan ⁷⁴
	Tryptophanase	β -replacement	
[¹¹C]Acetate	Glutamate-pyruvate transaminase	Transamination	<i>L</i> -[¹¹ C]Glutamate ⁶⁹
[¹¹C]Methanol	Alcohol oxidase/Catalase	Oxidation	<i>L</i> -[3- ¹¹ C]Serine ⁷⁵
	Serine Hydroxyl-methyltransferase	Hydroxymethylation	
[¹¹C]Hydrogen cyanide	D-amino acid oxidase/Catalase	Resolution/Redox reaction	<i>L</i> -[carboxy- ¹¹ C]Tyrosine ⁷⁶
	Glutamate-pyruvate transaminase	Transamination	
	D-amino acid oxidase/Catalase	Resolution/Redox reaction	<i>L</i> -[3- ¹¹ C]Tryptophan ⁷⁶
	Glutamate-pyruvate transaminase	Transamination	5-Hydroxy- <i>L</i> -[3- ¹¹ C]Tryptophan ⁷⁷
	Tryptophanase	β -replacement	
	D-amino acid oxidase/Catalase	Resolution/Redox reaction	<i>L</i> -[1- ¹¹ C]Alanine ⁷⁶
	Glutamate-pyruvate transaminase	Transamination	
	D-amino acid oxidase	Resolution	<i>L</i> -[¹¹ C]Leucine ⁷⁸
	D-amino acid oxidase/Catalase	Resolution/Redox reaction	<i>L</i> -[¹¹ C]Alanine ⁷⁹
[¹¹C]carbonate	Mutant strain of the <i>cyanobacterium Synechocystic</i> PCC 6803	Photosynthesis	<i>L</i> -[¹¹ C]Phenylalanine ⁸⁰

¹³N-amino acids

In the same way as the carbon-11, nitrogen-13 is an excellent radionuclide for the radiolabelling of organic molecules such as amino acids, due to its natural presence in its native structure. As explained in the section 2.3.4, nitrogen-13 is usually produced as nitrate ($[^{13}\text{N}]\text{NO}_3^-$), nitrite ($[^{13}\text{N}]\text{NO}_2^-$) and ammonia ($[^{13}\text{N}]\text{NH}_3$) and variations will depend on the material irradiated. But, as several enzymatic reactions use ammonia as nitrogen source, radiolabelled ammonia $[^{13}\text{N}]\text{NH}_3$ is the most common primary precursor for these kind of synthesis.

There are three main enzymatic routes to incorporate $[^{13}\text{N}]\text{NH}_3$ into amino acids (Figure 1.8): a) using amino acid synthetases that catalyse the introduction of $[^{13}\text{N}]\text{NH}_3$ into the ω -carboxylic group of acidic amino acids by using adenosine triphosphate (ATP)^{67,81}; b) using amino acid dehydrogenases, which catalyse the reductive amination of α -ketoacids, using $[^{13}\text{N}]\text{NH}_3$ as amine source and nicotinamide adenine dinucleotide (NADH) or nicotinamide adenine dinucleotide phosphate (NADPH) as redox cofactor and c) using bi-enzymatic system which comprehends an amino acid dehydrogenase and a transaminase that will transfer the radiolabelled amino group to another alfa keto acid.

By following this type of enzymatic routes, several amino acids have been synthesized, including L- $[^{13}\text{N}]\text{glutamine}$, L- $[^{13}\text{N}]\text{alanine}$, L- $[^{13}\text{N}]\text{methionine}$, L- $[^{13}\text{N}]\text{glutamate}$ and L- $[^{13}\text{N}]\text{leucine}$, among others (see Table 1.6).

The use of biosynthetic methods in radiosynthesis has proven efficient for the preparation of labelled compounds that would be difficult to label using chemical methods. Also, the biological relevance of amino acids inside living organisms makes these radiotracers promising probes to understand its metabolism, transport into cells and biological behaviour in the study and diagnosis of neurological disorders and tumours.

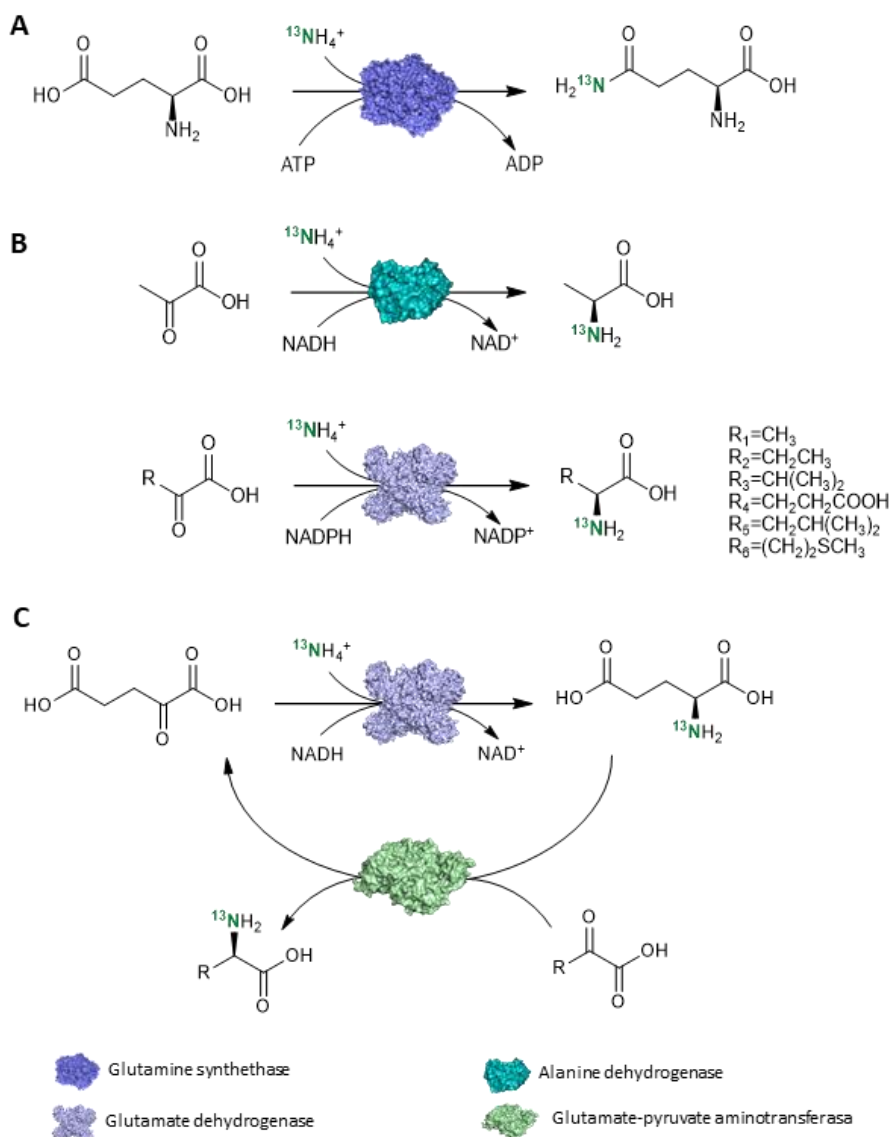


Figure 1.8. Examples of the major enzymatic routes used to incorporate $[^{13}\text{N}]\text{NH}_3$ into amino acids. A) Using amino acid synthetases; B) using amino acid dehydrogenases; C) using multi-enzymatic system formed by an amino acid dehydrogenase and an aminotransferase.

Chapter 1. General introduction

Table 1.6 Some examples of [¹³N]amino acids synthesized by following a biocatalytic route by using ¹³N-ammonia as ¹³N source. Adapted from the PhD thesis: da Silva, E., Application of enzymes in Nitrogen-13 radiochemistry: biocatalytic synthesis of PET radionuclides with biomedical interest. University of the Basque Country, 2017.

Radioactive precursor	Biosynthetic route	Reaction	Amino acid synthesized
¹³ N]Ammonia	Asparagine synthetase	Acid amide hydrolysis	L-[¹³ N]Asparagine
	Glutamate dehydrogenase	Reductive amination	L-[¹³ N]Glutamate ^{82,81}
	Glutamate dehydrogenase/Glutamate-pyruvate transaminase	Reductive amination	L-[¹³ N]Alanine ⁸¹
	Glutamine synthetase	Acid amide hydrolysis	L-[¹³ N]Glutamine ⁸¹
	Aspartate ammonia-lyase	Addition	L-[¹³ N]Aspartate ⁸¹
	Glutamate dehydrogenase	Reductive amination	L-[¹³ N]Glutamate L-[¹³ N]Valine L-[¹³ N]Methionine ^{66,83} L-[¹³ N]Leucine L-[¹³ N]Alanine
	Ornithine transcarbamylase Carbamyl phosphate synthetase	Carbamoylation Phosphorilation/Amination	L-[ω- ¹³ N]Citrulline ⁶⁷
	Phenylalanine dehydrogenase	Reductive amination	L-[¹³ N]Phenylalanine ⁸⁴ L-[¹³ N]Tyrosine ⁸⁴
	Alanine dehydrogenase	Reductive amination	L-[¹³ N]Alanine L-[¹³ N]Serine ⁴⁰ L-[¹³ N]Glycine

In contrast, one of the weaknesses that is presented about some of these radiolabelled amino acids is that some of the studies have been conducted more than 20 years ago, which reveals a lack of an actual re-evaluation with state-of-the-art imaging techniques. But nowadays, the development and accessibility of new carbon-11 and nitrogen-13 radiolabelling strategies have opened new avenues for the development of new (or reevaluation of already reported) imaging agents.

1.4 D-amino acids

D-amino acids have not been considered as relevant substrates in the mammalian metabolism. Therefore, it was assumed that the injection of a racemic mixture containing L and D-amino acids was not problematic. It was thought that D-amino acids were simply not metabolized and they will remain in the blood flow and then be excreted. However, it has been discovered that D-amino acids can play a crucial role in some diseases. The presence of particular D-amino acids in human body has been related to several diseases including amyotrophic lateral sclerosis⁸⁵, schizophrenia⁸⁶, and age-disordered conditions as cataract and atherosclerosis⁸⁷. They also play a relevant role in the development, pathophysiology, and treatment of cancer.

The potential role of D-amino acids in cancer was firstly published by Kögl and Erxleben in 1939⁸⁸. From then on, several studies have been performed and the controversy about the role played by D-amino acids has been a matter of debate^{89,90}. Nonetheless, D-glutamate and D-glutamine metabolism suggests to be regulated in patients of pancreatic cancer⁹¹. Also, patients with gastric cancer have shown increased concentration of D-alanine in the gastric juice⁹².

During the late 1970s, the administration of ¹⁴C-labeled D-amino acids to tumour-bearing mice was reported to present greater accumulation in tumour cells than when the administration was done with the corresponding L-amino acids⁹³. Sasamura *et al.*

also showed that the tumour cell proliferation was reduced after the administration of D-amino acids^{94,95}.

The stereoselective deamination of D-amino acids inside the body is catalysed by D-amino acid oxidase (DAAO) and this process will generate hydrogen peroxide (H₂O₂). This hydrogen peroxide is a reactive oxygen species (ROS), and it easily crosses the cellular membranes and damages DNA, lipids, and proteins, promoting their apoptosis. The poor presence of DAAO in mammalian cells suggest that the cytotoxicity of ROS can be harnessed by the administration of D-amino acids in tumour cells which have expressed DAAO in the cytoplasm⁹⁶. This suggests that the administration of D-amino acids could have a growth inhibitory function in tumours⁹⁴. D-amino acids have also been used to increase the half-life of anticancer drugs when they are incorporated into their backbone⁹⁷. Also, the incorporation of D-amino acids in cell-penetrating peptides boost their utilization as contrast agents to detect tumour cells⁹⁸.

Because all these reasons, the radiolabelling of D-amino acids becomes an interesting strategy to study cancer cell metabolism. In this PhD thesis, radiolabelled D-[*methyl*-¹¹C]alanine is synthesized and tested in a mice prostate cancer model.

1.5 Imaging prostate cancer

Nowadays, the diagnosis of prostate cancer is still majorly based on blood elevated levels of PSA (Prostate-Specific Antigen). PSA is a protein which values are elevated in men with prostate cancer. But these elevated levels are not only reflecting prostate cancer, as certain benign conditions can also result in elevated PSA levels in blood. With the PSA levels analysis, it is common to do a biopsy during the diagnosis of prostate cancer.

Also, imaging techniques help to diagnose advanced stages of cancer, in which prostate cancer cells can spread to other parts of the body. Magnetic Resonance Imaging (MRI) can help to confirm certain portion of prostate cancer lesions, although some of them

might be still missed. This is when molecular imaging provided by PET imaging gains relevance.

1.5.1 PSMA Imaging

PSMA, a transmembrane protein that is substantially overexpressed in most prostate cancer cells, both in primary and metastatic lesions, has become a target molecule for imaging techniques.

Prostate-specific membrane antigen imaging is a nuclear medicine exam based on positron emission tomography (PET) to detect prostate cancer. The PSMA PET analysis is accumulating evidence about its superior detection in comparison with conventional imaging tests such as CT scans. Some agents radiolabelled with gallium 68 (^{68}Ga) and fluorine 18 (^{18}F) are currently under study^{99,100}.

Two patient populations are being studied with the PSMA PET.

- Patients who have received a new diagnosis of high-risk prostate cancer. Conventional imaging techniques are not efficient in detecting high risk for metastases, and PSMA PET could help to change the surgical or oncological treatment plan.
- Patients who present biochemical recurrence. These patients present rising prostate-specific antigen (PSA) levels after treatment with surgery or radiation. PSMA PET can help to find sites of metastatic and recurrent disease⁹⁴.

The mouse cancer model used in the context of this PhD thesis does not over-express PSMA, and hence PSMA-specific tracers developed so far cannot be used for the evaluation of primary tumors or metastases. This said, the aim of this thesis is not the diagnosis of prostate carcinoma by using imaging techniques, but the investigation of metabolic aspects of prostate cancer in our particular cancer model. The findings may shed light on therapeutic targets in the future.

1.6 References

1. Sung, H. *et al.* Global Cancer Statistics 2020: GLOBOCAN Estimates of Incidence and Mortality Worldwide for 36 Cancers in 185 Countries. *CA. Cancer J. Clin.* **71**, 209–249 (2021).
2. Pienta, K. J. *et al.* The current state of preclinical prostate cancer animal models. *Prostate* **68**, 629–639 (2008).
3. Abdulkadir, S. A. & Kim, J. Genetically engineered murine models of prostate cancer: Insights into mechanisms of tumorigenesis and potential utility. *Futur. Oncol.* **1**, 351–360 (2005).
4. Simin, K. *et al.* Deciphering cancer complexities in genetically engineered mice. *Cold Spring Harb. Symp. Quant. Biol.* **70**, 283–290 (2005).
5. Kasper, S. Survey of genetically engineered mouse models for prostate cancer: Analyzing the molecular basis of prostate cancer development, progression, and metastasis. *J. Cell. Biochem.* **94**, 279–297 (2005).
6. Shen, M. M. & Abate-Shen, C. Pten inactivation and the emergence of androgen-independent prostate cancer. *Cancer Res.* **67**, 6535–6538 (2007).
7. Carver, B. S. & Pandolfi, P. P. Mouse modeling in oncologic preclinical and translational research. *Clin. Cancer Res.* **12**, 5305–5311 (2006).
8. Liao, C. P. *et al.* Mouse models of prostate adenocarcinoma with the capacity to monitor spontaneous carcinogenesis by bioluminescence or fluorescence. *Cancer Res.* **67**, 7525–7533 (2007).
9. Salmena, L., Carracedo, A. & Pandolfi, P. P. Tenets of PTEN Tumor Suppression. *Cell* **133**, 403–414 (2008).
10. Wang, S. *et al.* Prostate-specific deletion of the murine Pten tumor suppressor gene leads to metastatic prostate cancer. *Cancer Cell* **4**, 209–221 (2003).

Chapter 1. General introduction

11. Rangarajan, A. & Weinberg, R. A. Comparative biology of mouse versus human cells: Modelling human cancer in mice. *Nat. Rev. Cancer* **3**, 952–959 (2003).
12. Tong, X., Zhao, F. & Thompson, C. B. The molecular determinants of de novo nucleotide biosynthesis in cancer cells. *Curr. Opin. Genet. Dev.* **19**, 32–37 (2009).
13. Heiden, M. G. V., Cantley, L. C. & Thompson, C. B. Understanding the warburg effect: The metabolic requirements of cell proliferation. *Science (80-.)*. **324**, 1029–1033 (2009).
14. Currie, E., Schulze, A., Zechner, R., Walther, T. C. & Farese, R. V. Cellular fatty acid metabolism and cancer. *Cell Metab.* **18**, 153–161 (2013).
15. Giunchi, F., Fiorentino, M. & Loda, M. The Metabolic Landscape of Prostate Cancer. *Eur. Urol. Oncol.* **2**, 28–36 (2019).
16. DeBerardinis, R. J. *et al.* Beyond aerobic glycolysis: Transformed cells can engage in glutamine metabolism that exceeds the requirement for protein and nucleotide synthesis. *Proc. Natl. Acad. Sci. U. S. A.* **104**, 19345–19350 (2007).
17. Wise, D. R. & Thompson, C. B. Glutamine addiction: a new therapeutic target in cancer. *Trends Biochem. Sci.* **35**, 427–433 (2010).
18. Gambhir, S. S. Molecular imaging of cancer with positron emission tomography. *Nat. Rev. Cancer* **2**, 683–693 (2002).
19. Surasi, D. S., Bhambhani, P., Baldwin, J. A., Almodovar, S. E. & O'Malley, J. P. 18F-FDG PET and PET/CT patient preparation: A review of the literature. *J. Nucl. Med. Technol.* **42**, 5–13 (2014).
20. Jager, P. L. *et al.* Radiolabeled Amino Acids: Basic Aspects and Clinical Applications in Oncology ; Continuing Education. *J Nucl Med* **42**, 432–445 (2001).
21. Huang, C. & McConathy, J. Radiolabeled amino acids for oncologic imaging. *J. Nucl. Med.* **54**, 1007–1010 (2013).

22. Conti, M. & Eriksson, L. Physics of pure and non-pure positron emitters for PET: A review and a discussion. *EJNMMI Phys.* **3**, (2016).
23. Townsend, D. W. & Cherry, S. R. Combining anatomy and function: The path to true image fusion. *Eur. Radiol.* **11**, 1968–1974 (2001).
24. Townsend, D. W. & Beyer, T. A combined PET/CT scanner: The path to true image fusion. *Br. J. Radiol.* **75**, 24–30 (2002).
25. Carter, L. M. *et al.* The Impact of Positron Range on PET Resolution, Evaluated with Phantoms and PHITS Monte Carlo Simulations for Conventional and Non-conventional Radionuclides. *Mol. Imaging Biol.* **22**, 73–84 (2020).
26. Le Bars, D., Malleval, M., Bonnefoi, F. & Tourvieille, C. Simple synthesis of [1-¹¹C]acetate. *J. Label. Compd. Radiopharm.* **49**, 263–267 (2006).
27. Miller, P. W., Long, N. J., Vilar, R. & Gee, A. D. Synthesis of ¹¹C, ¹⁸F, ¹⁵O, and ¹³N radiolabels for positron emission tomography. *Angew. Chemie - Int. Ed.* **47**, 8998–9033 (2008).
28. Gómez-Vallejo, V. *et al.* Efficient system for the preparation of [¹³N]labeled nitrosamines. *Bioorganic Med. Chem. Lett.* **19**, 1913–1915 (2009).
29. Gómez-Vallejo, V. *et al.* Fully automated synthesis of ¹³N-labeled nitrosothiols. *Tetrahedron Lett.* **51**, 2990–2993 (2010).
30. Gaja, V. *et al.* Synthesis and evaluation of ¹³N-labelled azo compounds for β -amyloid imaging in mice. *Mol. Imaging Biol.* **16**, 538–549 (2014).
31. Joshi, S. M. *et al.* Synthesis of radiolabelled aryl azides from diazonium salts: Experimental and computational results permit the identification of the preferred mechanism. *Chem. Commun.* **51**, 8954–8957 (2015).
32. Joshi, S. M., Gómez-Vallejo, V., Salinas, V. & Llop, J. Synthesis of ¹³N-labelled polysubstituted triazoles: Via Huisgen cycloaddition. *RSC Adv.* **6**, 109633–109638 (2016).

33. Llop, J., Gómez-Vallejo, V., Bosque, M., Quincoces, G. & Peñuelas, I. Synthesis of S-[¹³N]nitrosoglutathione (13N-GSNO) as a new potential PET imaging agent. *Appl. Radiat. Isot.* **67**, 95–99 (2009).
34. Dence, C. S., Welch, M. J., Hughey, B. J., Shefer, R. E. & Klinkowstein, R. E. Production of [¹³N]ammonia applicable to low energy accelerators. *Nucl. Med. Biol.* **21**, 987–996 (1994).
35. Sobczyk, D. P., Van Grondelle, J., De Jong, A. M., De Voigt, M. J. A. & Van Santen, R. A. Production of chemically pure gaseous [¹³N]NH₃ pulses for PEP studies using a modified DeVarda reduction. *Appl. Radiat. Isot.* **57**, 201–207 (2002).
36. Berridge, M. S. & Landmeier, B. J. In-target production of [¹³N]ammonia: Target design, products, and operating parameters. *Appl. Radiat. Isot.* **44**, 1433–1441 (1993).
37. Krasikova, R. N., Fedorova, O. S., Korsakov, M. V., Landmeier Bennington, B. & Berridge, M. S. Improved [¹³N]ammonia yield from the proton irradiation of water using methane gas. *Appl. Radiat. Isot.* **51**, 395–401 (1999).
38. Schepis, T. *et al.* Absolute quantification of myocardial blood flow with ¹³N-ammonia and 3-dimensional PET. *J. Nucl. Med.* **48**, 1783–1789 (2007).
39. Kitsiou, A. N. *et al.* ¹³N-ammonia myocardial blood flow and uptake: Relation to functional outcome of asynergic regions after revascularization. *J. Am. Coll. Cardiol.* **33**, 678–686 (1999).
40. da Silva, E. S., Gómez-Vallejo, V., Baz, Z., Llop, J. & López-Gallego, F. Efficient Enzymatic Preparation of ¹³N-Labelled Amino Acids: Towards Multipurpose Synthetic Systems. *Chem. - A Eur. J.* **22**, 13619–13626 (2016).
41. Turner, P. V., Brabb, T., Pekow, C. & Vasbinder, M. A. Administration of substances to laboratory animals: Routes of administration and factors to consider. *J. Am. Assoc. Lab. Anim. Sci.* **50**, 600–613 (2011).

42. Suckow, M. A., Danneman, P. & Brayton, C. The laboratory mouse. *Lab. Mouse* 1–168 (2000).
43. Levin, C. S. & Hoffman, E. J. Calculation of positron range and its effect on the fundamental limit of positron emission tomography system spatial resolution. *Phys. Med. Biol.* **44**, 781–799 (1999).
44. Moses, W. W. Fundamental limits of spatial resolution in PET. *Nucl. Instruments Methods Phys. Res. Sect. A Accel. Spectrometers, Detect. Assoc. Equip.* **648**, S236–S240 (2011).
45. Filp, U., Pekošak, A., Poot, A. J. & Windhorst, A. D. Enantioselective synthesis of carbon-11 labeled L-alanine using phase transfer catalysis of Schiff bases. *Tetrahedron* **72**, 6551–6557 (2016).
46. Filp, U., Pekošak, A., Poot, A. J. & Windhorst, A. D. Stereocontrolled [11C]Alkylation of N-Terminal Glycine Schiff Bases To Obtain Dipeptides. *European J. Org. Chem.* **2017**, 5592–5596 (2017).
47. Pekošak, A., Filp, U., Poot, A. J. & Windhorst, A. D. From Carbon-11-Labeled Amino Acids to Peptides in Positron Emission Tomography: the Synthesis and Clinical Application. *Mol. Imaging Biol.* **20**, 510–532 (2018).
48. Bolster, J. M., Vaalburg, W., Elsinga, P. H., Wynberg, H. & Woldring, M. G. Synthesis of dl-[1-11C]methionine. *Int. J. Radiat. Appl. Instrumentation. Part 37*, 1069–1070 (1986).
49. Bolster, J. M. *et al.* Carbon-11 labelled tyrosine to study tumor metabolism by positron emission tomography (PET). *Eur. J. Nucl. Med.* **12**, 321–324 (1986).
50. Kilian, K. & Pełal, A. Synthesis of endogenous compounds labeled with 11C for positron emission tomography. *Acta Phys. Pol. A* **127**, 1475–1478 (2015).
51. Hubner, K. F. *et al.* Carbon-11-labeled amino acids for the rectilinear and positron tomographic imaging of the human pancreas. **20**, 507–513 (1979).

52. Qu, W. *et al.* Preparation and characterization of L-[5- ¹¹C]-glutamine for metabolic imaging of tumors. *J. Nucl. Med.* **53**, 98–105 (2012).
53. Ullrich, R. T. *et al.* Methyl-L-¹¹C-methionine PET as a diagnostic marker for malignant progression in patients with glioma. *J. Nucl. Med.* **50**, 1962–1968 (2009).
54. Glaudemans, A. W. J. M. *et al.* Value of ¹¹C-methionine PET in imaging brain tumours and metastases. *Eur. J. Nucl. Med. Mol. Imaging* **40**, 615–635 (2013).
55. Ogawa, T. *et al.* Clinical positron emission tomography for brain tumors: Comparison of fludeoxyglucose F 18 and L-methyl-¹¹C-methionine. *Am. J. Neuroradiol.* **17**, 345–353 (1996).
56. Halldin, C. The Buecherer-STrecker synthesis of D- and L-(¹¹C)tyrosine and the in vivo study of it in human brain using PET. *Eur J Nucl Med* **13**, 288–291 (1987).
57. Houston, A. & Craig, A. PET studies with L-[¹¹C]tyrosine, L-[methyl-¹¹C]methionine and ¹⁸F-fluorodeoxyglucose in prolactinomas in relation to bromocryptine treatment. *Eur. J. Nucl. Med.*, **18**, 453-460 (1991).
58. Kole, A. C. *et al.* Standardized Uptake Value and Quantification of Metabolism for Breast Cancer Imaging with Glucose metabolism of many malignant tumors is high. *J. Nucl. Med.* **38**, 692–696 (1997).
59. Washburn, C., Wieland, W. & Butler, [1-¹¹C] DL-Valine, a potential pancreas-imaging agent. *J. Nucl. Med.*, **19**, 77–83 (1977).
60. Corey, E. J., Xu, F. & Noe, M. C. A Rational Approach to Catalytic Enantioselective Enolate Alkylation Using a Structurally Rigidified and Defined Chiral Quaternary Ammonium Salt under Phase Transfer Conditions. *J. Am. Chem. Soc.* **119**, 12414–12415 (1997).
61. Abedi, D., Zhang, L., Pyne, M. & Chou, C. P. *Enzyme biocatalysis. Comprehensive Biotechnology* (2019).

62. Pollard, D. J. & Woodley, J. M. Biocatalysis for pharmaceutical intermediates: the future is now. *Trends Biotechnol.* **25**, 66–73 (2007).
63. Bommarius, A. S. & Broering, J. M. Established and novel tools to investigate biocatalyst stability. *Biocatal. Biotransformation* **23**, 125–139 (2005).
64. Bommarius, A. S. Biocatalysis: A Status Report. *Annu. Rev. Chem. Biomol. Eng.* **6**, 319–345 (2015).
65. Gelbard, A. S. Biosynthetic methods for incorporating positron-emitting radionuclides into compounds of biomedical interest. *J. Label. Compd. Radiopharm.*, No. 7, **XVIII**, 933-945 (1980).
66. Cooper, A. J. L. & Gelbard, A. S. The use of immobilized glutamate dehydrogenase to synthesize ¹³N-labeled l-amino acids. *Anal. Biochem.* **111**, 42–48 (1981).
67. Gelbard, A. S., Kaseman, D. S., Rosenspire, K. C. & Meister, A. Enzymatic syntheses of phosphate, l-citrulline, and N-carbamyl l-aspartate labeled with either ¹³N or ¹¹C. *Int. J. Nucl. Med. Biol.* **12**, 235–242 (1985).
68. Barrio, J. R., Egbert, J. E., Henze, E., Schelbert, H. R. & Baumgartner, F. J. l-[4-¹¹C]Aspartic Acid: Enzymatic Synthesis, Myocardial Uptake, and Metabolism. *J. Med. Chem.* **25**, 93–96 (1982).
69. Cohen, M. B. *et al.* The varying tissue distribution of L-glutamic acid labelled at three different sites. *Int. J. Appl. Radiat. Isot.* **33**, 613–617 (1982).
70. Bjurling, P. *et al.* Multi-enzymatic Synthesis of beta-¹¹C-Labelled L-Tyrosine and L-DOPA. *Acta Chemica Scandinavica*, **44** 183–188 (1990).
71. Halldin, C., Langstrom, B., Synthesis of [3-¹¹C]phenylpyruvic acid and its use in an enzymatic transamination to [3-¹¹C]phenylalanine. *J. Label. Compd. Radiopharm.* No. 7 715. **XXIII**, 715–722 (1985).
72. Kaneko, S., Ishiwata, K., Ishii, S. I., Omura, H. & Senda, M. Enzymatic synthesis of

Chapter 1. General introduction

- carbon-11 labeled methionine and its derivatives with immobilized γ -cyano- γ -aminobutyric acid synthase. *Appl. Radiat. Isot.* **51**, 285–291 (1999).
73. Bjurling, P. & Langstrom, B. The Synthesis a Useful Synthone, **39**, 627–630 (1988).
74. Bjurling, P., Watanabe, Y., Tokushige, M., Oda, T. & Långström, B. Syntheses of β -¹¹C-labelled L-tryptophan and 5-hydroxy-L-tryptophan using a multi-enzymatic reaction route. *J. Chem. Soc. Perkin Trans.* **1**, 1331–1334 (1989)
75. Svärd, H., Jigerius, S. B. & Långström, B. The enzymatic synthesis of L-[³-¹¹C]serine. *Int. J. Radiat. Appl. Instrumentation. Part* **41**, 587–591 (1990).
76. Bjurling, P. *et al.* Enzymatic Synthesis of Carboxy-¹¹C-Labelled L-Tyrosine, L-DOPA, L-Tryptophan and 5-Hydroxy-L-tryptophan. *Acta Chemica Scandinavica*, **44** 178–182 (1990).
77. Hartvig, P. *et al.* Brain kinetics of ¹¹C-labelled L-tryptophan and 5-hydroxy-L-tryptophan in the Rhesus monkey - A study using positron emission tomography. *J. Neural Transm.* **88**, 1–10 (1992).
78. Barrio, J. R., Keen, R. E. & Ropchan, J. R. L-[¹-¹¹C]leucine: Routine synthesis by enzymatic resolution. *J. Nucl. Med.* **24**, 515–521 (1983).
79. Ropchan, J., Barrio, J., Enzymatic synthesis of [¹-¹¹C]pyruvic acid, L-[¹-¹¹C]lactic acid and L-[¹-¹¹C]alanine via DL-[¹-¹¹C]alanine. *J. Nucl. Med.*, **25**, 887–892 (1984).
80. Labarre, J., Donie, P. & Crouzel, C. The biosynthesis of L-[¹¹C]phenylalanine using a mutant strain of a cyanobacterium (*Synechocystis* PCC 6803). *Int. J. Radiat. Appl. Instrumentation. Part* **42**, 659–663 (1991).
81. Baumgartner, F. J. *et al.* ¹³N-labeled L-amino acids for in vivo assessment of local myocardial metabolism. *J. Med. Chem.*, **24**, 764-766 (1981).
82. Gelbard, A. S. *et al.* Imaging of the human heart after administration of L-(N-¹³)glutamate. *J. Nucl. Med.* **21**, 988–991 (1980).

83. Barrio, J. R. *et al.* Synthesis and myocardial kinetics of N-13 and C-11 labeled branched-chain l-amino acids. *J. Nucl. Med.* **24**, 937–944 (1983).
84. Gelbard, A. S. *et al.* Methods for the enzymatic synthesis of tyrosine and phenylalanine labeled with nitrogen-13. *Int. J. Radiat. Appl. Instrumentation. Part 41*, 229–233 (1990).
85. Sasabe, J. *et al.* D-Amino acid oxidase controls motoneuron degeneration through D-serine. *Proc. Natl. Acad. Sci. U. S. A.* **109**, 627–632 (2012).
86. Verrall, L., Burnet, P. W. J., Betts, J. F. & Harrison, P. J. The neurobiology of D-amino acid oxidase and its involvement in schizophrenia. *Mol. Psychiatry* **15**, 122–137 (2010).
87. Fujii, N., Takata, T., Fujii, N., Aki, K. & Sakaue, H. D-Amino acids in protein: The mirror of life as a molecular index of aging. *Biochim. Biophys. Acta - Proteins Proteomics* **1866**, 840–847 (2018).
88. Kögl, F. & Erxleben, H. Zur Ätiologie der malignen Tumoren 1. Mitteilung über die Chemie der Tumoren. *Hoppe. Seylers. Z. Physiol. Chem.* **258**, 57–95 (1939).
89. Miller, J. A. Do Tumor Proteins Contain D-Amino Acids? A Review of the Controversy. *Cancer Res.* **10**, 65–72 (1950).
90. Stroud, E. D. & Smith, G. G. A search for d-amino acids in tumor tissue. *Biochem. Med.* **31**, 254–256 (1984).
91. He, X. *et al.* Serum metabolomics differentiating pancreatic cancer from new-onset diabetes. *Oncotarget* **8**, 29116–29124 (2017).
92. Nagata, Y. *et al.* High concentrations of D-amino acids in human gastric juice. *Amino Acids* **32**, 137–140 (2007).
93. Tamemasa, O., Goto, R., Suzuki, T., Preferential incorporation of some 14C-labeled D-amino acids into tumor-bearing animals. *Gann*, **69**, 517–523 (1978).

94. Sasamura, T., Matsuda, A. & Kokuba, Y. Tumor growth inhibition and nutritional effect of D-amino acid solution in AH109A hepatoma-bearing rats. *J. Nutr. Sci. Vitaminol.* **44**, 79–87 (1998).
95. Sasamura, T., Matsuda, A. & Kokuba, Y. Effects of D-methionine-containing solution on tumor cell growth in vitro. *Arzneimittel-Forschung/Drug Res.* **49**, 541–543 (1999).
96. Stegman, L. *et al.* Induction of cytotoxic oxidative stress by D-alanine in brain tumor cells expressing *Rhodotorula gracilis* D-amino acid oxidase: a cancer gene therapy strategy. *Human gene therapy*, **9**, 185–193 (1998).
97. Piossek, C. *et al.* Potent inhibition of angiogenesis by D,L-peptides derived from vascular endothelial growth factor receptor 2. *Thromb. Haemost.* **90**, 501–510 (2003).
98. Jiang, T. *et al.* Tumor imaging by means of proteolytic activation of cell-penetrating peptides. *Proc. Natl. Acad. Sci. U. S. A.* **101**, 17867–17872 (2004).
99. Jones, W., Griffiths, K., Barata, P. C. & Paller, C. J. PSMA theranostics: Review of the current status of PSMA-targeted imaging and radioligand therapy. *Cancers (Basel)*. **12**, (2020).
100. Maurer, T., Eiber, M., Schwaiger, M. & Gschwend, J. E. Current use of PSMA-PET in prostate cancer management. *Nat. Rev. Urol.* **13**, 226–235 (2016).

CHAPTER 2

Motivation and objectives of the thesis

Chapter 2. Motivation and objectives of the thesis

2.1 Justification of the study, hypothesis and objectives

In 2017, “La Caixa” Foundation funded a project to study the mechanism involved in the progression of prostate cancer, entitled “Eradicating prostate cancer metastasis before clinical manifestation”. The main objective of the project was to investigate how different molecular markers provide prostate cancer cells with metastatic capacity, and to exploit these markers for the development of imaging methods to identify metastatic cells. The project, led by Prof. Arkaitz Carracedo (CIC bioGUNE, Bilbao, Spain) required a multidisciplinary approach and involved different research institutions, including CIC biomaGUNE, with the participation of the Radiochemistry and Nuclear Imaging Group, led by Dr. Llop, and the Heterogeneous Biocatalysis Laboratory, led by Prof. López-Gallego.

One of the main specific objectives of the project was the development of radiolabelled molecular probes enabling more efficient and improved personalized diagnostic tools with application in positron emission tomography (PET) imaging. The development of such molecular probes asks for a multidisciplinary vision, comprising target and ligand structure identification, development of radiolabelling strategies and *in vivo* and *ex vivo* testing. Target and ligand structure identification was carried out by the group of Prof. Carracedo. Once the desired molecular probes had been identified, the (bio)synthesis of radiotracers following innovative radiolabeling strategies and the evaluation in animal models (provided by CIC bioGUNE) was carried out at CIC biomaGUNE.

The work conducted in the context of this PhD thesis has been divided in two main blocks, which constitute two experimental chapters (chapters 3-4).

The first part (chapter 3) is focused on all work related to the amino acid alanine. The work carried out comprises the development, refinement and automatization of synthetic strategies for the incorporation of two positron emitters, namely carbon-11

(^{11}C) and nitrogen-13 (^{13}N) in different positions of the native structure of alanine, by following synthetic and biocatalytic routes, respectively. The radiochemistry related to carbon-11 and nitrogen-13 labelling was carried out in the Radiochemistry and Nuclear Imaging Laboratory at CIC biomaGUNE, while the enzymatic strategies were designed and fine-tuned in the Heterogeneous Biocatalysis Laboratory. The use of two different radionuclides was expected to provide key information about the *in vivo* biodistribution, stability and uptake in different organs after administration to living organisms, in our case, a mouse model of prostate cancer which faithfully resembles the evolution of the human pathology. *In vivo* studies were complemented with *ex vivo* imaging studies and histological analyses.

The second part of the PhD thesis (chapter 4) is dedicated to all work that has been performed regarding the synthesis of glutamine radiolabelled with nitrogen-13 (^{13}N). Enzymatic strategies were designed and developed in the Heterogeneous Biocatalysis Laboratory, while radiolabelling strategies were carried out in the Radiochemistry and Nuclear Imaging Laboratory, both in CIC biomaGUNE. For this work, we had the collaboration of the Faculty of Chemistry and Chemical Technology at the University of Ljubljana (Slovenia) where some of the precursors were prepared.

2.2 Objectives

The general objective of this PhD thesis is the development of strategies for the radiolabelling of amino acids and study its biodistribution in a mouse prostate cancer model by positron emission tomography. To achieve this goal, the following specific objectives were defined:

1. To synthesize L-[*methyl*-¹¹C]alanine and D-[*methyl*-¹¹C]alanine with enough purity and enantiomeric excesses to perform imaging studies in mice, and to automatize the synthesis for both labelled amino acids, yielding a ready-to-inject radiotracer.
2. To produce Alanine Dehydrogenase by expression and purification of recombinant proteins, and apply the enzyme to the radiosynthesis of L-[¹³N]alanine.
3. To evaluate the *in vivo* biodistribution of L-[*methyl*-¹¹C]alanine, D-[*methyl*-¹¹C]alanine and L-[¹³N]alanine, after intravenous administration in a mouse prostate cancer model by using PET imaging and *ex vivo* complementary techniques, and correlate the findings with histological analysis.
4. To create a multi-enzymatic system capable of synthesizing L-glutamine from D-glutamine and express, purify and characterize the required enzymes.
5. To translate the method developed in objective 4 to the preparation of L-[¹³N]glutamine, using [¹³N]NH₃ as the labelling agent.

CHAPTER 3

Radiolabelled alanine

Chapter 3. Radiolabelled alanine

3.1 Introduction

Alanine-Serine-Cysteine-Threonine transporter type 2 (ASCT2, also known as SLC1A5), is an amino acid transporter that transports neutral amino acids into the cells to (i) preserve the concentration of neutral amino acids in cell plasma; and (ii) provide the cell with nutrients for metabolism¹. Among all ASCT2 substrates, L-alanine is known to be one of the dominants². ASCT2 transporter is well-known to be overexpressed in many tumors to satisfy their extraordinary demand of nutrients (Figure 3.1). Thus, it is considered as a promising biomarker in cancer.

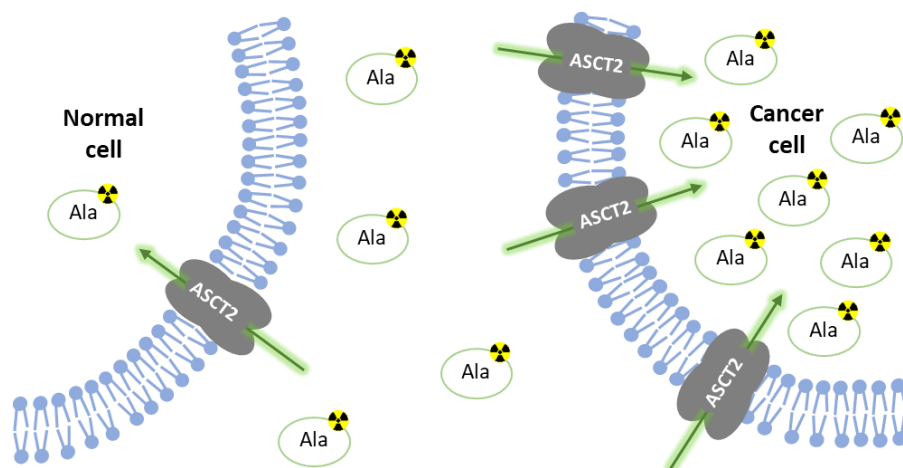


Figure 3.1 Schematic representation of membranes from normal cells and tumor cells, the latter with overexpressed ASCT2 and hence capable of uptaking more Alanine than normal cells.

In this context, the radiolabelling of alanine with a positron emitter could become a very interesting tool for the investigation of ASCT2 using Positron Emission Tomography (PET) imaging, both at the preclinical (animal models) and clinical levels.

Chapter 3. Radiolabelled alanine

Based on this narrative, we considered that the radiolabelling of L-alanine with different positron emitters (*i.e.* carbon-11 and nitrogen-13) may provide information on the expression of ASCT2 *in vivo* and at the whole body level, thus enabling the investigation of metabolic aspects of cancer cells in animal cancer models. Additionally, thanks to the incorporation of the radionuclide in different positions, information about the metabolism of the amino acid could be obtained.

As previously described by our group, the application of enzyme-mediated reactions applied to ^{13}N -radiochemistry is very promising. In this chapter, we used a previously described methodology for the enzymatic radiosynthesis of L- ^{13}N alanine with some modifications, aimed at improving the quality of the final radiotracer in terms of purity. Also, L-alanine was radiolabelled with carbon-11 by following a previously described methodology³, which was also applied to the preparation of ^{11}C D-alanine. It is worth mentioning that D-amino acids have gained a notable attention during the last years after the pioneering work of Tamemasa *et al.* in which by using ^{14}C -labelled amino acids in animal models, it was demonstrated that D-alanine, D-leucine, and D-tryptophan showed higher tumor accumulation than the corresponding L-forms⁴. Because of that, we hypothesized that the radiolabelling of both enantiomers could provide interesting information about differences in tumour uptake, enabling the development of new diagnostic or prognostic tools.

After radiolabelling, we evaluated the biodistribution and tumour accumulation of ^{11}C -labelled L- and D-alanine, and ^{13}N -labelled alanine in a mouse prostate cancer model using PET. First, fully automatic procedures for the radiosynthesis of the two enantiomeric forms of the ^{11}C -labelled amino acid were implemented. Also, an enzymatic methodology to produce ^{13}N -labelled alanine was implemented and refined. PET studies were carried out in an orthotopic animal model of Prostate Cancer (PC), driven by the conditional deletion of the tumour suppressor Phosphatase and tensin homolog (PTEN) in the prostate epithelia⁵. Contrary to most of the commonly used heterotopic cancer models, this animal model results in hyper-proliferative lesions that

lead to prostate cancer within 6 months of age, faithfully recapitulating the stepwise process of the disease in humans. Through PET studies, dynamic information of the biodistribution of labelled amino acids and tumour accumulation could be obtained in a non-invasive fashion. Imaging results were correlated to *ex vivo* analysis using PET imaging on excised prostates and histological studies.

3.2 Objectives

The specific objectives of this chapter are:

1. To synthesize L-[*methyl*- ^{11}C]alanine and D-[*methyl*- ^{11}C]alanine with enough purity and enantiomeric excesses to perform imaging studies in mice.
2. To automatize the enantioselective synthesis for both labelled amino acids, yielding a ready-to-inject radiotracer.
3. To produce Alanine Dehydrogenase by expression and purification of recombinant proteins, and apply the enzyme to the radiosynthesis of L-[^{13}N]alanine.
4. To evaluate the *in vivo* biodistribution of the three radiotracers after intravenous administration in a mouse prostate cancer model by using PET imaging and *ex vivo* complementary techniques, and correlate the findings with histological analysis.

3.3 Materials and methods

3.3.1 Reagents

N-(Diphenylmethylene)glycine *tert*-butyl ester (purity $\geq 98\%$), *O*-Allyl-*N*-(9-anthracenylmethyl)cinchonidinium bromide (purity $\geq 90\%$), cesium hydroxide monohydrate (purity $\geq 99.95\%$), ammonium formate (purity $\geq 99\%$), L-alanine (purity $\geq 98\%$), D-alanine (purity $\geq 98\%$) and sodium pyruvate (purity $\geq 99\%$) were purchased from Sigma Chemical Co. (St. Louis, IL, USA) and used without further purification. β -Nicotinamide adenine dinucleotide (NAD^+) and its reduced form (NADH), were purchased from GERBU Biotechnik GmbH (Wieblingen, Germany). Bradford protein assay reagent was purchased from BIO-RAD, USA.

Solid phase extraction (SPE) cartridges (Sep-Pak[®] C18 Plus and CM) were obtained from Waters (Waters[®] Association, MA, USA) and ion retardation resin (AG[®] 11-A8) was purchased from BIO-RAD, USA. The C18 cartridges were preconditioned with 10 mL ethanol, followed by 10 mL ultrapure water. The AG[®] 11-A8 resin packed column was preconditioned with 10 mL 0.5 M NaCl followed by 30 mL of ultrapure water.

The gene of L-alanine dehydrogenase (L-AlaDH) from *Bacillus subtilis*, was synthesized and cloned into pET28b by GenScript company (Piscataway, USA).

3.3.2 Synthesis of phase transfer catalyst 2 (PTC-2)

Synthesis of *N*-(9-anthracenylmethyl)cinchoninium chloride

To a solution of cinchonine (1 g, 3.4 mmol) in toluene (14 mL), 9-(chloromethyl)anthracene (770 mg, 3.74 mmol) was added. The reaction mixture was stirred at reflux overnight. Then, the solution was cooled to room temperature and poured onto 40 mL of diethyl ether and filtered. A light-yellow solid was obtained (1.389 g, 2.67 mmol, 78%).

Synthesis of *O*-Allyl-*N*-(9-anthracenylmethyl)cinchoninium bromide

N-(9-anthracenylmethyl)cinchoninium chloride (150 mg, 288 μmol) was dissolved in dichloromethane (DCM, 2 mL). To this solution, allyl bromide (78 μL , 684 μmol) and aqueous 50 % KOH (0.2 mL) were added. The resulting mixture was stirred vigorously at room temperature for 8 hours. The mixture was then diluted with water (10 mL) and extracted with dichloromethane (DCM; 3 x 15 mL). Organic fractions were combined, dried over Na_2SO_4 , filtered and concentrated to dryness in vacuo to give an orange solid. The solid was suspended in ice cold diethyl ether and filtered to give a light orange solid (139 mg, 221 μmol , 76%). A small fraction of filtered solid (*ca.* 40 mg) was purified by column chromatography (solvents DCM/MeOH 20:1).

3.3.3 Radiochemistry: production of L- and D-[methyl- ^{11}C]alanine

Carbon-11 (^{11}C) was produced in an IBA Cyclone 18/9 cyclotron by the $^{14}\text{N}(p,\alpha)^{11}\text{C}$ reaction. The reaction is produced via the bombardment of nitrogen gas containing small amounts of hydrogen gas with high energy protons (*ca.* 16 MeV). The beam current was maintained at 18 μA (pressure into the target during bombardment was 25 bar) to reach the desired integrated currents (1-4 μAh). This way, the so-called primary precursor [^{11}C]CH₄ was produced in the target.

[^{11}C]CH₄ was transferred to a TRACERlab FX_{C Pro} synthesis module (GE Healthcare, Waukesha, WI, USA) where [^{11}C]CH₃I was generated via the gas-phase method⁶. At the end of the process, [^{11}C]CH₃I was distilled under continuous helium flow (20 mL/min) and introduced in a closed reaction vial pre-charged with *N*-(Diphenylmethylene)glycine *tert*-butyl ester (3 mg), the phase transfer catalyst (*O*-Allyl-*N*-(9-anthracenylmethyl)cinchonidinium bromide for L-[methyl- ^{11}C]alanine; *O*-Allyl-*N*-(9-anthracenylmethyl)cinchoninium bromide for D-[methyl- ^{11}C]alanine; 1 mg), CsOH·H₂O (12 mg) as the base, toluene (100 μL) and DCM (15 μL). The reaction was allowed to occur for 4 minutes at room temperature, the mixture was diluted with mobile phase (ammonium formate 10 mM pH 8.3/acetonitrile/tetrahydrofuran; 1.5 mL; 30/52.5/17.5) and purified by means

of high-performance liquid chromatography (HPLC) using a semipreparative Mediterranean Sea 18 column (9.6 x 250 mm, 5 μ m particle size; Teknokroma, Barcelona, Spain) as the stationary phase (flow = 4 mL/min). The collected fraction (retention time: 12-13 min) was reformulated by dilution with water (20 mL), retention on a C-18 cartridge (Sep-Pak®Light, Waters, Milford, MA, USA) and elution with ethanol/1 M aqueous HCl solution (2 mL, 1:1). The eluted solution was introduced into a second reactor and heated at 100°C for 8 minutes to remove the protecting groups. The resulting solution was diluted with water (2 mL) and eluted through a C-18 cartridge (Sep-Pak®Light, Waters, Milford, MA, USA) and an AG® 11-A8 resin packed column connected in series. The eluate was collected in the final vial after filtration through a 0.22 μ m sterile filter, yielding ready-to-inject radiotracer. Total production time was *ca.* 45 min.

Quality control

Radiochemical purity was determined by HPLC, using an Agilent 1200 Series chromatograph equipped with a multiple wavelength UV detector (λ = 254 nm) and a Gabi radiometric detector (Raytest GmbH, Radeberg, Germany) connected in series. A great Smart RP18 (4.6 x 250 mm; 5 μ m) column was used as stationary phase and acetonitrile/10 mM ammonium formate pH 8.3 (70/30, v/v) as the mobile phase at a flow rate of 1 mL/min. Retention time for both L- and D-[*methyl*-¹¹C]alanine was 3 min.

Enantiomeric purity was determined by radio-HPLC using an analytic ReproSil Chiral-AA (8 μ m; 4.6 x 250 mm) column as the stationary phase and methanol/water (70/30, v/v) as the mobile phase (flow rate = 1 mL/min). UV monitoring was conducted at 214 nm. Retention times were 7 min and 19 min for L-[*methyl*-¹¹C]alanine and D-[*methyl*-¹¹C]alanine respectively.

3.3.4 Animal experimentation

General considerations

Animals were maintained and handled in accordance with the Guidelines for Accommodation and Care of Animals (European Convention for the Protection of Vertebrate Animals Used for Experimental and Other Scientific Purposes). All animal procedures were performed in accordance with the European Union Animal Directive (2010/63/EU). Experimental procedures were approved by the corresponding Ethical Committees. Animals were bred at CIC bioGUNE (Bilbao, Spain) and transferred to CIC biomaGUNE (San Sebastian, Spain) at the age of *ca.* 3 months. PET imaging sessions were carried out at the age of 4 and 7 months. Each animal underwent two PET scans. During the whole period, animals were housed in ventilated cages and fed on a standard diet *ad libitum*.

In vivo studies

Mice (29-36 g, PTEN) were anesthetized using a mixture of 4% isoflurane in O₂ for induction, and with 1-2% isoflurane for maintenance. Body temperature and respiration were monitored throughout the scan. The administration of L-, D-[*methyl*-¹¹C]alanine and L-[¹³N]alanine was performed through the tail vein and image acquisition (dynamic scan; 22 Frames: 4 x 10 s, 4 x 30 s, 4 x 60 s, 3 x 120 s, 3 x 240 s, 1 x 680 s; 1 bed position with an axial field of view of 10 cm, sufficient to cover the whole animal) was started immediately after administration using a β -CUBE preclinical platform (Molecubes, Gent, Belgium). After finalizing the PET imaging session, a whole-body computerized tomography (CT) scan (β -CUBE preclinical platform; Molecubes, Gent, Belgium) was acquired. PET data were reconstructed by 3D-OSEM iterative image reconstruction algorithm (30 iterations, with a reconstructed voxel size of 400 μ m) and processed with PMOD (PMOD Technologies LLC) software analysis tool. Volumes of interest (VOIs) were drawn in the brain, heart, lungs, liver, kidneys, prostate and bladder, and dynamic time-activity curves (TACs) were obtained over the whole duration of the scan. Animals were

Chapter 3. Radiolabelled alanine

scanned at 7 months old, in which hyper-proliferative lesions have already become cancer lesions (see Table 3.1 for scheme of the imaging schedule).

Ex vivo studies

Animals were sacrificed immediately after the *in vivo* acquisition carried out at the age of 7 months. After sacrifice, the prostates (still containing radioactivity) were excised and placed into the PET-CT scanner, and a 10 min PET scan was carried out using a MOLECUBES β -CUBE scanner. After the PET scan and to provide anatomical information of each prostate and the attenuation map for the reconstruction for the PET images, a CT acquisition was performed by using a MOLECUBES X-CUBE scanner.

Table 3.1 Scans established for the *in vivo* and *ex vivo* biodistribution studies.

Mice (n)	<i>in vivo</i> Scan			<i>ex vivo</i> Scan		
	L-[methyl- ¹¹ C]alanine	D-[methyl- ¹¹ C]alanine	L-[¹³ N]alanine	L-[methyl- ¹¹ C]alanine	D-[methyl- ¹¹ C]alanine	L-[¹³ N]alanine
1	✓	✓	✓	✓	-	-
2	✓	✓	✓	✓	-	-
3	✓	✓	✓	✓	-	-
4	✓	✓	✓	-	✓	-
5	✓	✓	✓	-	✓	-
6	✓	✓	✓	-	✓	-

3.3.5 Image quantification

PET and CT images of the same animal were co-registered and analyzed using PMOD image processing tool. For *in vivo* studies, volumes of interest (VOIs) were created on selected organs (brain, lungs, heart, liver, kidneys, prostate and bladder). The concentration of radioactivity (decay corrected to the start of the PET scan) in each organ was obtained as cps/cm³ and transformed into real activity (Bq/cm³) by using a calibration factor, previously obtained from scans performed on a phantom under the

same experimental conditions (isotope, reconstruction algorithm and energetic window).

3.3.6 Alanine dehydrogenase enzyme production

Expression. Overnight cultured of E.Coli BL21 (1 mL) transformed with the plasmid which codifies L-AlaDH from *Bacillus subtilis* was inoculated in a 50 mL of LB (Luria-Bertani) broth, containing the antibiotic kanamycin at a final concentration of 30 µg/mL. To reach the successful overexpression of Alanine dehydrogenase, the resulting culture was incubated at 37°C with vigorous shaking until the optical density at 600 nm (OD_{600nm}) reached 0.6. Then IPTG (1-thio-β-d-galactopyranoside) was added to the culture to a final concentration of 1 mM to induce protein synthesis. Cells were grown at 37°C for 3 hours and harvested by centrifugation at 1290g for 30 min.

Purification. The resulting pellet from 50 mL culture, was resuspended in 5 mL (one-tenth of its original volume) of sodium phosphate buffer (25 mM pH 7). Cells were broken by sonication at amplitude 50%, 0.5 s intervals during 20 min. The resulting suspension was centrifuged at 10528g for 30 min. The supernatant which contains the enzyme was collected and analyzed by 12% SDS-PAGE (Sodium dodecyl sulphate polyacrylamide gel electrophoresis) (Coomassie Blue staining) to determine enzyme purity.

3.3.7 Determination of the protein concentration

The protein concentration of the soluble enzyme was determined by Bradford's method by using bovine serum albumin (BSA) as protein standard. The soluble enzyme (5 µL) and Bradford reagent (200 µL) were mixed in a 96-well plate. The absorbance was measured in the spectrophotometer at 595 nm after 5 min of reaction at 25°C. For the standard curve, a series of BSA solutions with known concentrations (concentration = 0.06, 0.12, 0.25, 0.5 and 1 mg/mL) was used.

3.3.8 Determination of enzyme activity

Alanine dehydrogenase's activity was measured using the following protocol. Pyruvate (75 mM) was mixed with NADH (Nicotinamide-adenine dinucleotide, 0.5 mM) as the cofactor and NH_4Cl (500 mM) as the ammonia source, all dissolved in a total volume of 200 μL of phosphate buffer 100 mM pH 8. The reaction was started by the addition of 5 μL of AlaDH and the conversion of NADH into NAD^+ was followed in the spectrophotometer at 340 nm. 1 Unit of AlaDH was defined as the necessary amount of enzyme that was required for the reductive amination of 1 μmol of pyruvic acid per minute. Reaction was performed in 96-well transparent plates in a Varioskan™ Flash Multimode Reader (Thermo Scientific).

3.3.9 Enzymatic synthesis of L- ^{13}N]alanine

Production of the radiolabelling agent $^{13}\text{N}[\text{NH}_4\text{OH}]$

Nitrogen-13 (^{13}N) was produced in an IBA Cyclone 18/9 cyclotron by the $^{16}\text{O}(p,\alpha)^{13}\text{N}$ reaction. The target system consists in an aluminum insert (2 mL) covered with havar foil (thickness 25 μm , \varnothing 29 mm) and with an aluminum vacuum foil (thickness 25 μm , \varnothing 23 mm). The target, containing 1.7 mL of 5 mM EtOH aqueous solution, was irradiated with 18 MeV protons. The beam current was maintained at 22 μA (range pressure into the target during bombardment was 5-10 bar) to reach the desired integrated currents (1-4 μAh). The resulting solution was collected in a 10 mL vial, and the activity was measured in a dose calibrator (Capintec CRC®-25 PET, New Jersey, USA).

Production of L- ^{13}N]alanine

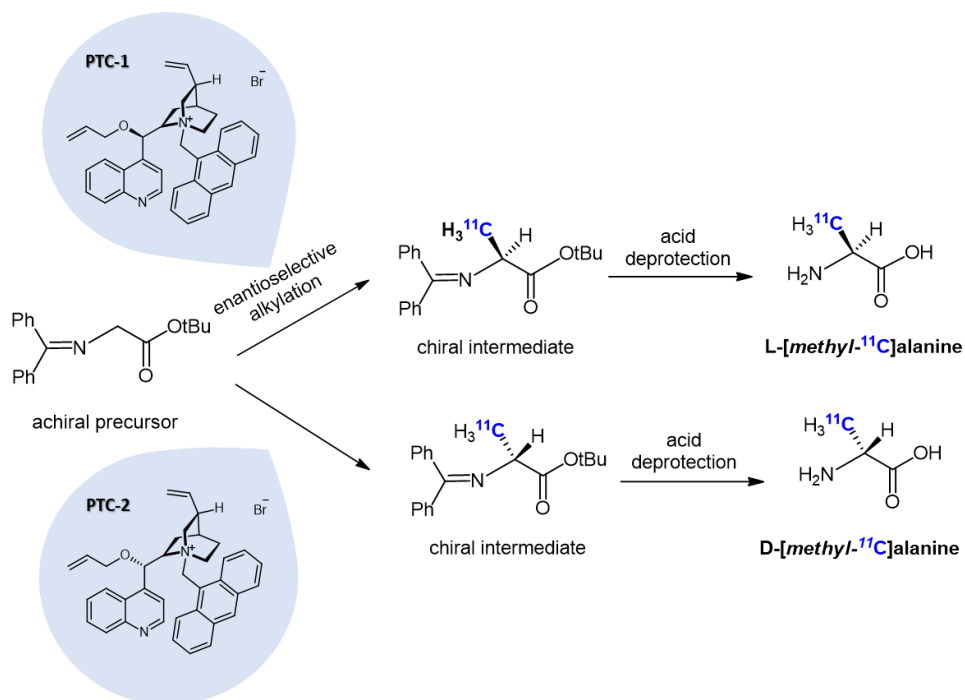
A mixture of pyruvic acid (26 μL from a 750 mM stock solution, final concentration in reaction: 65 mM) and NADH (13 μL from a 10 mM stock solution, final concentration in reaction: 0.5 mM) stocks were prepared in sodium phosphate buffer 325 mM pH 8. Additional 61 μL of the previous buffer were added. Then $^{13}\text{N}[\text{NH}_4\text{OH}]$ (100 μL , 310.8 MBq) was added and the reaction was started by the addition of Alanine Dehydrogenase (100 μL , 54 U/mg). The reaction was conducted for 10 minutes and stopped by centrifugation with a 30 kDa cut-off membrane. The filtrate containing the unreacted

$[^{13}\text{N}]\text{NH}_4\text{OH}$ and L- $[^{13}\text{N}]\text{alanine}$ was basified to pH 11 by addition of NaOH (10 μL , 1M) and heated during 15 minutes. Then, the solution was cooled to room temperature and neutralized by addition of HCl (10 μL , 1M) yielding a ready-to-inject radiotracer.

3.4 Results and discussion

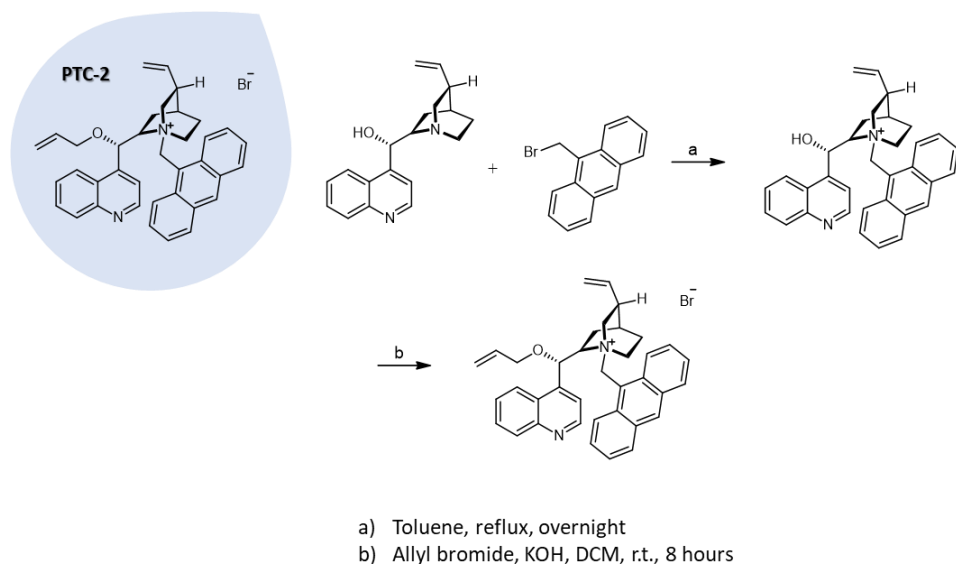
3.4.1 Synthesis of L- $[methyl-^{11}\text{C}]\text{alanine}$ and D- $[methyl-^{11}\text{C}]\text{alanine}$

The stereoselective synthesis of L- and D- $[methyl-^{11}\text{C}]\text{alanine}$ was accomplished by adapting a recently published method using a phase-transfer catalyst^{3,7}, via asymmetric alkylation of glycine-derived precursors and using $[^{11}\text{C}]\text{methyl iodide}$ ($[^{11}\text{C}]\text{CH}_3\text{I}$) followed by acid-catalyzed hydrolysis of the protecting groups (Scheme 3.1).



Scheme 3.1 Synthetic pathway for the enantioselective radiosynthesis of L- and D- $[methyl-^{11}\text{C}]\text{alanine}$ *via* asymmetric alkylation of a glycine-derived Schiff base with $[^{11}\text{C}]\text{CH}_3\text{I}$.

The catalyst required for the enantioselective production of the L- enantiomer was commercially available (PTC-1 in Scheme 1). We anticipated that the diastereoisomer of this catalyst (PTC-2 in Scheme 1) could catalyze the synthesis of the D- amino acid. PTC-2 was not commercially available, and hence we first tackled its preparation by reacting cinchonine and 9-methyl-antraceni bromide to yield the intermediate alcohol, which was then alkylated to yield the desired phase transfer catalyst 2 (Scheme 3.2).



Scheme 3.2 Synthetic pathway for the production of phase transfer catalyst-2 (PTC-2) required for the enantioselective synthesis of D-[*methyl*- ^{11}C]alanine; DCM: dichloromethane; r.t.: room temperature.

The process was initially carried out manually, in order to have better control on the different synthetic steps, and the reaction was monitored via radio-HPLC. Alkylation, performed as the first step, was successful as revealed by the presence of a radioactive peak in the chromatogram with a retention time around 9 minutes (Figure 3.2, A). Despite the identity of the compound was not confirmed by co-elution with reference standard, the fact that the retention time is longer than the retention time of the precursor (*ca.* 1 minute difference between retention times) strongly suggests the formation of the methylated species, which is less polar than the precursor and hence is

Chapter 3. Radiolabelled alanine

more strongly retained in reverse phase chromatography. This radioactive peak was the one selected for collection during the automatization of the process (see below).

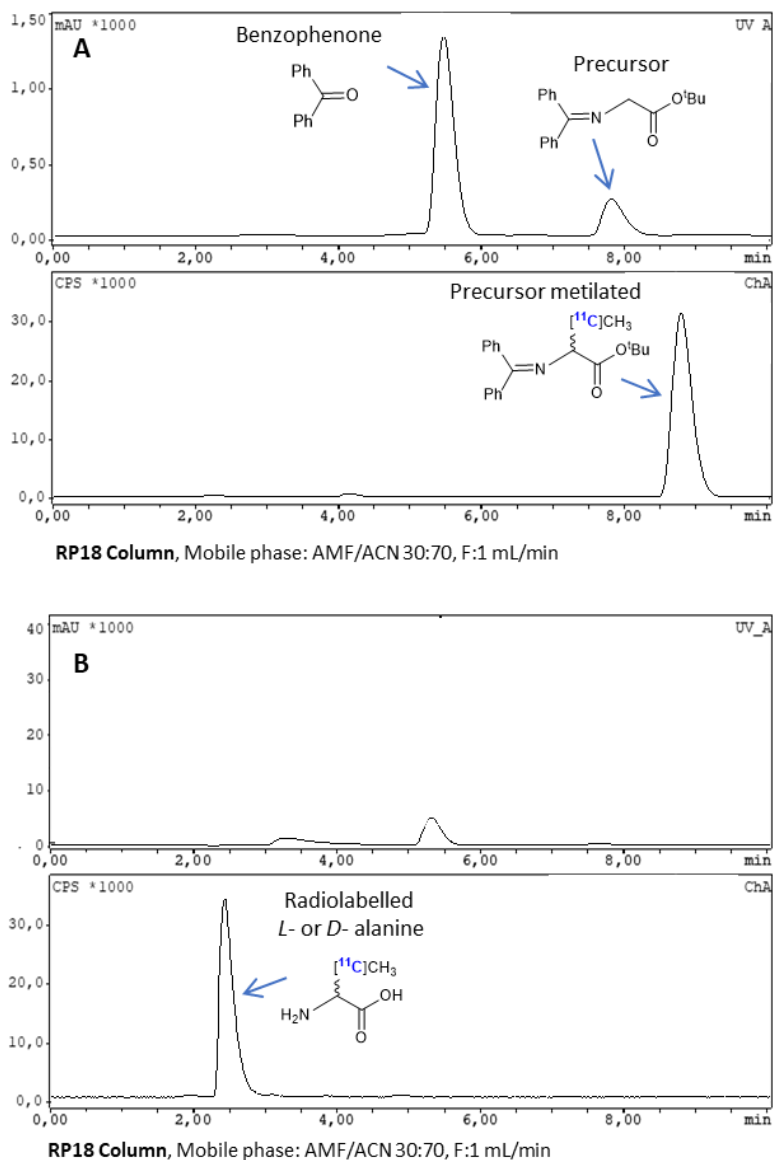


Figure 3.2 HPLC profiles corresponding to UV (top) and radioactive (bottom) detectors. A) Signals after alkylation step of the precursor with $[^{11}\text{C}]\text{CH}_3$; B) Signals after deprotection step.

After alkylation, the acidic deprotection was carried out and the reaction crude was analyzed. First, the same chromatographic conditions as above were applied (Figure 3.2, B). As it can be seen, the peak with retention time = 9 min disappeared, and a major peak with retention time around 3 minutes appeared, corresponding to L-[methyl- ^{11}C]alanine or D-[methyl- ^{11}C]alanine.

The chromatogram (UV detector) also revealed the presence of a major with retention time of approximately 5.5 min, corresponding to benzophenone. Indeed, benzophenone is a by-product originated from the precursor. Despite the presence of this by-product, the chromatogram obtained with the radioactive detector confirmed that the reaction gives *quasi*-quantitative conversion under these conditions, and virtually all methyl iodine (retention time = 3 min) is incorporated to the precursor. At this stage, it was not possible to discriminate between the two enantiomers, as both would have identical retention times under the chromatographic conditions used.

In order to assess the enantiomeric purity of the labelled species, HPLC analysis using a chiral column was carried out and the enantiomeric excess was determined (see Figures 3.3A and 3.3B for the L- and D- enantiomers, respectively).

In both cases enantiomeric excesses were 90%, values that are considered to be sufficient for subsequent *in vivo* studies.

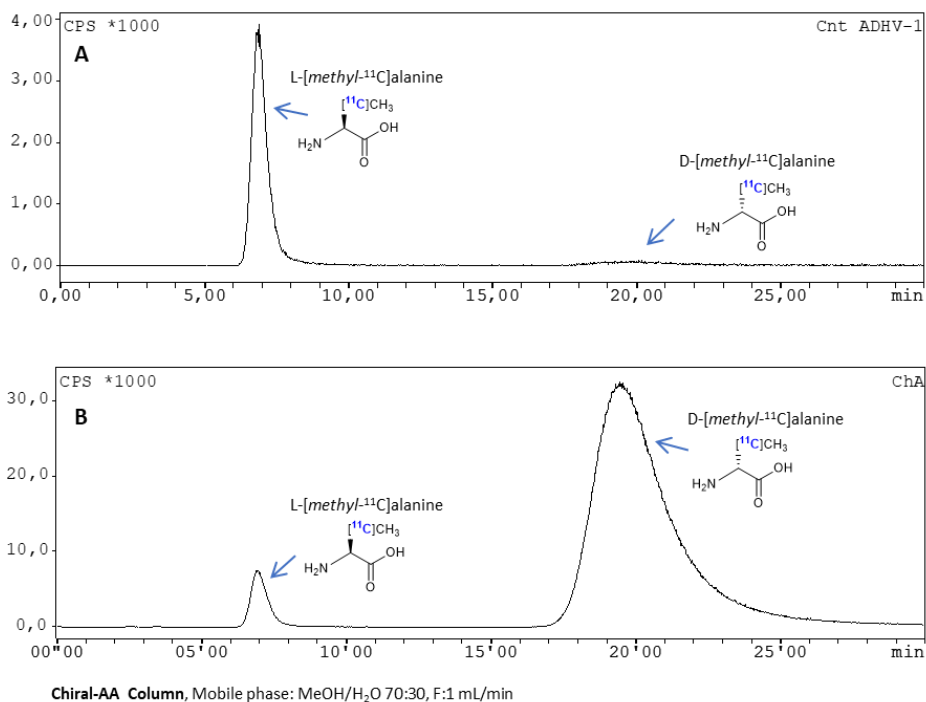


Figure 3.3 HPLC profiles of the radioactive signal corresponding to L-[methyl- ^{11}C]alanine (A) and D-[methyl- ^{11}C]alanine (B).

3.4.2 Automatization

Even though the preparation of L-[methyl- ^{11}C]alanine has been already reported³, the methodology requires further development in order to achieve fully automated production, which would allow *in vivo* studies at the preclinical level and eventual translation into the clinics. The use of automated synthesis modules for the preparation of radiopharmaceuticals has several advantages, including: (i) facilitates transfer of the methodology to other institutions; (ii) as all the synthetic procedure can be controlled remotely and the synthesizer is located in a shielded “hot cell”, the radiation dose received by personnel involved in the production is dramatically minimized; and (iii) different variables during the process can be controlled and monitored, and all

Chapter 3. Radiolabelled alanine

individual steps are carried out always in the same way, thus facilitating translation of the conditions to a good manufacturing practices (GMP)-compliant laboratory.

In our case, the automated process was implemented in a TRACERlab FXC_{pro} synthesizer (see Fig. 3.4 for scheme).

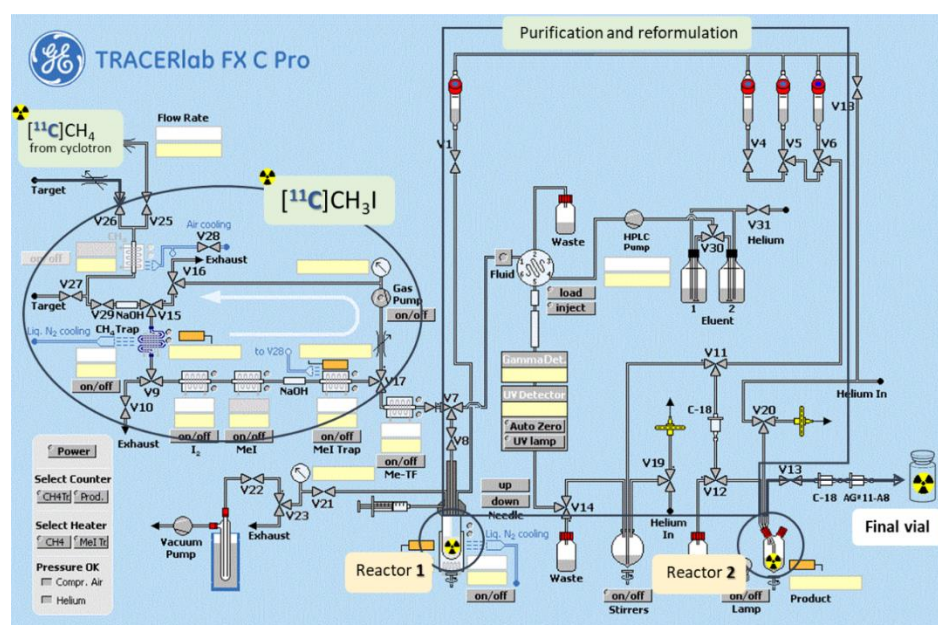


Figure 3.4 Scheme representing the TRACERlab FX C pro synthesizer and the general synthetic steps.

In the synthetic process, radioactive carbon-11 is first produced in the cyclotron target as radioactive methane. After finishing the cyclotron beam, the radioactive methane is transferred to the hot cell, and it enters in a circuit to produce radioactive methyl iodine ($[^{11}\text{C}]\text{CH}_3\text{I}$). The production of $[^{11}\text{C}]\text{CH}_3\text{I}$ is based on the iodination of $[^{11}\text{C}]\text{methane}$ ($[^{11}\text{C}]\text{CH}_4$).

$[^{11}\text{C}]\text{CH}_4$ is trapped in a Carbosphere trap pre-cooled to -180°C . After complete trapping, heating is applied and $[^{11}\text{C}]\text{CH}_4$ is released and introduced in a circulating loop, where it is mixed with iodine at 720°C . $[^{11}\text{C}]\text{CH}_3\text{I}$ is continuously generated and retained in a

second trap, while unreacted [^{11}C]CH₄ is recirculated to undergo subsequent reaction steps with iodine using a pump.

After 6-7 reaction cycles, [^{11}C]CH₃I is distilled into a reaction vessel, pre-charged with all reagents required for the first reaction step (methylation). After this step, a purification step is carried out via semi-preparative HPLC, and the fraction corresponding to the pure labelled amino acid (still bearing protective groups) is collected in a 100 mL container (bulb vessel) pre-charged with water. The resulting solution is flushed through a C18 Sep-Pak cartridge in which the product will be trapped. This step allows removal of the solvents used during purification via HPLC. After elution of the labelled species using an acidic solution and collection in a second reactor (reactor 2) the protective groups are removed by heating under acidic conditions. After hydrolysis, the pure labelled amino acid is obtained by purification using two solid phase extraction cartridges connected in series: one C18 Sep-Pak cartridge (to trap possible non-hydrolyzed species) and AG[®]11 A8 resin, which is an ionic exchange resin that neutralizes the final solution by removing the excess protons. Final filtration through a sterile filter into the final vial yields the pure amino acid ready to be injected.

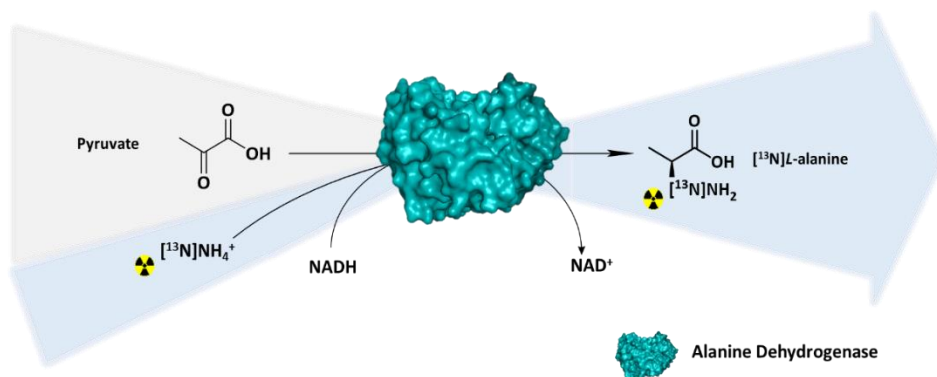
Both radiotracers, L- and D-[*methyl*- ^{11}C]alanine could be successfully synthesized using the above mentioned automated process. L- and D-[*methyl*- ^{11}C]alanine were obtained in a non-decay corrected radiochemical yield (RCY) of $10.2\pm 1.2\%$ (N = 25) and $10.3\pm 1.1\%$ (N = 20) respectively, with respect to [^{11}C]CH₃I in less than 40 min from the end of bombardment, including purification and reformulation. Radiochemical purities were >99% in all cases. Chiral HPLC analysis of the final products demonstrated enantiomeric excess were >90% in both cases.

The RCY values obtained are similar to those recently reported for the synthesis of D-[^{11}C]-Ala(decay-corrected RCY reported: $39.2\pm 3.3\%$, radiochemical purity reported >95% and enantiomeric excess reported: 89.2%)⁷. Noteworthy, in this previous work the purification of the labelled amino acid was not achieved by HPLC, but using solid phase extraction, which is a simpler and faster methodology. Still, this previous method

required the recovery of the compound from the purification cartridge using trifluoroacetic acid, which was then eliminated by three evaporation cycles using acetonitrile. This step was difficult to automate in our hands, and hence we decided to apply HPLC purification followed by reformulation. This reformulation by trapping the reaction intermediate into a C18 Sep-pak cartridge can be done thanks to the presence of the protecting groups, which are already present after the methylation step. These protecting groups make the amino acid more hydrophobic and due to the reverse phase nature of the extraction cartridge, it can be easily retained.

3.4.3 Radio-Enzymatic synthesis of L-[¹³N]alanine

Radiolabelled L-[¹³N]alanine was produced by a one-pot radiosynthesis catalyzed by L-alanine Dehydrogenase from *Bacillus subtilis* (Scheme 3.3). The reductive amination of pyruvate is catalyzed using NADH as cofactor and cyclotron-produced, no-carried-added [¹³N]NH₄OH as amine source⁸.



Scheme 3.3 Radio-enzymatic synthesis of L-[¹³N]alanine starting by pyruvate and using [¹³N]NH₄OH as ammonia source and NADH as enzyme's cofactor.

This synthesis has already been reported by our research group⁸. However, significant modifications were implemented during this PhD thesis, mainly in the purification step.

In previous works, the purification was based on filtration through a cut-off membrane, which also served as a means to quench the reaction. This approach may lead to the presence of unreacted [^{13}N] NH_4OH in the final solution. To overcome this problem, we implemented an additional step in which after quenching the enzymatic reaction by centrifugal filtration using a cut-off membrane, the resulting solution was collected and basified to pH 11 by adding aqueous NaOH (1 M, 10 μL), in order to have all free ammonia in the form [^{13}N] NH_3 . Heating at 100°C for 15 min resulted in elimination of all unreacted ammonia. This process was validated previously to being used in routine syntheses. With that aim, [^{13}N] NH_4OH produced in the cyclotron was basified as above and submitted to heating (100°) for 5, 10 and 15 min. Subsequent analysis via HPLC demonstrated that ammonia almost gets removed from the solution after 15 min of heating, because the area of the radioactive peak decreases significantly (Figure 3.5, A). In parallel, a solution containing non-labelled alanine was submitted to the same treatment, and it was analyzed by HPLC (UV detection, $\lambda = 220$ nm, wavelength in which alanine can be detected). With this process, we confirmed that alanine is not removed from the solution or decomposed after 15 min of heating (Figure 3.5, B). Also, control experiments to demonstrate the relevance of the pH of the solution was carried out. With that aim, the same process was repeated but the pH of the solution was adjusted at 8. As expected, during this control neither ammonia nor alanine could be removed from the solution (Table 3.2).

Before injection, the solution was neutralized with HCl (1 M, 10 μL). It is well known that it is not recommended the use of strong acids or bases to modify the pH of the solutions, because a small error can drastically change the pH from one extreme to the other. In our case, this approach was appropriate as: (i) the solution to be neutralized already contained a phosphate buffer (325 mM); and (ii) the use of a strong acid allowed for neutralization with a minimal impact on the reaction volume (that was 250 μL). Indeed, an increase in the reaction volume would decrease the concentration of radioactivity, and hence higher volumes would be required to perform *in vivo* studies.

Chapter 3. Radiolabelled alanine

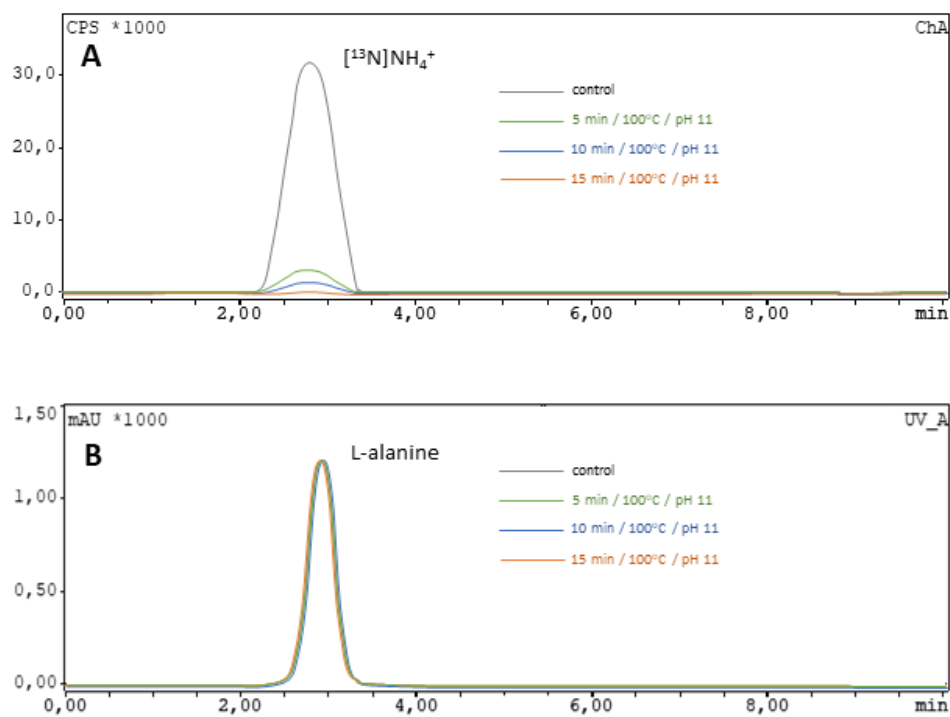


Figure 3.5. A) radio-HPLC obtained for an [¹³N]NH₄OH solution before and after being heated at 100°C, pH=11 for 5, 10 and 15 min. B) HPLC profile (UV detector, λ=220 nm) corresponding to non-labelled L-alanine before and after being heated at 100°C, pH=11 for 5, 10 and 15 min .

Table 3.2. Percentages obtained after heating a mixture of radioactive ammonia and cold alanine during different times and pH values, based on the comparison of HPLC areas.

Heating time	Ammonia % C.P.S.			Alanine % UV 220nm		
	5 min	10 min	15 min	5 min	10 min	15 min
pH 8	100%	100%	100%	100%	100%	100%
pH 11	14%	4.1%	0.1%	100%	100%	100%

By following this methodology, L-[^{13}N]alanine could be produced with a radiochemical yield (decay-corrected) of $40.3 \pm 2.1\%$ in overall production time of *ca.* 30 min from EOB.

3.4.4 Whole body dynamic *in vivo* PET studies

Whole-body bio-distribution PET studies of L- and D-[*methyl*- ^{11}C]alanine and L-[^{13}N]alanine in diseased animals was carried out to see differences in radiotracer accumulation in major organs such as the brain, the heart, the lungs, the liver, the kidneys and the bladder. As explained in the materials and methods section, animals were scanned at the age of 7 months. We decided to focus our imaging study only in the results obtained at 7 months because at this point, we know with certainty that hyper-proliferative lesions are become prostate cancer. Dynamic images obtained immediately after intravenous injection of the labelled amino acids at the age of 7 months showed a different biodistribution pattern depending on the isotope an enantiomer injected (Figure 3.6).

Major organs can be easily identified on the CT images, and hence these images were used to manually delineate volumes of interest (VOIs) in each organ. VOIs were then transferred to PET images and the concentration of radioactivity in each organ could be determined as a function of time (Figure 3.7).

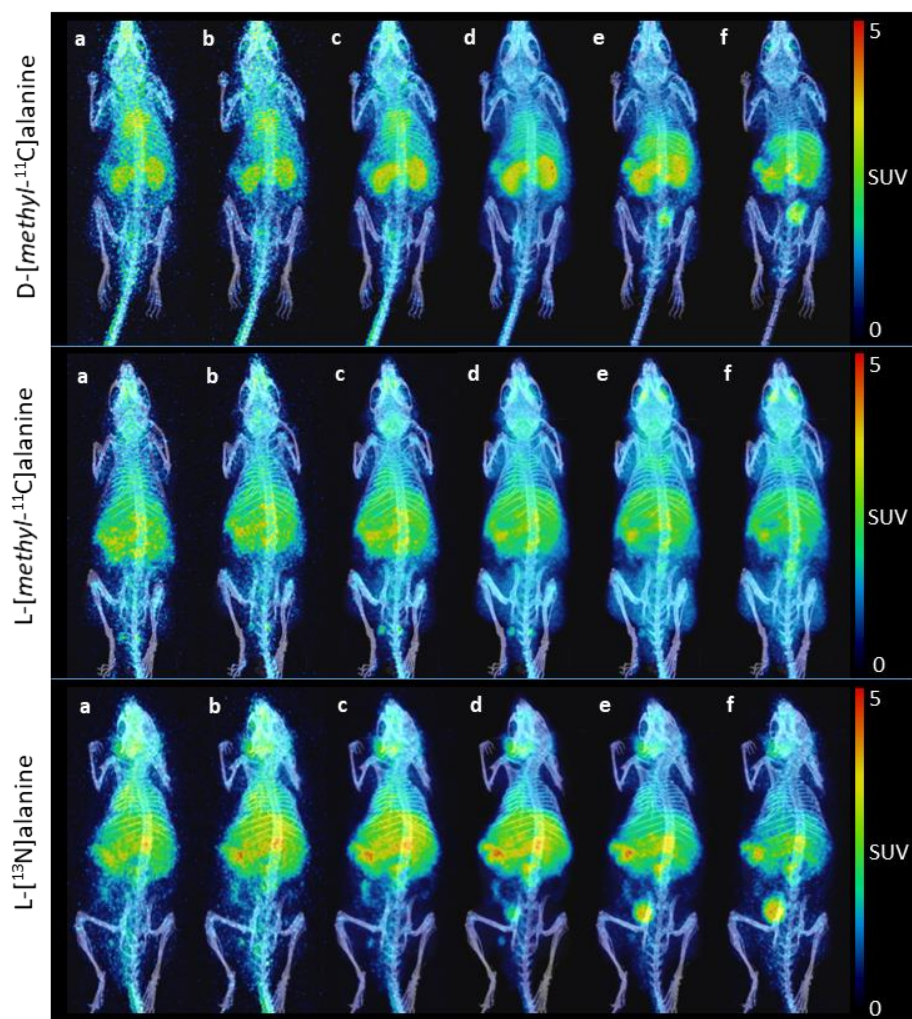


Figure 3.6 PET images (coronal projections) co-registered with representative CT slices for co-localization of the radioactive signal, obtained at different times after intravenous administration of the three labelled amino acids, at the age of 7 months. Images are maximum intensity projections (MIP), expressed as standard uptake value (SUV), and correspond to averaged data of the following time frames: (a) 0-0.5 min; (b) 0.5-1 min; (c) 1-4 min; (d) 4-16 min; (e) 16-30 min; (f) 30-60 min.

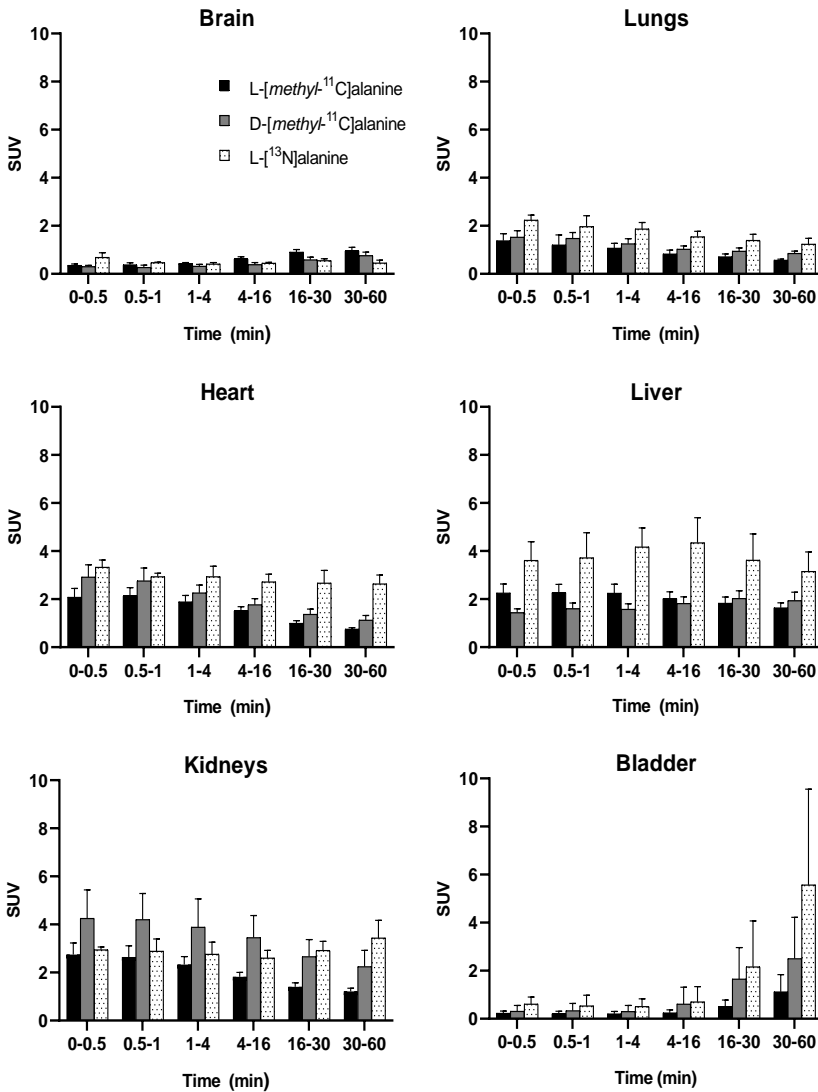


Figure 3.7. Amount of radioactivity in different organs at different time points after administration of L-[methyl-¹¹C]alanine, D-[methyl-¹¹C]alanine and L-[¹³N]alanine, as determined by quantification of PET images. Values (mean ± standard deviation, n=6) are expressed as standardized uptake value (SUV).

As expected, visual inspection of the images already suggested major accumulation in the liver, in the kidneys and the bladder, irrespective of the enantiomer and the labelling

position. However, interesting differences among the different labelled species could be observed when the images were quantified.

Focusing on the kidneys, maximum accumulation was observed for D-[*methyl*-¹¹C]-alanine. This can be explained by the elevated amount of D-amino acid oxidase (DAAO) enzyme that is present in this organ; in fact, this enzyme, which catalyzes the oxidative deamination of D-amino acids, is mostly expressed in the kidneys and D-alanine is one of its main physiologic substrates ⁹.

Moreover, differences between L-alanine radiolabelled with carbon-11 and nitrogen-13 were observed. When L-alanine enters the body, its first metabolic reaction is the oxidative deamination to produce pyruvate. When alanine is radiolabelled with nitrogen-13, the deamination results in the formation of labelled ammonia, which enters the urea cycle and is excreted via urine. Whereas when alanine is radiolabelled with carbon-11, the resulting radiolabelled product after the first metabolic reaction is pyruvate. Because of this, elimination is not as fast as in the case of L-[¹³N]alanine.

During the quantification of the brain and the lungs, no relevant differences between the three radiotracers were observed. On the other hand, differences were observed in the heart. The concentration of radioactivity in the heart after administration of both L- and D-[*methyl*-¹¹C]alanine progressively decreases with time, while the concentration of radioactivity in this organ after administration of L-[¹³N]alanine remains almost constant, with a very slight trend to decrease. It is worth mentioning that the VOI drawn in the heart covers both the ventricles and the myocardium, as these regions are not distinguishable on CT images. Hence, the measured concentration of radioactivity in the heart is a result of the contribution of both, the myocardium, and the blood present in the ventricles. Although not proven, we hypothesize that, on the one hand L-[¹³N]alanine is progressively cleared from the blood. On the other hand, the formation of [¹³N]NH₄OH (used to measure the myocardial activity¹⁰) after metabolic degradation of L-[¹³N]alanine results in accumulation of radioactivity in the myocardium. The result

of the two contributions results in a quasi-stable concentration of radioactivity in the heart.

After the whole body biodistribution study in major organs, a detailed analysis of the abdominal region was carried out to identify potential differences in the accumulation of the radiotracers in the prostate. The identification and delineation of the prostate in CT images is extremely challenging. Because of this, we performed an attempt to discriminate between the prostate and the bladder based on PET images. We hypothesized that the uptake kinetics in both organs would be different and determined voxel-by-voxel the dynamic time-activity curves. For ^{11}C -labelled amino acids, two different types of curves could be identified: those that showed a progressive increase over the whole duration of the scan, and those that showed a maximum and progressively decreased afterwards (see Figure 3.8 for illustrative example). Voxels showing a progressive increase were identified as the bladder, and voxels showing a maximum were identified as the prostate. Subsequently, voxels corresponding to both organs were pooled (Figure 9) to define whole VOIs, and time-activity curves for each VOI were determined (Figure 10).

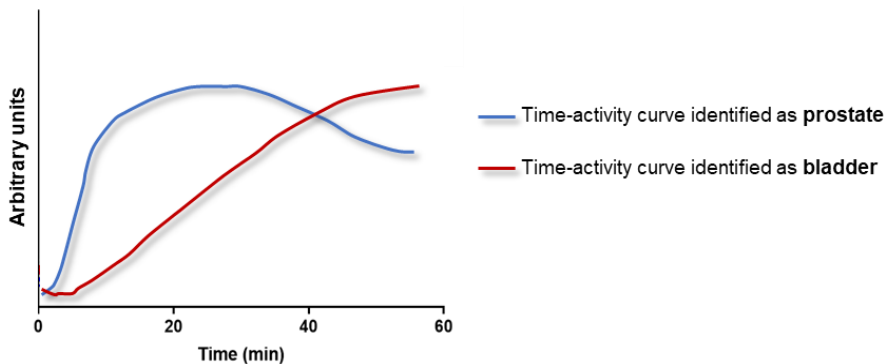


Figure 3.8 Time-activity curves for VOI identified as prostate (blue line) and for VOI identified as bladder (red line).

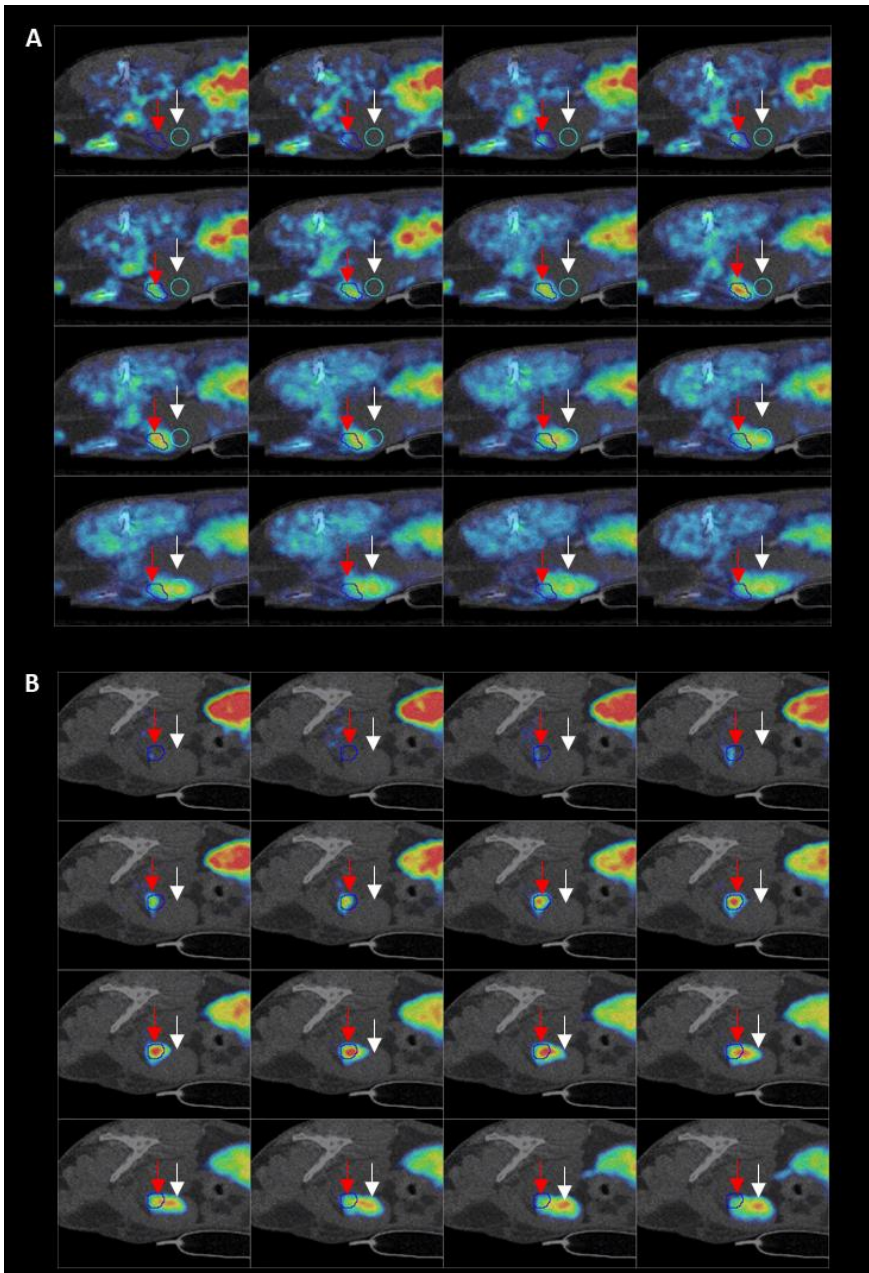


Figure 3.9 Sagittal projection from the *in vivo* PET scan from two animals (A and B) injected with carbon-11 radiolabelled alanine. Prostate's uptake is pointed in red, and bladder uptake is point in white.

Visual inspection of the images (Figure 9) clearly showed that the relative position of the prostate with respect to the bladder was animal-dependent, thus adding difficulty to the identification of the different regions of interest. In some sagittal projections, VOIs identified as the prostate are located in the upper part of the bladder, while in other animals the VOI is located in a ventral position. It is also possible that regions showing high uptake correspond to different lobes of the prostate, although this could not be confirmed from in vivo images.

Importantly, quantification of the different VOIs showed interesting differences between the two ^{11}C -labelled enantiomers (Figure 11). Indeed, the uptake of D-[*methyl*- ^{11}C]alanine in the prostate was significantly higher than the uptake of the L-enantiomer. These results are in line with previous studies that have demonstrated that for some cancer types, D-amino acids are uptaken by cancer cells at a higher ratio than the L-enantiomers,^{4,13,14,15} and position D-[*methyl*- ^{11}C]alanine as a potential diagnostic tool for prostate cancer.

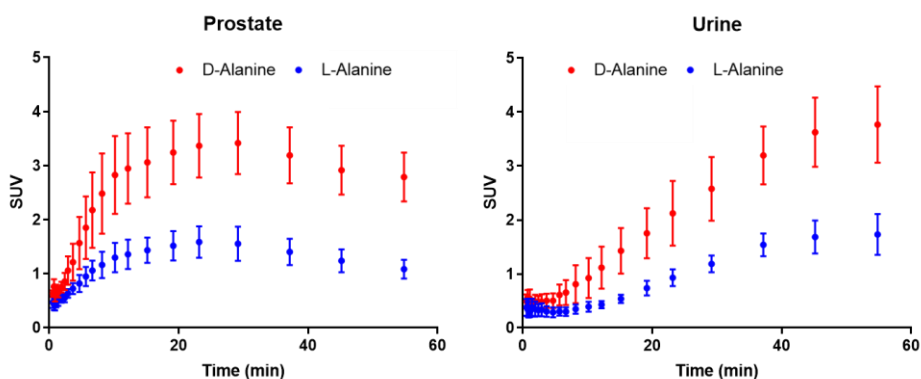


Figure 3.10 Quantification of prostates and bladder from the in vivo PET images. Values (mean \pm standard deviation, n=6) are expressed as standardized uptake value (SUV).

Contrarily to ^{11}C -labelled amino acids, animals injected with L-[^{13}N]-alanine showed very rapid accumulation of radioactivity in the bladder, and regions with time-activity curves

showing increase followed by decrease could not be observed. This made identification of the prostate impossible, and hence comparative data could not be achieved.

Due to the interesting results obtained during the *in vivo* Scan of animals injected with L- and D-[methyl-¹¹C]alanine, prostates of animals injected with these radiotracers were submitted to an *ex vivo* analysis.

3.4.5 Prostate-specific Pten deletion cancer model: *ex vivo* studies

Immediately after the *in vivo* PET-CT scan at the age of 7 months, animals were sacrificed, and still radioactive hypertrophied prostates were harvested. These prostates were placed into the PET-CT scan next to a urine sample from the same animal, collected in a vial, and a static scan was performed for ten minutes. Quantification of these prostates was carried out by measuring the activity that remains in the central part of the prostate, regarding the whole reproductive system (Figure 3.12) and also quantification of the urine inside the vial.

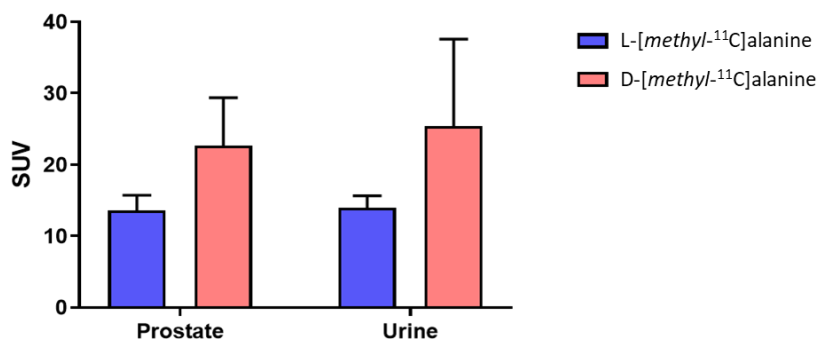


Figure 3.12 Accumulation of L-[methyl-¹¹C]alanine and D-[methyl-¹¹C]alanine in the prostate and urine of diseased animals determined by *ex vivo* PET imaging. Values (mean \pm standard deviation, n=6) are expressed as standardized uptake value (SUV).

Accordingly to the *in vivo* quantification, the *ex vivo* image quantification showed higher uptake in prostates of those animals injected with D-[methyl-¹¹C]alanine in comparison

with those injected with L-[*methyl*-¹¹C]alanine. These results confirm the key role that D-amino acids can play in cancer cell proliferation.

3.4.6 Histological analysis

After being analyzed by imaging techniques, prostates were collected and preserved into formalin solution 5% and they were sent to Cancer Cell Signaling Lab at CIC bioGUNE, where they were histologically analyzed to study the characteristics of the prostate tissue. During histological analysis, different staining was used to identify different structures, cells, tissues, or other components.

Hematoxylin and eosin staining

The Hematoxylin/eosin staining technique is one of the most common tinctions used in histological analysis. Hematoxylin is a cationic/basic substance that stains basophile structures (*i.e.* the nuclei) with a purple-blue coloration. On the contrary, eosin is an anionic/acid substance that stains acidophilic components (*i.e.* cellular cytoplasm) with a pink coloration

Figure 3.13 is a comparison between a heterozygous mice model, which presents only one allele of PTEN, that presents focal pre-malignant lesions (A) and will serve as a control, and the prostate cancer mouse model (with complete deletion of Pten in the prostate epithelium) (B). A lesion is considered as malignant when cells acquire invasive properties (leading to an invasive carcinoma).

In Figure 3.13-A is possible to see two glands, the blue arrow depicts a normal gland, the red arrow points to a gland that presents histological alterations. The normal structure of the gland is lost, and epithelial cells fill the lumen. However, these cells are confined to the gland and do not break the basal lamina. This lesion is defined as PIN (Prostatic Intraepithelial Neoplasm), a premalignant lesion.

Figure 3.13-B corresponds to the prostate histology found in prostate-specific Pten deficient mice. These mice develop adenocarcinoma lesions. The picture shows a high level of stromal reaction, and epithelial lesions with signs of invasion. Stroma is the

tissue in which glands are found, and it's easy to appreciate that in this image, the stroma is denser and richer.

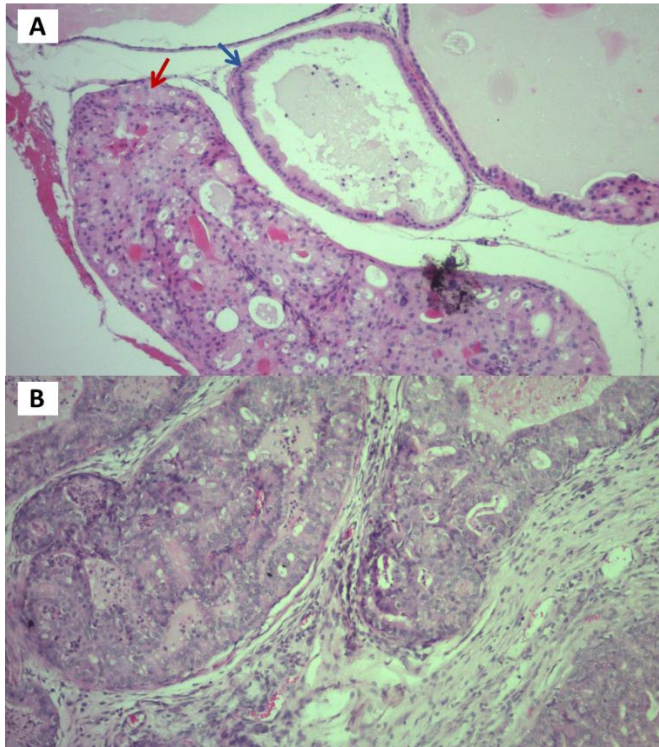


Figure 3.13 Hematoxylin-eosin staining corresponding to A) Tissue from control mice which have normal prostatic glands, or PIN lesions and B) Tissue from PTEN-knock out mice prostate cancer model with malignant lesions.

p-AKT staining

Protein kinase B, also known as AKT, plays a key role in cellular processes. AKT is one of crucial proteins in the AKT/PI3K/PTEN signaling pathway. This AKT/PI3K/PTEN pathway is known to be a cellular survival route and it takes part in several cellular transduction signals.

In PTEN knock-out mice model, AKT proteins present higher phosphorylation. Once AKT is phosphorylated (p-AKT) it gets activated and plays an important role in the process of malignant transformation. Figure 3.14 represents a comparison of p-AKT staining from a control tissue (A) and a p-AKT staining from one of our prostate cancer model mice under study (B).

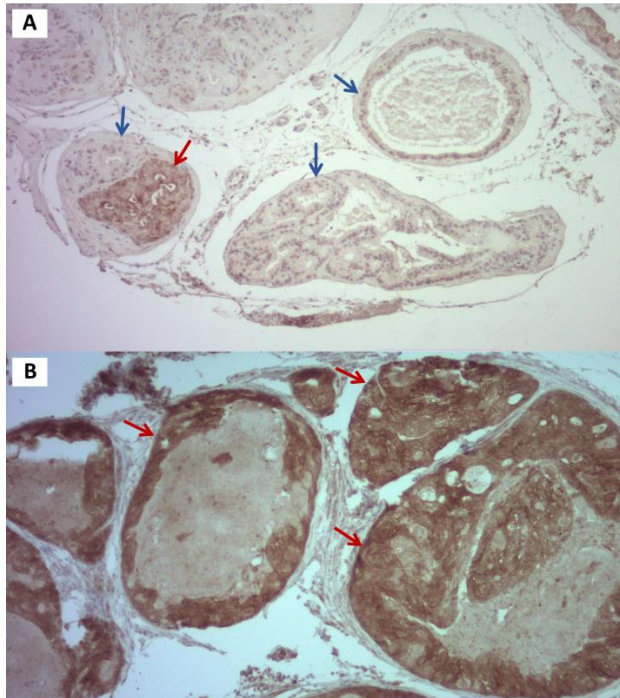


Figure 3.14 p-AKT staining of: A) Tissue from control mice which have normal prostatic glands, or pre-malignant lesions and B) Tissue from PTEN-knock out mice prostate cancer model with malignant lesions.

When a tissue presents some PIN lesions, AKT signal will increase in the cellular membrane, presenting an intense membrane brown coloration. In Figure 3.14-A, it is possible to see two glands which present low p-AKT tinction (right blue arrows), and other one in the left part, which present a low p-AKT in the outer part (blue arrow), but also a zone in which p-AKT is activated, which histologically corresponds to a PIN lesion (red arrow).

In Figure 3.14-B, it is easily appreciated intense membranous p-AKT staining.

CK-5 staining

Citokeratin 5 staining labels basal cells in the prostate. The disappearance of the basal cell layer is a key feature of invasive cancerous lesions. As in previous examples, Figure 3.15 is composed of: A) tissue from control mice, and B) tissue from our mice prostate cancer model. In Figure 3.15-A, is possible to see a thin label-positive line surrounding the gland (blue arrows). On the contrary, in Figure 3.15-B, it is possible to see that there is a discontinuous line of basal cells (blue arrows), with areas where these cells are absent (red arrows). These alterations are more localized than in the other staining, but this loss of the line is indicative of an invasive lesion.

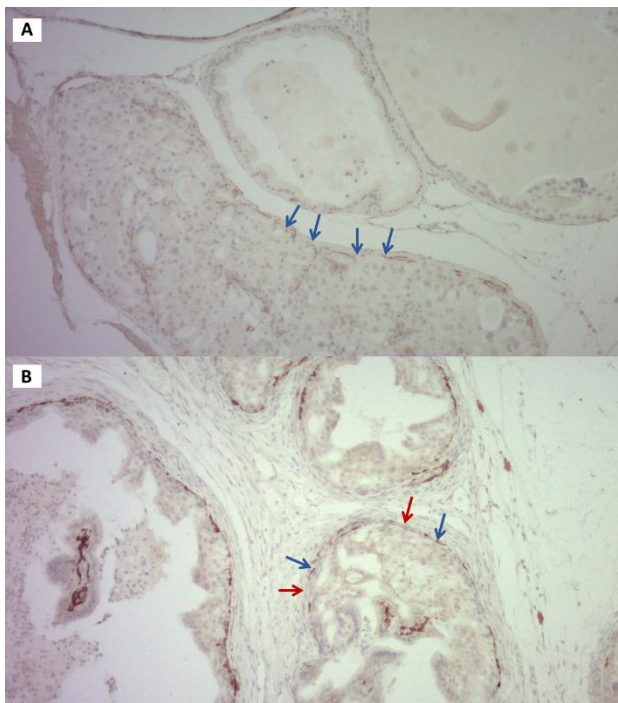


Figure 15. CK-5 staining of corresponding to A) Tissue from control mice which have normal prostatic glands, or only pre-malignant lesions and B) Tissue from PTEN-knock out mice prostate cancer model with malignant lesions.

3.5 Summary and conclusions

In this chapter, it has been demonstrated that nuclear imaging techniques such as PET, are perfectly suited to investigate the *in vivo* biodistribution of radiolabelled amino acids. We have demonstrated the relevance of the enantiomer and radioisotope selection to perform an imaging study. Our results confirm that prostates from the tumour model based on the deletion of PTEN in the prostate epithelia present an elevated uptake of amino acids to support their fast proliferation rate. Moreover, an elevated uptake of the D- with respect to the L-enantiomer was observed. The histological analysis confirmed the malignancy of the tissue.

3.6 References

1. Utsunomiya-Tate, N., Endou, H. & Kanai, Y. Cloning and functional characterization of a system ASC-like Na⁺-dependent neutral amino acid transporter. *J. Biol. Chem.* **271**, 14883–14890 (1996).
2. Kekuda, R. *et al.* Cloning of the sodium-dependent, broad-scope, neutral amino acid transporter B(o) from a human placental choriocarcinoma cell line. *J. Biol. Chem.* **271**, 18657–18661 (1996).
3. Filp, U., Pekošak, A., Poot, A. J. & Windhorst, A. D. Enantioselective synthesis of carbon-11 labeled L-alanine using phase transfer catalysis of Schiff bases. *Tetrahedron* **72**, 6551–6557 (2016).
4. Into, P., Animals, I., Some, O. F. & Tumor-bearing, C. D. A. The development of radioactive agents which have a strong affinity for tumor is one of the most important subjects in the field of radiopharmaceuticals . Among tumor-scanning agents being used at present , ^{99m}Tc pertechnetate for the diagnosis of cerebr. **69**, 517–523 (1978).
5. Carracedo, A., Alimonti, A. & Pandolfi, P. P. PTEN level in tumor suppression: How much is too little? *Cancer Res.* **71**, 629–633 (2011).

6. Larsen, P., Ulin, J., Dahlstrøm, K. & Jensen, M. Synthesis of [11C]iodomethane by iodination of [11C]methane. *Appl. Radiat. Isot.* **48**, 153–157 (1997).
7. Parker, M. F. L. *et al.* Sensing Living Bacteria in Vivo Using d-Alanine-Derived 11C Radiotracers. *ACS Cent. Sci.* **6**, 155–165 (2020).
8. da Silva, E. S., Gómez-Vallejo, V., Baz, Z., Llop, J. & López-Gallego, F. Efficient Enzymatic Preparation of 13N-Labelled Amino Acids: Towards Multipurpose Synthetic Systems. *Chem. - A Eur. J.* **22**, 13619–13626 (2016).
9. Koga, R. *et al.* Mouse D -Amino-Acid Oxidase : Distribution and Physiological Substrates. **4**, 1–10 (2017).
10. Muzik, O. *et al.* Validation of nitrogen-13-ammonia tracer kinetic model for quantification of myocardial blood flow using PET. *J. Nucl. Med.* **34**, 83–91 (1993).
11. Fletcher, J. W. *et al.* Recommendations on the use of 18F-FDG PET in oncology. *J. Nucl. Med.* **49**, 480–508 (2008).
12. Shreve, P. D., Anzai, Y. & Wahl, R. L. Pitfalls in oncologic diagnosis with FDG PET imaging: Physiologic and benign variants. *Radiographics* **19**, 61–77 (1999).
13. Kögl, F. & Erxleben, H. Zur Ätiologie der malignen Tumoren 1. Mitteilung über die Chemie der Tumoren. *Hoppe. Seylers. Z. Physiol. Chem.* **258**, 57–95 (1939).
14. He, X. *et al.* Serum metabolomics differentiating pancreatic cancer from new-onset diabetes. *Oncotarget* **8**, 29116–29124 (2017).
15. Nagata, Y. *et al.* High concentrations of D-amino acids in human gastric juice. *Amino Acids* **32**, 137–140 (2007).

CHAPTER 4

Radiolabelled glutamine

Chapter 4. Radiolabelled Glutamine

4.1 Introduction

During the last years, scientists have been doing a great effort investigating cancer metabolism both to understand the mechanism of tumour proliferation and to develop new treatments, which specifically target the metabolic pathways sustaining the tumour growth. Such pathways, in which glycolysis and glutaminolysis are involved, might be exploited for therapeutic purposes^{1,2}.

The second most abundant nutrient in blood (after glucose) is glutamine, with a concentration about 0.5 to 1 mM. Glutamine complements glucose metabolism, takes part in bioenergetics, protect cells against oxidative stress and is also a nitrogen donor for nucleotide and amino acid synthesis³.

After entering the cell, glutamine is first converted to glutamate by glutaminase, and then, glutamate dehydrogenase removes the remaining ammonia group from glutamate to produce the α -ketoglutarate. The latter enters directly into the tricarboxylic acid cycle (TCA cycle) to produce metabolic substrates and energy (Figure 4.1).

One therapeutic approach to starve cancer cells to death is based on the inhibition of glutaminolysis. Stopping cancer cells from using glutamine can be achieved by blocking either the glutamine transporters or glutaminase, which is the first metabolic enzyme.

Glutamine is transported into the cell through at least three different amino acid transporters: a) Sodium-neutral amino acid transporters (SNAT); b) alanine, serine, cysteine-preferring transporter 2 (ASCT2); and c) large neutral amino acid transporter 1 (LAT1). These transporters are not specific to glutamine but the ASCT2 transporter appeared to be the most notable and unregulated transporter for glutamine uptake in cancer cells. Hence, the blocking of the glutamine transporter ASCT2 is nowadays an active area of therapeutic development^{4,5}.

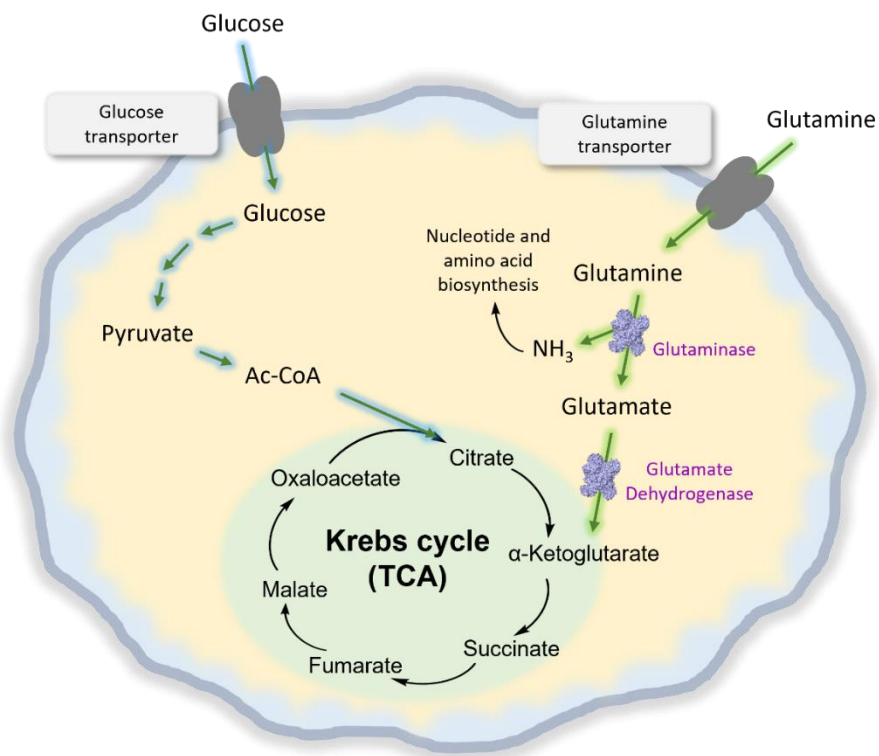


Figure 4.1 Schematic drawing of intracellular metabolism of glucose and glutamine, showing glycolysis and glutaminolysis. Ac-CoA = acetyl-coenzyme A.

Today, positron emission tomography imaging is an important tool to monitor and diagnose cancer⁶. The radiopharmaceutical 2-[¹⁸F]fluoro-2-deoxy-D-glucose (also known as [¹⁸F]FDG or FDG) takes advantage of the elevated glucose uptake that is present in many cancer cells. As an alternative to FDG, the idea of radiolabelling glutamine to study glutaminolysis has gained notable interest among the scientific community.

Although radiolabelled analogues of L-glutamine, such as ¹⁸F-(2S,4R)4F-Gln, ¹⁸F-(2S,4S)4F-Gln, ³H-(2S)-Glutamine and 5-¹¹C-(2S)-Glutamine have been already reported (Figure 4.2)^{7,8,9,10,11,12}, glutamine has not yet been prepared in its ¹³N-radiolabelled form. This radiotracer offers some advantages over the use of carbon-11 and fluorine-18 labelled counterparts. Firstly, when glutamine is radiolabelled with nitrogen-13, the

Chapter 4. Radiolabelled glutamine

chemical structure remains unaltered; hence, contrarily to [^{18}F]FGln, conserves unmodified pharmacokinetic, metabolic and catabolic properties. Additionally, the shorter physical half-life of nitrogen-13 in comparison with carbon-11 and fluorine-18 results in lower radiation dose on the investigated subject and enables repeated scans on the same subject within one day.

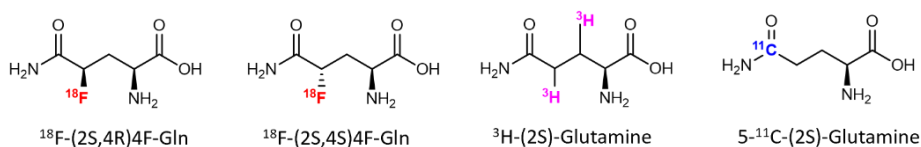


Figure 4.2 Analogues of glutamine labelled with ^{18}F ($T_{1/2}=109.65$ min), and glutamine labelled with tritium ($T_{1/2}=12.32$ years), and carbon-11 ($T_{1/2}=20.40$ min).

Biocatalysis offers a great opportunity to radiolabel glutamine with nitrogen-13. As previously shown by our group in other radioenzymatic syntheses in which ^{13}N -labelled ammonia was used as the labelling agent, enzymes could be the perfect catalysts to perform the amination reaction^{13,14}. Indeed, enzymes offer some advantages over traditional chemical catalysis. They present excellent selectivity and high turnover numbers at low substrate concentration, enabling fast chemical conversions and high yield under mild conditions, which is mandatory when radionuclides with short radioactive half-life are used.

This chapter collects our efforts to synthesise L- ^{13}N]glutamine using [^{13}N]NH₄OH as the labelling agent.

4.2 Objectives

The specific objectives of this chapter are:

1. To create a multi-enzymatic system capable of synthesizing L-glutamine from D-glutamine.
2. To express, purify and characterize the required enzymes for the system.
3. To assess the function of the system under radioactive conditions by using radioactive ammonia to produce L-[¹³N]glutamine.

4.3 Materials and methods

4.3.1 Reagents

D-glutamine (purity ≥ 98%), L-glutamine (purity ≥ 98%), L-glutamate (purity ≥ 98%), oxo-ketoglutaric acid (purity 99%), o-phenylenediamine (OPD; purity >99.5%), ammonium chloride (NH₄Cl; purity ≥ 99.5%), and pyroxidal 5'-phosphate (PLP, purity ≥ 98%) were purchased from Sigma Chemical Co. (St. Louis, IL, USA) and used without further purification. Marfey's Reagent (purity 99%) was purchased from Thermo Fisher Scientific, (Waltham, MA, USA) and used without further purification. β-Nicotinamide adenine dinucleotide phosphate disodium dihydrate (NADP⁺) and its reduced form (NADPH), were purchased from GERBU Biotechnik GmbH (Wieblingen, Germany). The genes of transaminases (ωTA) from *Hallomonas elongate*, *Pseudomonas fluorescence* and *Chromobacterium violaceum* were synthesized and cloned into pET28b by GenScript company (Piscataway, USA).

Glutamate dehydrogenase from beef liver (10 units/mg protein, lyophilized), Catalase from bobine liver (2000-5000 units/mg protein, lyophilized powder), and Peroxidase from horseradish (150 units/mg protein, lyophilized powder) were purchased from

Chapter 4. Radiolabelled glutamine

Sigma Chemical Co. (St. Louis, IL, USA). D-amino acid oxidase from *Trigonopsis variabilis* (TvDAAO) was kindly donated by Recordati.

Bio-Rad Protein Assay Dye Reagent Concentrate was purchased from Bio-Rad Laboratories (Madrid, Spain).

4.3.2 Enzyme production

Transaminase gene (ω TA) Production

Hallomonas elongate (He), *Pseudomonas fluorescens* (Pf), and *Chromobacterium violaceum* (Cv)

Expression. A total of 1 mL of an overnight culture of *E.coli* BL21 transformed with the respective plasmid (pRESTb or pET28b or pMP89b, from *Hallomonas elongata* (He), *Pseudomonas fluorescens* (Pf) and *Chromobacterium violaceum* (Cv) respectively), was inoculated in a 50 mL of LB (Luria-Bertani) broth, containing the antibiotic kanamycin in a final concentration of 30 $\mu\text{g mL}^{-1}$. To reach the successful overexpression of ω TA, the resulting culture was incubated at 37 °C with energetic shaking until the optical density at 600 nm ($\text{OD}_{600\text{nm}}$) reached 0.6. Then IPTG (1-thio- β -d-galatopyranoside) was added to the culture to a final concentration of 1 mM to induce protein synthesis. Cells were grown at 21 °C overnight and harvested by centrifugation at 1290g rpm for 30 min.

Purification. All transaminases were purified as follows: The resulting pellet from 50 mL culture, was resuspended in 5 mL (one-tenth of its original volume) of HEPES buffer solution (100 mM, pH 8) containing PLP (pyroxidal phosphate, 0.1 mM). Cells were broken by sonication at amplitude 50 %, 0.5 s intervals during 20 min. The resulting suspensions were centrifuged at 10528 g for 30min. The supernatant containing the enzyme was collected and samples were analysed by 12 % SDS-PAGE (Sodium dodecyl sulphate polyacrylamide gel electrophoresis) (Coomassie Blue staining) after each protein production to determine enzyme purity.

4.3.3 Determination of the protein concentration

Determination of protein concentration, when needed, was performed by Bradford's method, using bovine serum albumin (BSA) as protein standard. The soluble enzyme (5 μL) and Bradford reagent (200 μL) were mixed in a 96-well plate. The absorbance was measured in the spectrophotometer at 595 nm after 5 min of reaction at 25 °C. For the standard curve, a series of BSA solutions were used (concentration= 0.06, 0.12, 0.25, 0.5 and 1 mg mL^{-1}).

4.3.4 Determination of enzyme activity

GluDH Quality Control

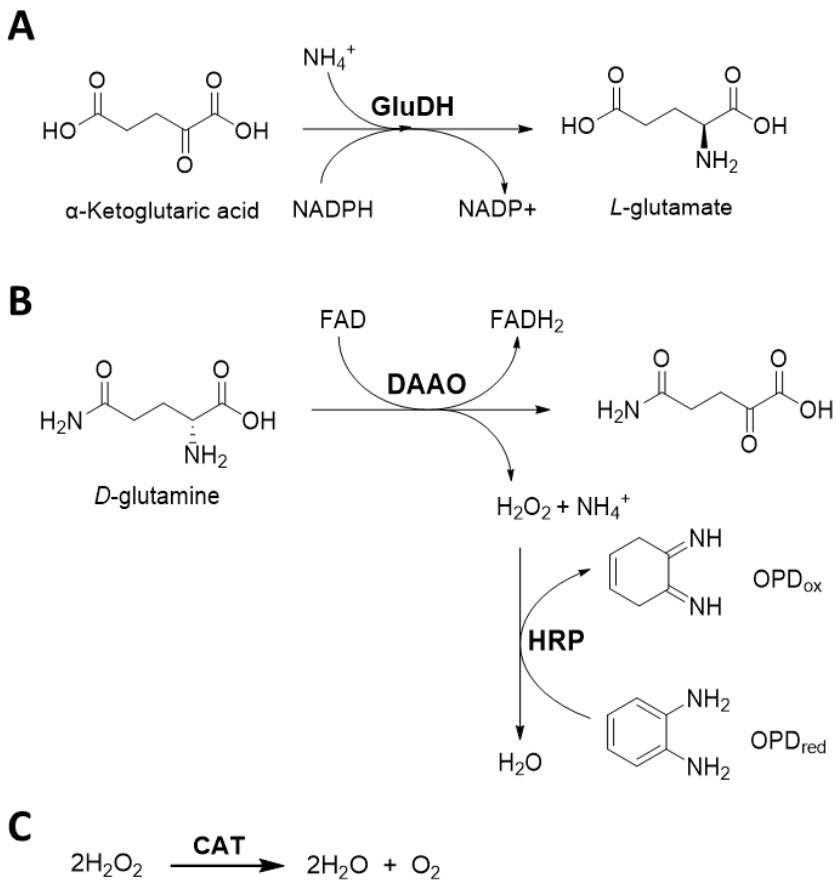
Glutamate dehydrogenase's activity was measured as follows: α -ketoglutaric acid (75 mM) was mixed with NADPH (Nicotinamide adenine dinucleotide phosphate, 0.5 mM) as the cofactor and NH_4Cl (125 mM) as the ammonia source, all dissolved in phosphate buffer 25 mM pH 7. The reaction was started by addition of GluDH and the conversion of NADPH into NADP^+ was followed by spectrophotometry at 340 nm. 1 Unit of GluDH was defined as the necessary amount of enzyme required for the reductive amination of 1 μmol of α -ketoglutaric acid per minute (Scheme 4.1, A)

DAAO Quality Control

D-amino acid oxidase's activity was determined as follows: D-glutamine (10 mM) was mixed with OPD (*o*-phenylenediamine, 0.8 mM) and HRP (Horseradish peroxidase, 0.045 mg mL^{-1}), all dissolved in phosphate buffer 25 mM pH 7. The oxidative deamination was started by adding DAAO. Hydrogen peroxide produced by the oxidative deamination is used by HRP to catalyse the OPD oxidation, yielding a brownish coloration that can be followed by monitoring the absorbance at 450 nm. 1 Unit of DAAO was defined as the necessary amount of enzyme required for the oxidation of 1 μmol of *D*-glutamine per minute (Scheme 4.1, B).

Catalase Quality Control

Catalase's activity was evaluated as follows: a mixture composed of hydrogen peroxide (35 mM) and Catalase (10 mg mL⁻¹) was dissolved in phosphate buffer 50 mM pH 7. The reaction was followed by spectrophotometry, by monitoring the decrease in the absorbance at 240 nm. 1 Unit of Catalase was defined as the necessary amount of enzyme required to produce 1 μmol of H₂O₂ per minute (Scheme 4.1, C).



Scheme 4.1. Quality control used to determine the enzymatic activity of GluDH (A), DAAO (B) and CAT (C).

Chapter 4. Radiolabelled glutamine

Transaminases (from Pf, Cv and He) Quality Control

Transaminases quality control was measured as follows:

A mixture of pyruvate (final concentration 2 mM, from stock solution 750 mM prepared in water), pirydoxal phosphate (PLP) (final concentration 0.1 mM, from stock solution of PLP 10 mM prepared in buffer HEPES 100 mM pH 8), and phenylethylamine (final concentration 2 mM, from stock solution 1 M prepared in acetonitrile (ACN)) was prepared. The reaction was started by addition of the Transaminase and was followed in the spectrophotometer by monitoring the absorbance at 245 nm.

GluDH for deamination

L-glutamate or L-glutamine (final concentration 75 mM) was mixed with NADP⁺ (final concentration 0.5 mM) as the cofactor, all dissolved in phosphate buffer 25 mM pH 7. The measurement was started by the addition of GluDH, and it was followed in the spectrophotometer at 340 nm.

4.3.5 Synthesis of L-glutamine

Multi-enzymatic system under non-radioactive conditions

A mixture with final concentrations of D-glutamine (10 mM), NADPH (1 mM), NH₄Cl (125 mM), Catalase (100 U), and Glutamate Dehydrogenase (1 U) was prepared in 250 µL of phosphate buffer 25 mM pH 8. The reaction cascade was started by the addition of D-amino-acid oxidase (0.1 U). The reaction was conducted for 1 hour and was quenched by centrifugation with a 30 kDa cut-off membrane. The filtrate was then derivatized by Marfey's method and analysed by HPLC (see below for detailed explanation of the Marfey's method).

4.3.6 Synthesis of L-[¹³N]glutamine

Production of the radiolabelling agent [¹³N]NH₄OH

Nitrogen-13 (¹³N) was produced in an IBA Cyclone 18/9 cyclotron by the ¹⁶O(*p*, α)¹³N reaction. The target system consists in an aluminium insert (2 mL) covered with havar foil (thickness 25 μ m, \varnothing 29 mm) and with an aluminium vacuum foil (thickness 25 μ m, \varnothing 23 mm). The target, containing 1.7 mL of EtOH 5 mM in water, was irradiated with 18 MeV protons. The beam current was maintained at 22 μ A (range pressure into the target during bombardment was 5-10 bar) to reach the desired integrated currents (1-4 μ Ah). The resulting solution was collected in a 10 mL vial, and the activity was measured in a dose calibrator (Capintec CRC®-25 PET, New Jersey, USA).

Multi-enzymatic system under radioactive conditions

A mixture of 2-oxoglutaramate lithium salt (LiOGA) in its cyclic form (5 mg, to have 0.66 M final concentration), NADPH (0.5 mg, to have 10 mM final concentration) and Glutamate dehydrogenase (24 mg, 48 U) was prepared in a reaction vial without any buffer or solvent. The reaction was started by the addition of [¹³N]NH₄OH (aqueous solution, 562.4 MBq, 50 μ L) in phosphate buffer 325 mM pH 8. The reaction was conducted for 1 hour and was quenched by centrifugation with a 30 kDa cut-off membrane. The filtrate was then derivatized by Marfey's method during 30 min and analysed by radio-HPLC.

4.3.6 HPLC and radio-HPLC analysis

Marfey's derivatization

The reaction sample (20 μ L) was mixed with sodium bicarbonate (8 μ L, 1 M) and Marfey's reagent (20 μ L, 15 mM) in acetone and it was incubated for 1 hour at 50 °C and 400 rpm in a shaker-incubator. Afterwards, derivatisation reaction was stopped by the addition of HCl (8 μ L, 2M). Then, samples were diluted with ultrapure water (50 μ L) and

centrifugated at 10621g for 10 minutes. The resulting supernatant was ready to be injected into the HPLC. Samples must be submitted immediately to the HPLC to avoid the formation of solids, inherent to the Marfey's methodology. Derivatized samples were analysed by HPLC, with a Mediterranea SEA C18 5 μm column (15 cm x 0.46 cm, Teknokroma) as the stationary phase. Mobile phases were A: Trifluoroacetic acid 0.1% in water and B: Acetonitrile. Elution was performed at 1 mL/min following a gradient from 10% of B to 40% in 45 minutes, to then recover the initial conditions in 15 additional minutes. Detection of compounds was done using a variable wavelength detector ($\lambda = 340 \text{ nm}$).

4.4 Results and discussion

In our attempt to prepare L- ^{13}N glutamine, enzymatic amination of the glutamine's α -keto-acid, also known as 2-oxoglutaramate (OGA), was envisaged, using ^{13}N ammonium hydroxide (^{13}N NH₄OH) as the ammonia source, similar to our previously described method for the production of ^{13}N -labelled amino acids¹³. For this purpose, different enzymes were prepared to allow their use in further enzymatic reactions.

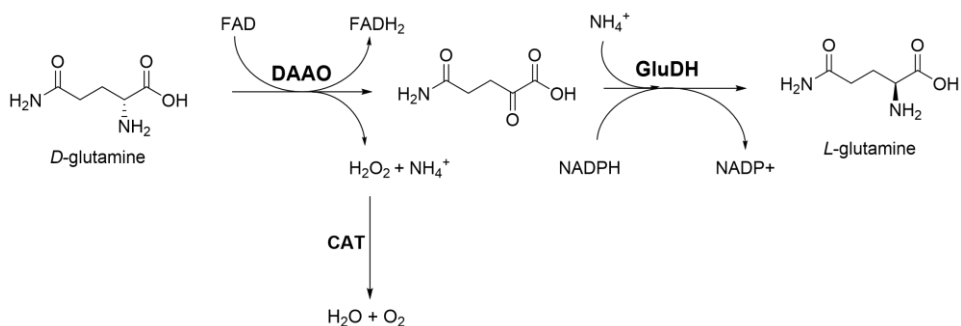
4.4.1 Multi-enzymatic system under non-radioactive conditions

Our first attempt was the one-pot enzyme-assisted oxidative deamination-reductive amination sequence, by using D-amino acid oxidase (DAAO), Catalase (CAT) and Glutamate dehydrogenase (GluDH). This enzyme combination presented an attractive synthetic route using D-glutamine as the precursor and ^{13}N NH₄OH as the labelling agent. The idea was to set up experimental conditions under non-radioactive conditions in a first step, to then translate the reaction to radioactive conditions.

By using this approach, DAAO catalyses the oxidative deamination of D-glutamine to form 2-oxoglutaramate (OGA), which subsequently can undergo GluDH-assisted reductive amination using ammonia as amine donor to yield L-glutamine (Scheme 4.2).

Chapter 4. Radiolabelled glutamine

As DAAO releases hydrogen peroxide as by-product, Catalase was added to disproportionate hydrogen peroxide to molecular oxygen and water, thus avoiding its accumulation which might damage the enzymes involved in the cascade.



Scheme 4.2. Multi-enzymatic system which catalysed the production of L-glutamine starting from D-glutamine.

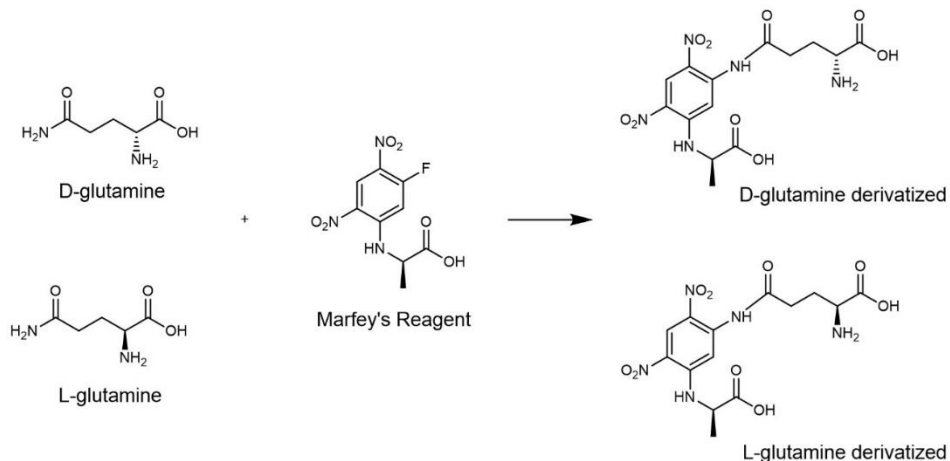
Before testing the complete multi-enzymatic system, each enzyme was freshly prepared and submitted to quality control to ensure proper activity. GluDH activity was measured by using α -ketoglutaric acid, its natural substrate, and NADPH as cofactor. DAAO activity was measured by using D-glutamine as substrate, using O-phenylenediamine and Horseradish peroxidase to spectrophotometrically monitor the amount of H₂O₂ produced by the DAAO. Finally, Catalase was measured by using hydrogen peroxide as substrate (more details in the materials and methods section).

When tackling enzymatic reactions, it is crucial to know the exact activity of each enzyme just before testing the multi-enzymatic system, in order to add the required amount of all the components. Once all activities were known, first trials of the multi-enzymatic system were carried out.

To analyse the reaction products, Marfey's derivatization was selected as analytical methodology, to follow the reaction by HPLC¹⁵. This approach constitutes an exceptional tool as it allows the differentiation between amino acids and enantiomers (Scheme 3).

Chapter 4. Radiolabelled glutamine

This way, it is possible to know if there is still unreacted D-glutamine and if L-glutamine has been formed. This method perfectly fits with the analysis of our purpose, which is the stereo inversion of glutamine.



Scheme 4.3 Marfey's derivatization of both glutamine enantiomers yielding a diastereoisomers mixture.

During these first trials of the multi-enzymatic system, no products were observed under non-radioactive conditions. The absence of products suggests that the ammonium needed for the second step may be interfering with the first step, affecting DAAO's activity. Despite not being a reversible enzyme, DAAO releases ammonia into the reaction media and the external ammonia added to the solution, to perform the second step, was probably reducing the catalytic activity of DAAO.

To confirm this hypothesis, an experiment consisting of measuring the activity of both enzymes (DAAO and GluDH) with different amounts of ammonia was performed (Figure 4.3). With that aim, ammonia was added to the enzymatic activity assay to see how the activity changes when the concentration of ammonia increases.

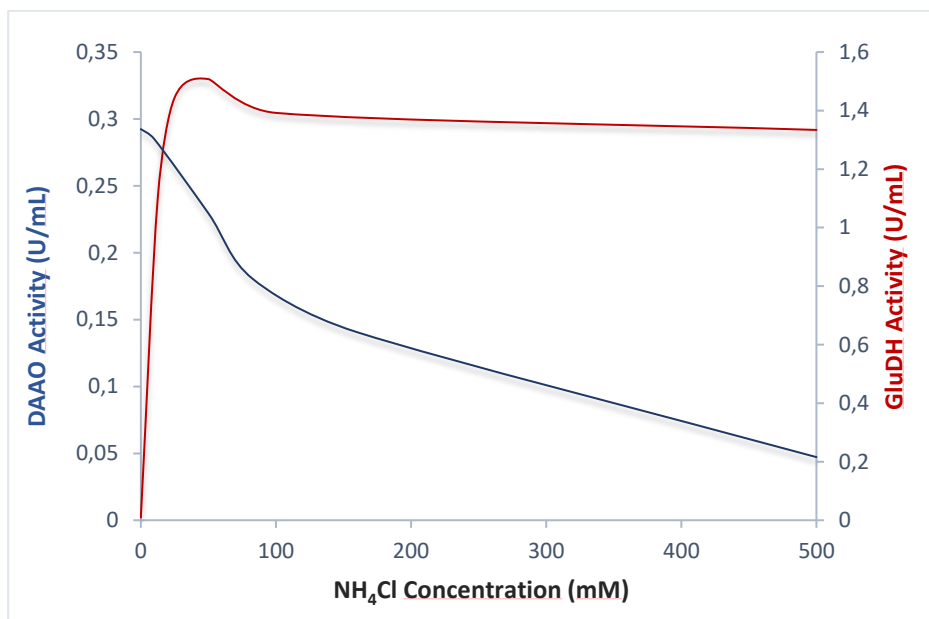


Figure 4.3 Enzymatic activity curves of DAAO and GluDH expressed at Units per milliliter, at different NH₄Cl concentrations during their quality control.

As predicted, DAAO's enzymatic activity decreases when ammonia concentration increases. Also, at higher ammonia concentrations, GluDH is working close to its maximum of activity; however, if the ammonia concentration is too low, GluDH is much less active. This experiment confirmed that there is an optimum ammonia concentration, in which both enzymes work very close to its maximum capacity.

In our initial attempts (see above) the ammonia concentration used in the multi-enzymatic reaction was 500 mM, based on the typical ammonia concentration that is used during the routinary quality control tests of amino acid dehydrogenases.

Then, the multi-enzymatic system was tested also without adding any NH₄Cl, to know if the ammonia released by DAAO is enough to saturate the GluDH in the second step. Unfortunately, L-glutamine could not be detected under our analytic methodology.

Chapter 4. Radiolabelled glutamine

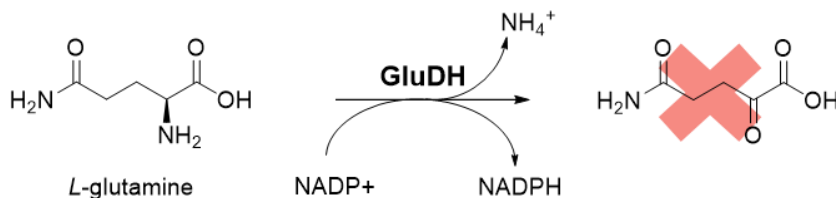
An optimal ammonia concentration was found at 125 mM. At this point, using 125 mM ammonia, the activity of GluDH was 92% of the maximum (at 50 mM ammonia), while the DAAO activity was 53% of its maximum (without ammonia). A surprising result was observed when lower concentrations of ammonia (less than 125 mM) were used, because no products were observed. According to Figure 3, it could be expected that at lower concentrations of ammonia, the system works very fast because both enzymes were in its higher values. But the lack of formation of the products suggests that the multi-enzymatic system is not as simple as expected.

After adjusting the ammonia concentration at 125 mM, the multi-enzymatic reaction resulted in the formation of L-glutamine in 30% yield after 60 minutes of reaction at room temperature. This yield is lower than expected considering the enzymatic units that are present in the system. Regarding the first step, D-glutamine must be converted into the corresponding keto-acid in 25 min. This can be calculated considering that 1 enzymatic Unit (U) means the conversion of 1 μmol of substrate per minute, as 0.1 U of DAAO were present and the concentration of D-glutamine is 10 mM in a total volume of 250 μL . On the other hand, the time corresponding to the second step reaction, the formation of L-glutamine from the keto-acid, can be also calculated considering that the cofactor (NADPH) is going to be the limiting factor. Then, having 1 U of GluDH and 1 mM of NADPH in a total volume of 250 μL , the reaction must be completed in less of 1 minute. Therefore, the reaction time assayed should be sufficient to produce 100% of L-glutamine.

One possible explanation for the low yields may be the reversible activity of GluDH towards the cascade product L-glutamine. To see if that is the case, GluDH was tested in the deamination sense, by using L-glutamine as substrate and NADP^+ as cofactor (Scheme 4.3). Fortunately, it did not yield any product, which means that GluDH catalyses the amination step more favourably. This is very important, because if GluDH could take L-glutamine, and produce its keto-acid OGA, our multi-enzymatic system

Chapter 4. Radiolabelled glutamine

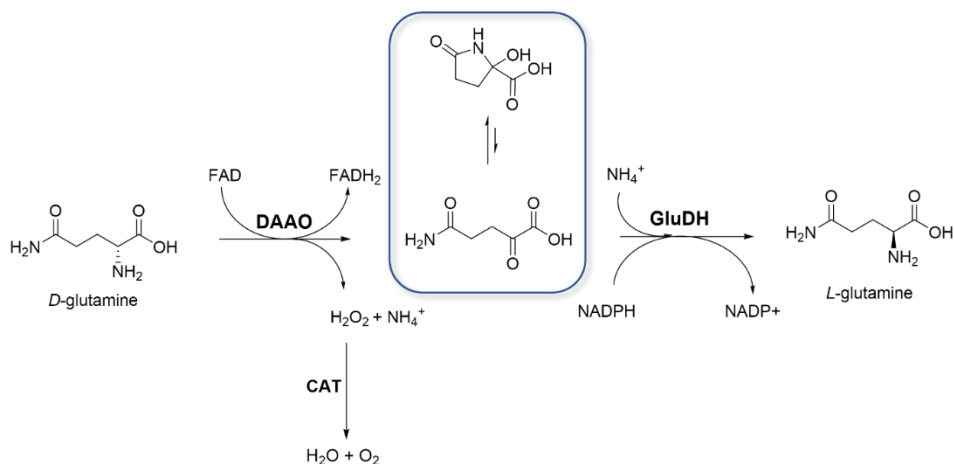
could be less favoured. Therefore, we discarded the reversible product deamination as a potential reason behind the failed production of L-glutamine.



Scheme 4.3 Enzymatic deamination of L-glutamine by using GluDH and NADP⁺ as cofactor.

Another possible reason for the lack of quantitative conversion in our multi-enzymatic reaction is the equilibrium between the linear and the cyclic forms of the keto-acid. As demonstrated in previous works, 2-oxoglutarate (OGA) predominantly exists in a cyclic hydroxylactame form, because the equilibrium between cyclic and acyclic forms is shifted to the cyclization^{16,17} (Scheme 4). Because of that, and based on the results, we hypothesised that the enzyme is not able to aminate the cyclic form. In this scenario, the formation of the cyclic form dramatically decreases the concentration of the linear form, thus hampering the formation of L-glutamine. Moreover, this lack of L-glutamine formation is also hampered if low ammonia concentration is used. Because if cyclic form is predominant over the linear one, and low concentrations of ammonium are used, the chances of both (linear form, and ammonium) being at the same time in the enzyme active site are reduced.

Although no quantitative formation of the desired amino acid could be achieved, we decided to move forward and assay the reaction under radioactive conditions, using [¹³N]NH₄OH instead of ammonia. The fact that radiochemical reactions take place under very small concentrations of the labelling agent and the fact that yields are determined based on the radioactive species, may lead to different results from those obtained under non-radioactive conditions.



Scheme 4. Multi-enzymatic system with the formation of the cyclic form, which is in equilibrium with the linear form.

4.4.2 Multi-enzymatic system under radioactive conditions

Translation of the reaction parameters from the non-radioactive conditions to radioactive conditions is often not straightforward. When a carrier-free radioactive precursor is used, as $[^{13}\text{N}]\text{NH}_4\text{OH}$, the concentration of this specie is particularly low, in the micro molar order, while the concentration used in cold (non radioactive) conditions was at the mili molar range. Hence, the reaction's kinetics might be considerably altered, and meticulous refinements of the experimental conditions are required.

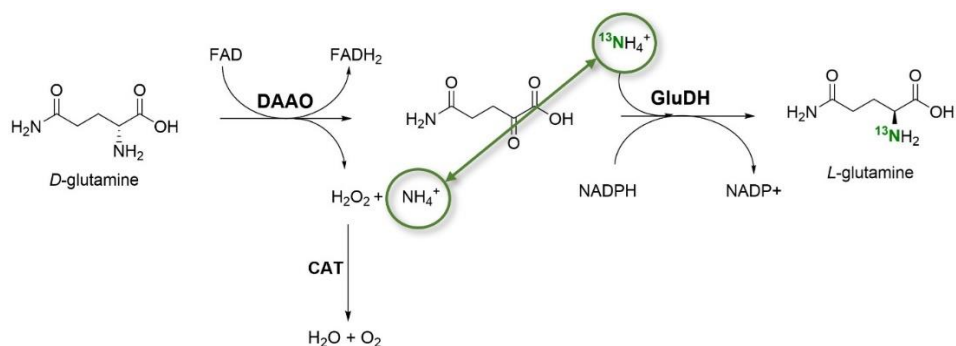
The multi-enzymatic reaction system was initially tested following the same procedure as for non-radioactive conditions, but replacing the ammonia added into the solution for its radioactive counterpart ($[^{13}\text{N}]\text{NH}_4\text{OH}$). Unfortunately, no radioactive species beside the labelling agent could be detected in the solution. As the only modification with respect to the reaction carried out under non-radioactive conditions was the replacement of ammonia by $[^{13}\text{N}]\text{NH}_4\text{OH}$, we hypothesised that the problem might be related to the concentration of the labelling agent.

Chapter 4. Radiolabelled glutamine

Ammonia competition

One of the most likely reasons for the failure to produce the radiotracer, was the competition between radioactive and non-radioactive ammonia that occurs in this multi-enzyme cascade (Scheme 4.5). While radioactive ammonia is added to the system, its quantity is far inferior to the quantity of the non-radiolabelled ammonia that is formed *in situ* and released after first reaction step (1:1000 radioactive/non-radioactive ammonia).

Assuming that both isotopes of ammonia (^{13}N and ^{14}N) have similar preference to enter the enzymatic amination pathway, the low concentration of $[^{13}\text{N}]\text{NH}_4\text{OH}$ could be responsible for the low labelling yield. Even when the product was formed, the concentration might be too low to be detected using radio-HPLC, despite the reaction was assayed using significant amounts of starting radioactivity (up to 500 MBq).



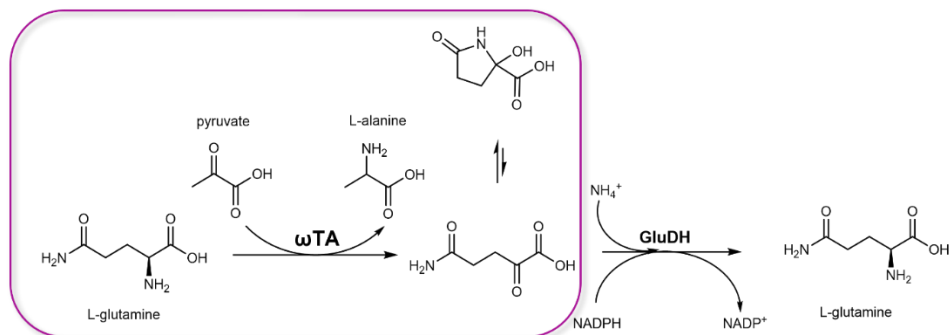
Scheme 4.5 Ammonia competition in the multi-enzymatic system composed of DAAO, CAT and GluDH.

Modification of the original multi-enzymatic system by using a Transaminase

The combination of these two factors (ammonia competition, and cyclic-acyclic equilibrium) makes the performance of this reaction under radioactive conditions even more challenging. Because of that, and to avoid the competition problem, D-amino acid

Chapter 4. Radiolabelled glutamine

oxidase/catalase system was replaced by a Transaminase, which is not expected to release ammonia into the reaction media (Scheme 4.6).



Scheme 4.6 Multi-enzymatic system in which first step is conducted by a Transaminase.

The first step of the enzymatic cascade was firstly tested. If the reaction works, Marfey's derivatization followed by HPLC should show the formation of derivatised L-alanine, while the peak corresponding to derivatised L-glutamine should decrease with reaction time. Three transaminases, from different micro-organisms (*Cromobacterium violaceum*, *Halomonas elongata* and *Pseudomonas fluorescense*) were expressed, purified, and tested. Also, three different reaction time-points were investigated: one hour, three ours and overnight (Table 4.1).

Table 4.1 Conditions tested for the first step reaction by using different transaminases and reaction times. *Pf*: *pseudomonas fluorescense* *Cv*: *cromobacterium violaceum* *He*: *halomonas elongata*

ωTA (conc)	L-Gln	Pyr	PLP	buffer	Time points	Quality Control
ωTA from <i>Pf</i> (4 mg/mL)	10 mM	10 mM	0.5 mM	HEPES 200mM pH 8	1 h 3 h Overnight	Marfey's derivatization
ωTA from <i>Cv</i> (4 mg/mL)						
ωTA from <i>He</i> (4 mg/mL)						

The reaction was conducted in a total volume of 250 μL in an amicon filter, with a cut-off membrane to quench the reaction by centrifugation. Surprisingly, no products were observed under non-radioactive conditions. All products were analysed by Marfey's

derivatization, and in none of the cases the peak corresponding to the derivatized alanine could be observed (Figure 4.4).

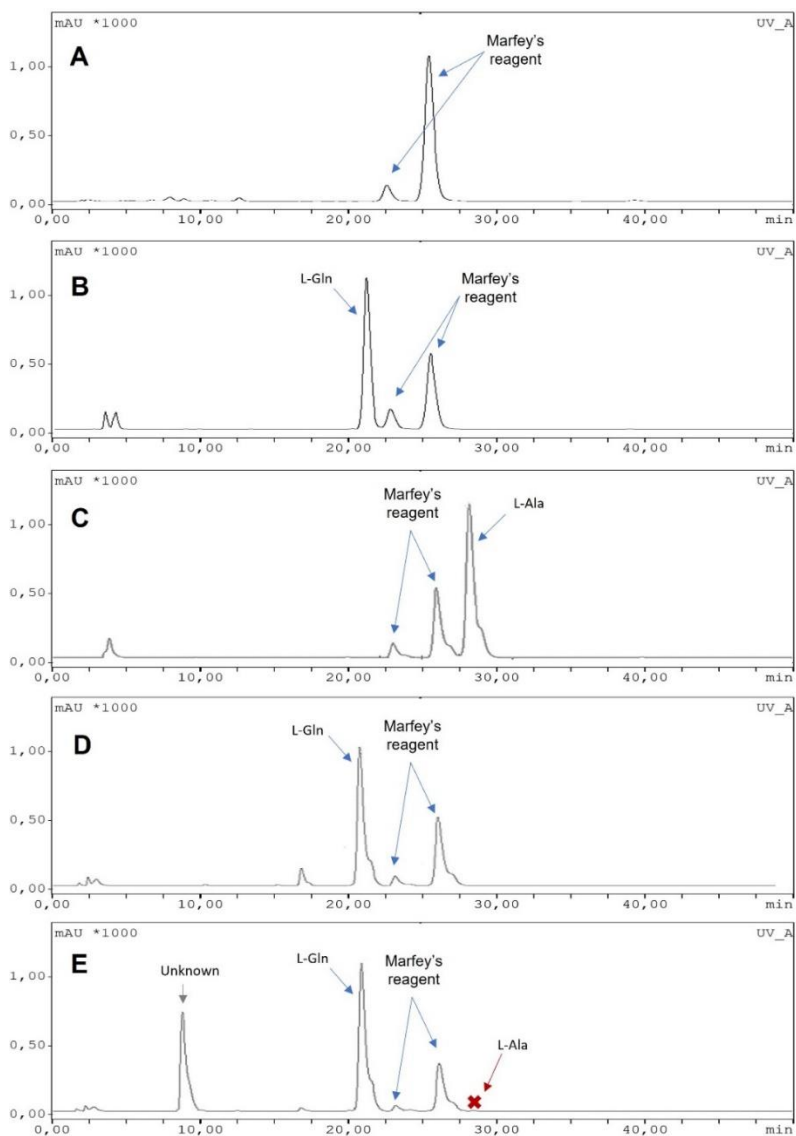


Figure 4.4 Chromatograms from: A) Marfey's reagent; B) L-glutamine standard derivatized; C) L-alanine standard derivatized ; D) Reaction control without enzyme; E) Enzymatic reaction with ω -TA.

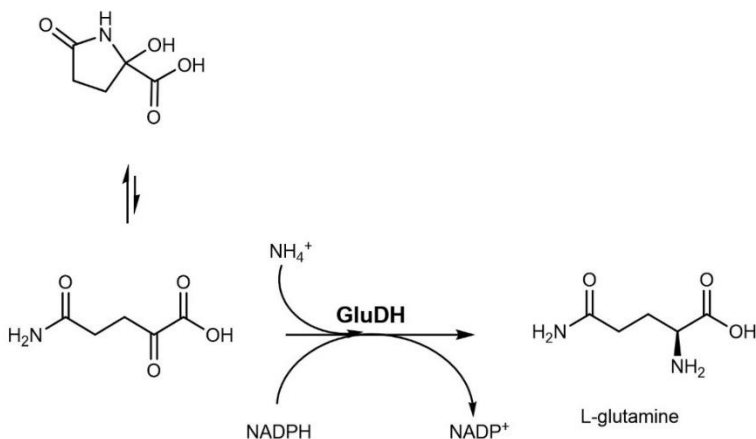
Chapter 4. Radiolabelled glutamine

Possible reasons for the lack of success include: (i) too short reaction time; or (ii) L-glutamine is not a good substrate for these enzymes. In any case, the reaction was not suitable to be assayed under radioactive conditions.

4.4.3 Separated synthesis of 2-oxoglutarate

In order to overcome the problem related to the formation of the cyclic form of glutamine's keto-acid, we anticipated that 2-oxoglutarate could be prepared using conventional synthetic chemistry, to then tackle the preparation of L-glutamine using a one-enzymatic process. By following this approach, the concentration of intermediate in its cyclic form can be increased. This should lead to an increase in the concentration of both the cyclic and the acyclic forms, thus favouring the reaction for the formation of the desired amino acid via reductive amination. The formation of L-glutamine should at the same time favour the formation of the linear form of OGA.

This simplified method consists of a one-step enzymatic amination from the glutamine's α -keto acid (Scheme 4.7).

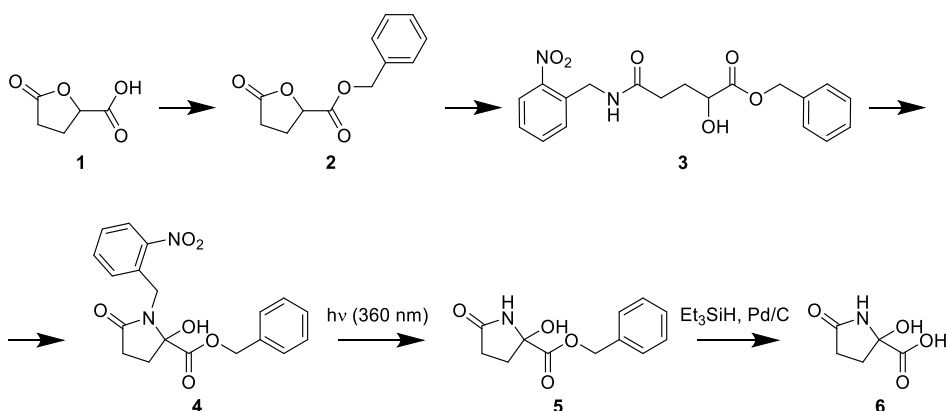


Scheme 4.7 Enzymatic synthesis of L-glutamine starting from OGA in its cyclic hydroxylatame form and catalyzed by Glutamate Dehydrogenase.

Chapter 4. Radiolabelled glutamine

This approach is less complicated from an enzymatic point of view, although it required the preparation of OGA using synthetic methods. The complexity in the production of this molecule makes it non-commercially available and its synthesis has only been described in one peer reviewed paper¹⁸ and one patent¹⁹. Isolation of the α -keto acid has previously been described in the literature; but it was biochemically prepared, which only affords low amounts of the compound and was not planned to be used in further reactions.

As none of the previously reported methods was anticipated to be appropriate for our purposes, a new synthetic route for the preparation of OGA in its cyclic hydroxylactame form was developed in collaboration with University of Ljubljana (Scheme 4.8).



Scheme 4.8 Synthetic route for the production of Oxoglutaramate in its cyclic hydroxylactame form.

The synthetic route consists on the esterification of the starting lactone **1** to produce compound **2**. Then the aminolysis using 2-nitrobenzyl amine resulted in the secondary alcohol **3** in high yield. This alcohol underwent Dess-Martin oxidation reaction to produce the lactone **4**. Photochemical de-benzylation reaction yielded the mono-protected product **5**, which was isolated by extraction from acetonitrile/water reaction mixture and chromatographically purified before further use. Subsequently, catalytic

hydrogenation was performed on palladium via *in situ* formation of hydrogen and afforded the desired cyclic OGA 6. Also, to enable its easy handling, OGA was reformulated as a lithium salt, by using aqueous lithium hydroxide, resulting in a white crystalline solid, LiOGA.

The product was obtained in the cyclic form as LiOGA. Hence, the acyclic precursor was still in substantial deficit. Nevertheless, once the precursor will be dissolved, equilibrium with the linear form should be reached.

4.4.4 Enzymatic synthesis starting from cyclic LiOGA

Once the keto-acid was obtained as a white powder, the reaction was tested under non-radioactive conditions. Before that, the activity of the enzyme was evaluated at different pH values (Figure 4.5). The results confirmed that the activity of the enzyme was maximum in the pH range between 7 and 9. Because of that, pH values of 7, 8 and 9 were selected to assay the preparation of L-glutamine under non-radioactive conditions (Table 4.2). Indeed, despite Figure 5 clearly shows that the optimal pH is 8, the other pH values were assayed as it was anticipated that pH could have an effect on the equilibrium between the cyclic and the linear forms of OGA, with the consequent effect on reaction yield.

Table 4.2. Experimental conditions assayed for the production of L-glutamine under non-radioactive conditions, using synthetically prepared OGA (as LiOGA, in its hydroxylactame form) at different pHs.

pH	OGA (mM)	NADPH (mM)	GluDH (U)	NH ₄ Cl (mM)	Reaction time (min)	Analysis
7	10	1	10	125	60	Marfey's
8						
9						

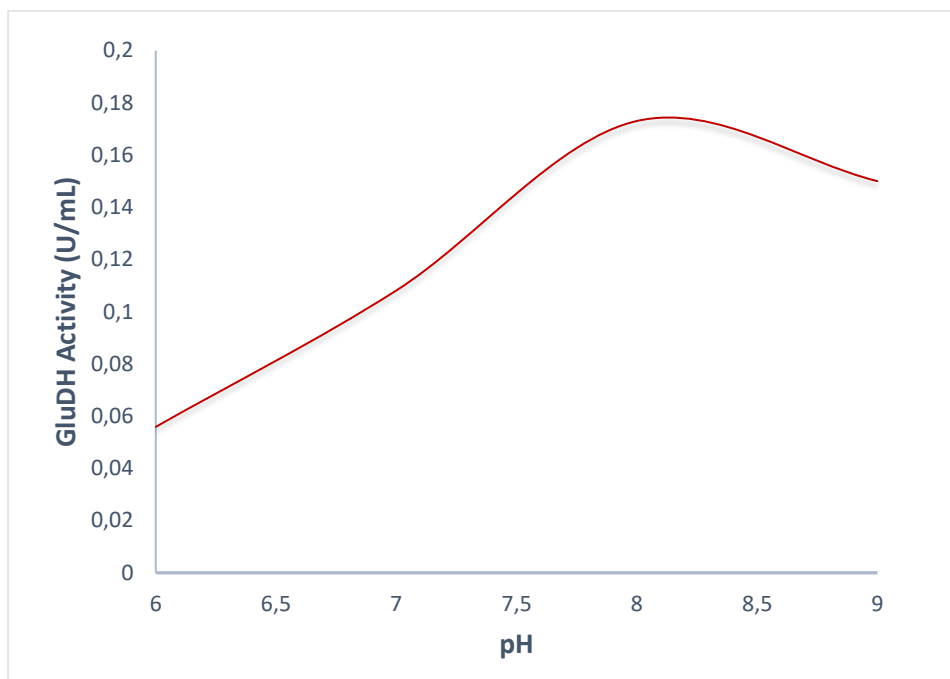


Figure 4.5 Relationship between Glutamate dehydrogenase activity and pH following the quality control GluDH conditions.

Under non-radioactive conditions, the reaction produced the desired L-glutamine in an 80% conversion irrespective of the pH in 60 min, based on HPLC analysis of the resulting products by Marfey's derivatization (Figure 4.6). This yield is calculated considering that maximum yield of L-glutamine is 1 mM, because the concentration of the cofactor NADPH, that is 1 mM, is the limiting factor. These results confirmed that the catalytic system successfully incorporated ammonia to the substrate.

Encouraged by these results, the reaction was reproduced under radioactive conditions, using exactly the same experimental conditions but replacing the non-radioactive ammonia by [^{13}N]ammonia (Scheme 4.9).

Chapter 4. Radiolabelled glutamine

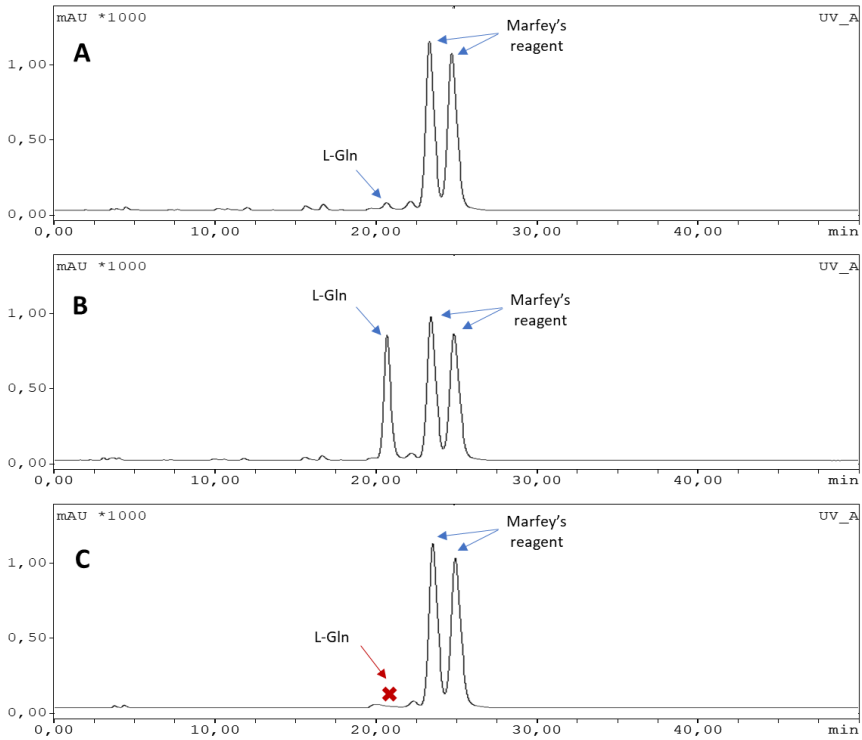
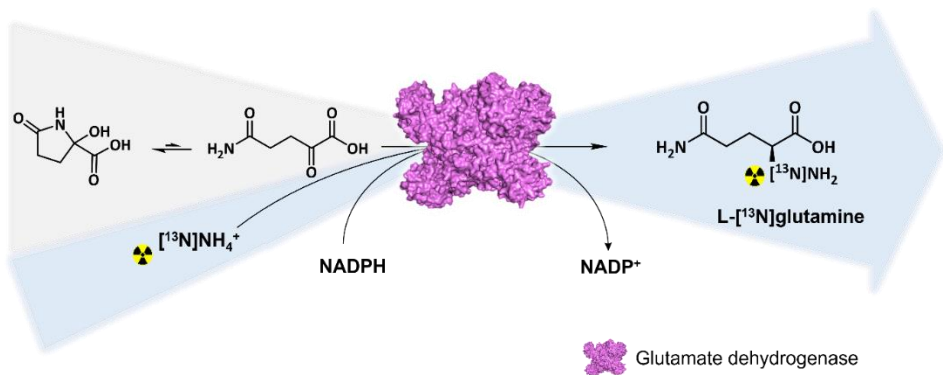


Figure 4.6 Chromatograms from: A) Enzymatic reaction product derivatized; B) Enzymatic reaction product with standard L-Gln 10 mM derivatized; C) Enzymatic reaction control without enzyme derivatized.



Scheme 4.9 Enzymatic radiolabelling of L-[¹³N]glutamine starting from LiOGA in its hydroxylactame form, and [¹³N]NH₄OH as radiolabelling agent.

Chapter 4. Radiolabelled glutamine

Unfortunately, the reaction was not successful and the formation of L-[¹³N]glutamine could not be detected. One of the main problems of our approach was the long synthesis time required (60 min) which is not compatible with the short half-life of nitrogen-13. Different attempts were made to increase the radiochemical yield, by modifying the reaction temperature from 4 to 37 °C. Additionally, pH of the reaction mixture was also modified in the range 5-10, to increase substrate availability in linear form and catalytic activity of the enzyme (Table 4.3, entries 1-15). Nevertheless, no radioactive product was formed irrespectively of the experimental conditions.

Table 4.3 Conditions tested under radioactive conditions for the synthesis of nitrogen-13 labelled glutamine.

Entry	pH	Temperature (°C)	LiOGA (mM)	GluDH (U)	NADPH (mM)	Yield %
1	5	4	10	10	1	-
2		r.t.				-
3		37				-
4	7	4	10	10	1	-
5		r.t.				-
6		37				-
7	8	4	10	10	1	-
8		r.t.				-
9		37				-
10	9	4	10	10	1	-
11		r.t.				-
12		37				-
13	10	4	10	10	1	-
14		r.t.				-
15		37				-
16	8	r.t.	660	24	10	6
17				48		20

Chapter 4. Radiolabelled glutamine

Dramatic increase of the precursor and enzyme's concentrations

After carefully reviewing the experimental approach, we realised that in the experiments listed in table 4.3 (entries 1-15) both the concentrations of the precursor and ammonia were in deficit, which is not ideal. Because of that, a drastic increase of LiOGA, GluDH and NADPH concentration was assayed. Using a higher amount of GluDH (12 mg, 24 U), NADPH cofactor (10 mM), and LiOGA (0.66 M) in phosphate buffer (325 mM, pH 8) at room temperature, the formation of the ^{13}N -labelled product could be detected in 60 min, with an overall radiochemical chromatographic yield of 6 % (Figure 4.6; and Table 4.3, entry 16).

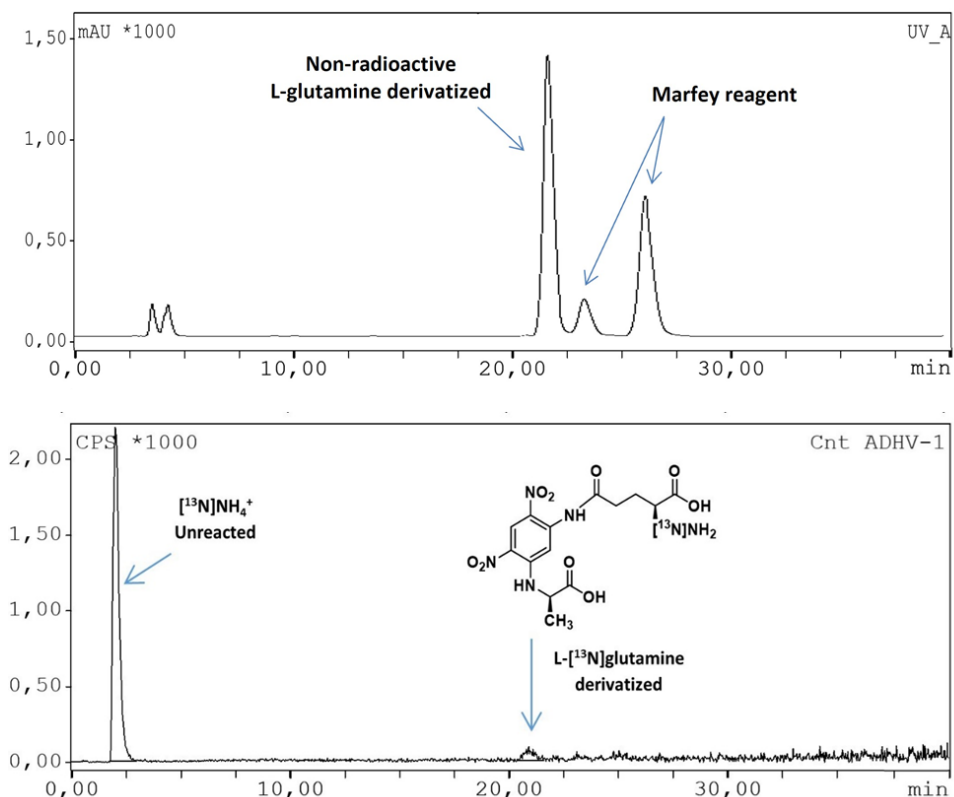


Figure 4.6. radio-HPLC corresponding to the Marfey's derivatization of the enzymatic reaction for the production of L-[^{13}N]glutamine with a 6% of chromatographic yield.

Chapter 4. Radiolabelled glutamine

The low reaction yield was attributed to low probability of the crucial elements in the reaction, namely the precursor, $[^{13}\text{N}]$ ammonia, NADPH cofactor and the enzyme, to coincide in favourable way. Chromatographic yield could be slightly improved up to 20 % (Figure 4.7) (Table 4.3, Entry 17) by increasing GluDH concentration from 24 to 48 U (this is, to saturation).

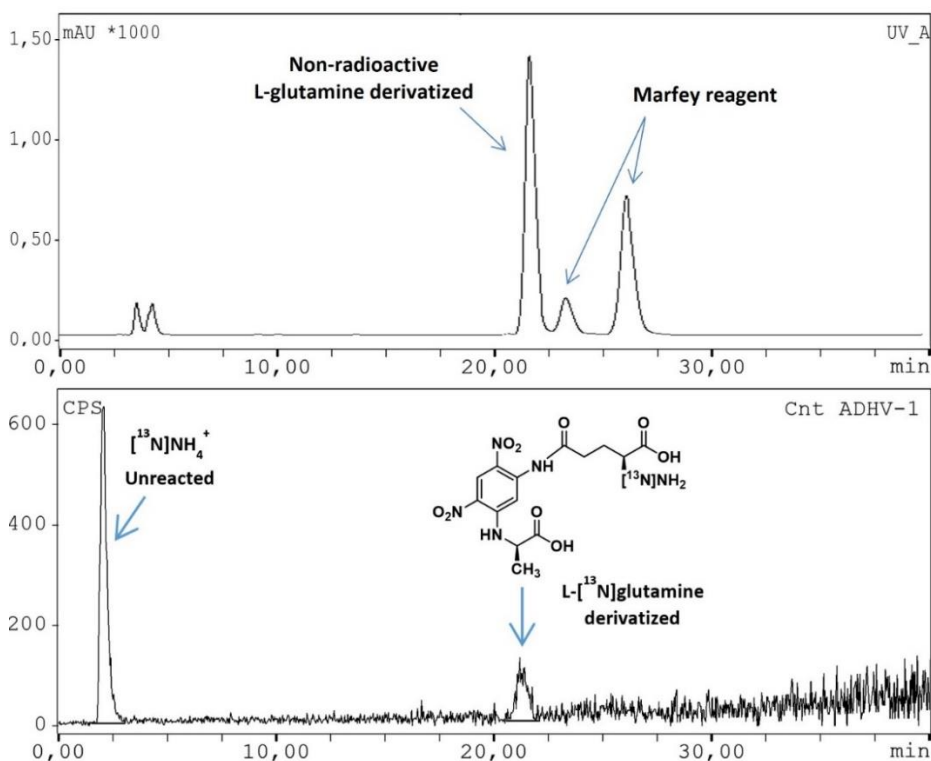


Figure 4.7 radio-HPLC corresponding to the Marfey's derivatization of the enzymatic reaction for the production of L- $[^{13}\text{N}]$ glutamine with a 20% of chromatographic yield.

This methodology successfully demonstrated production of ^{13}N -radiolabelled L-glutamine in its native form and is a promising step towards utilization of this radiotracer in PET imaging studies. This adds to the toolbox of diagnostic protocols and strategies to determine mechanism of different diseases.

4.4.5 Future perspectives

Although the formation of the desired labelled compound could be observed, future works should focus on optimising the reaction conditions to increase radiochemical yield. This is a necessary step for future application of the tracer in vitro or in vivo. Modification of the experimental conditions, e.g. performing the reaction under increased pressure or using micro/nano reactors, together with an increase in the concentration of the reagents, may increase production yields, eventually in shorter reaction times.

Also, a future work should focus on the pivotal role that the enzyme plays in the reaction. The production of Glutamate Dehydrogenase mutants could result very promising. The purpose of this mutants will be the better accommodation of the oxoglutaramate linear form (OGA) in its active site, improving their selectivity towards this precursor, which is not actually the natural one. Within that aim, we propose two mutants which could help to increase the reaction yield.

The first letter of the mutant's nomenclature indicates the amino that will be replaced, followed by the position of the amino acid in the enzyme's structure, and next to it, the new amino acid that is going to occupy the position.

Two mutants are proposed and the amino acid that will be replaced is the Lysine (K) of the position 92, by an Alanine (A) or an Asparagine(N), respectively (Figure 8C and 8D).

The natural substrate of Glutamate dehydrogenase is the α -ketoglutaric acid. This keto-acid fits in the active site of the enzyme and interacts with the lysine from the 92 position by forming a salt bridge (Figure 4.8A). As glutamine's keto-acid (oxoglutaramate, OGA) has an amine group instead of a hydroxyl group in this position, the interaction forming a salt bridge will not be possible (Figure 4.8B).

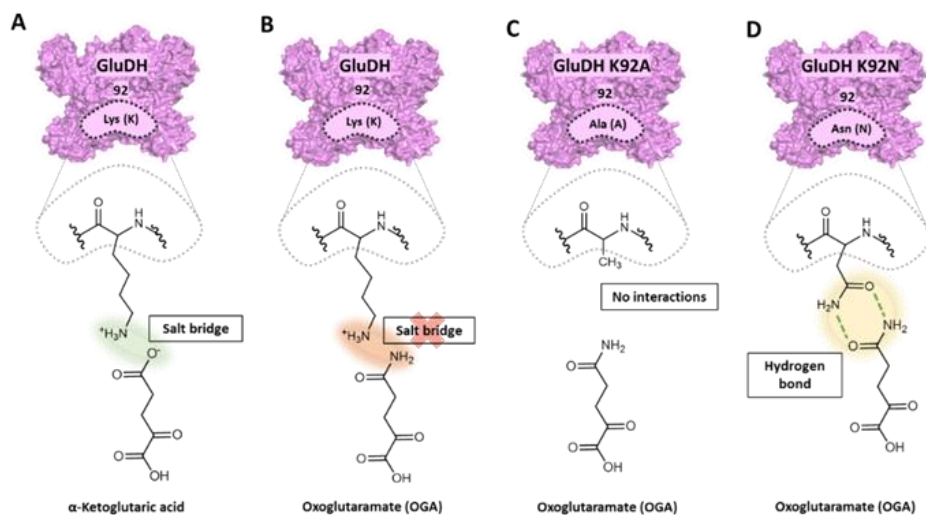


Figure 4.8 Schematic representation of GluDH and the modifications in the 92 position of the corresponding mutants. A) GluDH interaction with its natural substrate α -ketoglutaric acid; B) GluDH interaction with oxoglutaramate linear form (OGA); C) GluDH mutant K92A interaction with oxoglutaramate linear form (OGA); D) GluDH mutant K92N interaction with oxoglutaramate linear form (OGA).

The first mutant envisaged, the K92A will leave more space in the enzyme's active site to accommodate the oxoglutaramate (Figure 4.8C). The second one, the K92N, is thought to create a perfect interaction with the oxoglutaramate by forming two hydrogen bonds (Figure 4.8D).

These two mutants have only been designed and will be expressed, purified and tested in the future by following the same enzymatic conditions in which the system works to know if the yield increases.

4.5 Summary and conclusions

We have opened a new biosynthetic route to produce nitrogen-13 radiolabelled L-glutamine, to be used in future preclinical PET studies.

In this chapter, it has been demonstrated that L-[¹³N]glutamine can be synthesized by reductive amination of OGA using an enzymatic process starting from the cyclic hydroxylactame form, that can be spontaneously but reversibly linearized to the mentioned alpha-ketoacid.

We have reached this point by finding and selecting an enzymatic system, which allows the stereoisomeric inversion from D-glutamine to L-glutamine under non-radioactive conditions. However, when radioactive conditions were used the system did not work, due to two factors: (i) the low concentration of radioactive ammonia available to reach the enzyme; and (ii) the OGA cyclization, which significantly decreases the amount of linear form available for the enzyme.

As the low concentration of ammonia was inherent to the radiosynthetic processes, we thought that the concentration of the OGA in its linear form could be increased by putting the system into saturation conditions. With that purpose, OGA was synthesized separately as a lithium salt, allowing its use directly in the enzymatic reaction by using higher concentrations. With this approach, the desired radiolabelled product was identified, because higher yield was achieved.

Thanks to the use of a biocatalytic process, enantioselective problems were avoided and the best synthetic conditions were reached by a combination of traditional synthetic procedures and enzymatic chemistry. Our method, despite not directly applicable to perform preclinical studies, opens future opportunities. Further work will be required to increase the yield of the production of L-[¹³N]glutamine.

4.6 References

1. Pavlova, N. N. & Thompson, C. B. The Emerging Hallmarks of Cancer Metabolism. *Cell Metab.* **23**, 27–47 (2016).
2. Altman, B. J., Stine, Z. E. & Dang, C. V. From Krebs to clinic: Glutamine metabolism to cancer therapy. *Nat. Rev. Cancer* **16**, 619–634 (2016).
3. Lane, A. N. & Fan, T. W. M. Regulation of mammalian nucleotide metabolism and biosynthesis. *Nucleic Acids Res.* **43**, 2466–2485 (2015).
4. Wang, Q. *et al.* Targeting ASCT2-mediated glutamine uptake blocks prostate cancer growth and tumour development. *J. Pathol.* **236**, 278–289 (2015).
5. Schulte, M. L., Khodadadi, A. B., Cuthbertson, M. L., Smith, J. A. & Manning, H. C. 2-Amino-4-bis(aryloxybenzyl)aminobutanoic acids: A novel scaffold for inhibition of ASCT2-mediated glutamine transport Dedicated to the memory of Eric S. Dawson, Ph.D. *Bioorganic Med. Chem. Lett.* **26**, 1044–1047 (2016).
6. Gambhir, S. S. Molecular imaging of cancer with positron emission tomography. *Nat. Rev. Cancer* **2**, 683–693 (2002).
7. Zhu, L., Ploessl, K., Zhou, R., Mankoff, D. & Kung, H. F. Metabolic imaging of glutamine in cancer. *J. Nucl. Med.* **58**, 533–537 (2017).
8. Padakanti, P. K. *et al.* Automated synthesis of [11C]L-glutamine on Synthra HCN plus synthesis module. *EJNMMI Radiopharm. Chem.* **4**, (2019).
9. Rosenberg, A. J., Nickels, M. L., Schulte, M. L. & Manning, H. C. Automated radiosynthesis of 5-[11C]L-glutamine, an important tracer for glutamine utilization. *Nucl. Med. Biol.* **67**, 10–14 (2018).
10. Qu, W. *et al.* Preparation and characterization of L-[5- 11C]-glutamine for metabolic imaging of tumors. *J. Nucl. Med.* **53**, 98–105 (2012).
11. Hassanein, M. *et al.* Preclinical Evaluation of 4-[18F]Fluoroglutamine PET to

- Assess ASCT2 Expression in Lung Cancer. *Mol. Imaging Biol.* **18**, 18–23 (2016).
12. Qu, W. *et al.* Synthesis of optically pure 4-fluoro-glutamines as potential metabolic imaging agents for tumors. *J. Am. Chem. Soc.* **133**, 1122–1133 (2011).
 13. da Silva, E. S., Gómez-Vallejo, V., Baz, Z., Llop, J. & López-Gallego, F. Efficient Enzymatic Preparation of ^{13}N -Labelled Amino Acids: Towards Multipurpose Synthetic Systems. *Chem. - A Eur. J.* **22**, 13619–13626 (2016).
 14. da Silva, E. S., Gómez-Vallejo, V., López-Gallego, F. & Llop, J. Biocatalysis in radiochemistry: Enzymatic incorporation of PET radionuclides into molecules of biomedical interest. *J. Label. Compd. Radiopharm.* **61**, 332–354 (2018).
 15. Bhushan, R. & Brückner, H. Marfey's reagent for chiral amino acid analysis: A review. *Amino Acids* **27**, 231–247 (2004).
 16. Hersh, L., Rat liver ω -amidase. Purification and properties. *Biochemistry*, **10**, No 15, 2884-2891 (1971)
 17. Heuson, E., Charmantray, F., Petit, J. L., de Berardinis, V. & Gefflaut, T. Enantioselective Synthesis of d- and l- α -Amino Acids by Enzymatic Transamination Using Glutamine as Smart Amine Donor. *Adv. Synth. Catal.* **361**, 778–785 (2019).
 18. Shen, D., Kruger, L., Deatherage, T. & Denton, T. T. Synthesis of α -Ketoglutaramic acid. *Anal. Biochem.* **607**, 113862 (2020).
 19. Martinez *et al.* United States Patent. Patent No.: US6288240 B1(2001).

CHAPTER 5

General Conclusions

Chapter 5. General conclusions

1. L-[*methyl*-¹¹C]alanine and D-[*methyl*-¹¹C]alanine can be produced *via* asymmetric alkylation of a glycine-derived Schiff base using [¹¹C]CH₃I as the labelling agent. Automation of the process allowed the preparation of ready-to-inject enantiopure amino acids with high radiochemical purity in moderate yields.
2. L-[¹³N]alanine can be efficiently produced with high radiochemical and enantiomeric purity by using an improved biocatalytic process based on reductive amination and using [¹³N]NH₄OH as the labelling agent.
3. The three labelled amino acids, L-[*methyl*-¹¹C]alanine, D-[*methyl*-¹¹C]alanine and L-[¹³N]alanine, show different biodistribution patterns after intravenous administration in a mouse model of prostate cancer, based on the deletion of PTEN in prostate epithelia. D-[*methyl*-¹¹C]alanine showed the highest accumulation in the tumour, highlighting the impact of the enantiomer, the radionuclide and the labelling position on imaging studies. These results were confirmed by *ex vivo* imaging and histological analysis.
4. The preparation of L-glutamine starting from D-glutamine using a multi-enzymatic process allowing stereoisomeric inversion, results in moderate yields under non-radioactive conditions. Translation into radioactive conditions did not result in the formation of L-[¹³N]glutamine, probably due to the low concentration of the labelling agent ([¹³N]NH₄OH) and the linear form of the reaction intermediate oxoglutaminate (OGA) which is in equilibrium with the cyclic form.
5. The enzymatic preparation of L-[¹³N]glutamine could be achieved by using chemically synthesized OGA and a high concentration of glutamate dehydrogenase, although radiochemical yields (20% chromatographic yield) and long reaction times required (60 min) demand for further refinement of the synthetic conditions.

ACKNOWLEDGEMENTS

ACKNOWLEDGEMENTS

Acknowledgements

En primer lugar, quiero mostrar mi agradecimiento al Prof. Manuel Martín Lomas, al Prof. Luis Liz-Marzán y a Prof. Aitziber López Cortajarena, anteriores y actual director científico de CIC biomaGUNE, respectivamente. Gracias por darme la oportunidad de desarrollar el trabajo experimental de esta tesis en las increíbles instalaciones del centro. Ha sido un placer crecer como científica en un ambiente tan multi disciplinar y multi cultural.

Quiero mostrar mi agradecimiento a mi codirector de tesis el Dr. Jordi Llop, por darme la oportunidad de llevar a cabo mi tesis bajo su supervisión, enseñándome tanto sobre este apasionante campo y por su puerta siempre abierta, siempre listo para responder cualquier duda durante estos tres años. Gracias por enseñarme a ser más fuerte cada día.

También, a mi codirector el Prof. Arkaitz Carracedo, gracias por darme la oportunidad de formar parte de este fascinante proyecto sobre el cáncer de próstata.

Me gustaría también expresar mi más sincero agradecimiento al Prof. Fernando López-Gallego. A pesar de no haber sido oficialmente mi director de tesis ha actuado como uno, y uno de los buenos. Gracias por enseñarme tantos valiosos conocimientos sobre el mundo de la biocatálisis. Gracias por ser siempre amable, comprensivo y profesional.

Gracias a la Dr. Vanessa Gómez-Vallejo por su apoyo durante todo el trabajo experimental en radioquímica.

También me gustaría expresar mi agradecimiento a mi querida Dr. Susana Velasco-Lozano. Gracias por todos los consejos extremadamente valiosos que me has dado durante estos años, científicos y personales. Ha sido un placer poder trabajar a tu lado, eres el mejor ejemplo de lo que significa ser una gran científica y una gran persona.

ACKNOWLEDGEMENTS

Aprovecho también para agradecer a todos mis compañeros del grupo de Radioquímica e Imagen nuclear y del grupo de Biocatálisis Heterogénea, ha sido un placer conocerlos a todos y compartir estos años juntos.

Gracias a mi Muchitanga (Aitor, Xabi, Unai y Kepa Z) por todos los increíbles momentos que hemos vivido dentro y fuera del laboratorio. Dentro de la muchitanga, especialmente a mis Neskak (Anica, Roxi y Cris) por estar siempre ahí, apoyándonos mutuamente cada día y creando momentos inolvidables, y a mi Quintico (Víctor), gracias por tu valioso apoyo técnico y por nuestras largas conversaciones. También a mi querida AnaB, gracias por estar siempre cuando más hace falta. Estoy muy segura de que nuestros caminos no se separan aquí.

Gracias también a mis amigos de Luceni y Donosti, no hay nada como una cerveza y una conversación con vosotros para ser feliz.

Nadie es más importante para mí que mi familia, y especialmente mis padres, gracias por estar siempre ahí, siempre apoyándome durante toda mi vida. Soy muy afortunada de tenerlos a mi lado.

Por último, pero no menos importante, gracias a ti, Ibai. Ni en sueños podría haber imaginado un mejor compañero de vida.



CICbiomaGUNE

MEMBER OF BASQUE RESEARCH
& TECHNOLOGY ALLIANCE



EXCELENCIA
MARÍA
DE MAEZTU

CICbioGUNE

MEMBER OF BASQUE RESEARCH
& TECHNOLOGY ALLIANCE



EXCELENCIA
SEVERO
OCHOA